DEVELOPMENT OF A METHOD FOR BWR SUBCHANNEL ANALYSIS

by

ARTUR JOSE GONÇALVES FAYA

DOCTOR OF PHYSOLOPHY

at the

MASSACHUSETTS INSTITUTE OF TECHNOLOGY

October 1979

DEVELOPMENT OF A METHOD FOR BWR SUBCHANNEL ANALYSIS

by

ARTUR JOSE GONÇALVES FAYA

E.E., Instituto Tecnologico de Aeronautica, Brazil, (1972)

M.S., Universidade de Sao Paulo, Brazil, (1975)

SUBMITTED IN PARTIAL FULFILLMENT OF THE

REQUIREMENTS FOR THE

DEGREE OF

DOCTOR OF PHILOSOPHY

at the

MASSACHUSETTS INSTITUTE OF TECHNOLOGY

OCTOBER 1979

Signature of Author _____
Department of Nuclear Engineering, Oct.24, 1979

Certified by _____
Thesis Supervisor

Accepted by _____
Chairman, Department Committee on Graduate Students

Orientador Lothar Wolf

Title of Thesis: Development of a Method for BWR Subchannel Analysis

Name of Author: Artur José Gonçalves Faya

Submitted to the Department of Nuclear Engineering, October 1979, in partial fulfillment of the requirements for the Degree of Doctor of Philosophy.

ABSTRACT

This study deals with the development of a computer program for steady-state and transient BWR subchannel analysis. The conservation equations for the subchannels are obtained by area-averaging of the two-fluid model conservation equations and reducing them to the drift-flux model formulation. The conservation equations are solved by a marching type technique which limits the code to analysis of operational transients only. The transfer of mass, momentum and energy between adjacent subchannels is split into diversion cross-flow and turbulent mixing components. The transfer of mass by turbulent mixing is assumed to occur in a volume-for-volume scheme reflecting experimental observations. The phenomenon of lateral vapor drift and mixing enhancement with flow regime are included in the mixing model of the program. The following experiments are used for the purpose of the assessment of the code under steady-state conditions:

1) GE Nine-Rod tests with radially uniform and nonuniform heating
2) Studsvik Nine-rod tests with strong radial power tilt
3) Ispra Sixteen-rod tests with radially uniform heating

Comparison of calculated results with these data shows that the program is capable of predicting the correct trends in exit mass velocity and quality distributions.

Thesis Supervisor: Lothar Wolf
Title: Associate Professor of Nuclear Engineering

Thesis Supervisor: Neil E. Todreas
Title: Professor of Nuclear Engineering

ACKNOWLEDGEMENTS

The author wishes to express his gratitude to Professor Lothar Wolf for his advice and criticism. His encouragement at times when the results were not so clear is deeply appreciated.

Thanks are also due to Professor Neil Todreas for his patience and valuable guidance during the last part of this work.

The author wishes to thank FAPESP - Fundacão de Amparo à Pesquisa do Estado de São Paulo, Brazil, for granting him a scholarship during the course of this work.

The author wishes to thank IPEN - Instituto de Pesquisas Energéticas e Nucleares for granting him a leave on absence during which this work was performed.

Special thanks are due to my wife, Su Chiang, for her understanding and encouragement. Her skillful typing of this thesis is deeply appreciated.

TABLE OF CONTENTS

LIST OF FIGURES

LIST OF TABLES

NOMENCLATURE

A	flow area	m^2
C_o	void concentration parameter	-
c_p	specific heat	$J/Kg-^oK$
D_e	Hydraulic diameter	m
$\dot{E}$	energy flux	W/m^2
f	friction factor	-
F	friction force term	Kg/m^2-s^2
g	gravitational acceleration	m/s^2
G	mass velocity	Kg/m^2-s
h	enthalpy	J/Kg
h	heat transfer coefficient	W/m^2-^oK
h_{fg}	latent heat of vaporization	J/Kg
j	superficial velocity	m/sec
j_v^*	$j_v\rho_v^{0.5}\left[gD(\rho_\ell-\rho_v)\right]^{-0.5}$	-
j_ℓ^*	$j_\ell\rho_\ell^{0.5}\left[gD(\rho_\ell-\rho_v)\right]^{-0.5}$	-
k	thermal conductivity	$W/m-^oK$
K_a	empirical parameter appearing in the mixing model	-
L_i	number of fuel rods adjacent to subchannel i	-
$\dot{M}$	momentum flux	$Kg/m-s^2$
N_i	number of subchannel adjacent to subchannel i	-
p	pressure	N/m^2
Pr	Prandtl number	-

Q	energy source term	W/m^3
q''	heat flux	W/m^2
Re	Reynolds number	-
S_{ik}	gap spacing between subchannels i and k	m
T	temperature	^oC
t	time	s
$\tilde{u}$	turbulent component of the transverse velocity	m/s
v	velocity	m/s
V	volume	m^3
V_{vj}	drift velocity between the vapor and the mixture center-of-volume	m/s
W	mass flow rate per unit of axial length	Kg/s-m
x	quality	-
Δy_{ik}	mixing length between subchannels i and k	m
z	axial coordinate	-
α	void fraction	-
β	mixing constant	-
Γ_v	vapor source term	Kg/m^3-s
ϵ	empirical parameter which appears in the model for the subcooled region	-
θ	two-phase mixing multiplier	-
μ	viscosity	Kg/m-s
ρ	density	Kg/m^3
σ	surface tension	Kg/s^2

$\phi_{\ell o}$	two-phase friction multiplier	-

subscripts

av	average
d	donor subchannel
d	void detachment
fc	forced convection
i	subchannel i
j	axial node j
k	adjacent subchannel k
ℓ	liquid
m	adjacent rod m
nb	nucleate boiling
sp	single-phase
tp	two-phase
v	vapor
w	wall

CHAPTER 1 - INTRODUCTION

1.1 Background

One of the primary goals for the safe operation of nuclear power reactors is to have accurate predictions of thermal hydraulic conditions in the core. In both design and operation it is important to anticipate the fluid conditions at which failure of the fuel may occur due to overheating. The prediction of the average fluid density throughout the core is also important for neutronic calculations and fuel management schemes.

Many experimental and analytical studies have been performed on the parallel rod array geometry which is typical of the reactor core design. The study of this geometry is difficult to conduct due to geometric complexity of the array and the two-phase flow and heat transfer conditions involved in nuclear reactors.

The geometric complexity stems from the high degree of freedom associated with parallel rod arrays. Rod diameter, rod-to-rod pitch, rod spacers and their location and bundle length are the principal geometric parameters that affect the thermal hydraulic performance of rod bundles.

Fig.1.1 is a representation of a parallel array of rods typical of LWR design. The term subchannel is usually associated with the flow passages between the fuel rods. The boundary between subchannel is chosen to be the minimum distance between close adjacent rods or a normal to wall from the center of the adjacent rod. This convention has been adopted universally and is commonly termed coolant-centered approach. Gaspari /G1/ and more recently Sha et al. /S3/ adopted a rod-centered scheme where the subchannel boundaries are defined around the fuel rods as indicated in Fig.1.2.

This approach has advantages in simulating the bundle behavior in the annular flow regime condition where the liquid tends to adhere to the fuel rods and bundle wall. However, it becomes difficult to quantify the interaction between neighboring subchannels since most experimental setups extract coolant from coolant-centered subchannels.

The two-phase flow situation of the coolant compounds the difficulties by introducing additional variables such as the vapor volume fraction, velocity and temperature of the phases and distribution of the phases within the complex flow configuration in the bundle. In addition, radial and axial variations of the fuel rod power generation cause the coolant flow rate and coolant thermal conditions to vary considerably throughout the array.

1.2 Models for Two-Phase Flow

Two-phase flow is a complicated phenomenon to model in a BWR core, for example, the flow consists of a turbulent mixture of vapor and liquid. For all practical purposes it is impossible to account for all of the physical vapor-liquid interfaces which appear and the interactions between them. For this reason it has been become customary to approximate each phase as a continuous field. This done by volume averaging of the local conservation equations governing the balance of mass, momentum and energy for each phase. By this procedure two sets (one for each phase) of volume-averaged conservation equations (or field equations) are obtained. New quantities are introduced, namely, the phasic volumetric fraction and interaction terms reflecting the transport of mass, momentum and energy across the vapor-liquid interface.

Basically, all existent two-phase models should start

from this point. Restrictions are then imposed which allow reduction of the number of initial field equations. When field equations are removed they are replaced by constitutive equations. For example it is possible to remove one of the energy equations by assuming that one of the phases is saturated. The two-phase models differ from each other by the number of field equations retained. In decreasing order of complexity, following Hughes /H6/, the most commonly used two-phase models are:

(a) Two-Fluid Model - In this model all field equations are retained and no restrictions are imposed. Constitutive equations must be provided to account for the three imterfacial interaction terms. This constitute one of the main problems which are presently under invertigation in the development of the two-fluid model.

(b) Drift-Flux Model - In this model the field equations consist of one continuity equation for the vapor, one continuity equation for the mixture (or for the liquid), one mixture momentum equation and one mixture energy equation. The four field equations are supplemented by a constitutive equation for the velocity difference between the phases, a thermal constraint (usually the assumption of one of the phases saturated) and a relation for the rate of evaporation (or condensation) which is the interfacial interaction term present in the phasic continuity equations.

(c) Homogeneous Equilibrium Model - In this model the field equations are three: one continuity, one momentum and one energy equation for the mixture. The field equations are supplemented with the assumption that both phases flow at the same speed and both phases are saturated.

Table 1.1 summarized the information above and indicates the codes that use the various models described. A glance at this table reveals that the majority of today's subchannel

computer codes employ the homogeneous model.

For a complete picture of the two-phase models the reader is referred to the paper by Boure /B7/ who has summarized all possible combinations of retained field equations and imposed restrictions.

1.3 Purpose of this Study

The purpose of this work is to develop a subchannel code (CANAL) capable of giving a reliable assessment of the thermal margins in BWR bundles for steady-state and operational transient conditions. Presently, there is no code specifically designed for the thermal-hydraulic analysis of BWR core. The widely used COBRA codes fail to display some important trends observed in rod bundle experiments as it will be discussed in next section. Therefore, there is a strong motivation for developing such a code.

Selection of the two-phase model

In the light of what was discussed in the foregiong section the drift-flux model constitutes an appropriate choice between simplicity and complexity. This model certainly describes the interaction between the vapor-liquid mixture and the system better than the homogeneous model. The two-fluid model is, of course, the most advanced one but for subchannel analysis it may be rather costly in terms of computational time. The potential of the two-fluid model resides in accurate physical models to describe the interfacial interaction terms mentioned in Section 1.2. Presently, however, there are uncertainties in modeling these terms.

The drift-flux model seems to be appropriate for solving problems with strong local coupling between the phases, i.e., dispersed flows. However even for problems with moderate

local coupling the drift flux is also appropriate since the axial dimensions of the engineering systems are usually large enough to give sufficient interaction times /I3/.

Code Objectives

In general the transient scenario affects the definition of the objectives as well as the scope for both the analysis and the computer code development. The Loss-of-Coolant-Accident (LOCA) and the Anticipated Transient Without Scram (ATWS) are postulated accidents with the most severe consequences. Whereas LOCA leads to high temperatures of the fuel element in the reactor core, ATWS leads to high pressures in the primary systems. It is obvious that the elimination of the LOCA analysis as code objective will greatly simplify the task of program development. However, besides the great significance of the transient scenario there are still other phenomena which have not been consistently simulated by common subchannel codes in steady-state BWR bundle analysis yet. These will be discussed in Chapter 3.

In short, the main objectives of the CANAL code can be stated as follows:

1) It should predict the experimental trends found in BWR bundle geometry;

2) It should handle all the ATWS transients except those where reverse flow occurs. This leads to simplifications in the numerical scheme adopted.

1.4 Previous Studies

Many subchannel computer codes have been developed in recent years. A review of the methodology employed in all codes is not necessary here. The papers by Rogers and Todreas /R2/ and Lahey and Schraub /L1/ present a good survey on subchannel work done up to 1968. An excellent review of more

recent work has been given by Weisman and Bowring /W2/.

One of the unique features of subchannel analysis is the transverse interchange of mass, momentum and energy at the imaginary interface which defines the subchannels. Although the flow is predominantly in the axial direction the quantification of this transverse phenomena is essential for accurate predictions of the flow quantities. The split of the transverse flow into a turbulent component and a diversion flow component has been almost universally adopted. In most of the codes presently in use the turbulent transverse exchange processed are assumed to occur in a mass-for-mass basis. That is to say, only momentum and energy are transported by turbulent exchange across the imaginary subchannel boundaries. This is a good assumption for single-phase flow where adjacent subchannels have nearly the same density. However, this assumption is questionable for two-phase flow conditions.

Differences in the present generation of subchannel codes exist only in the manner how the various mixing models are coupled. In HAMBO /B9/, for instance, it is assumed that the diversion crossflow and turbulent exchange are dependent upon each other. Other differences exist with respect to the treatment of transverse pressure gradients. Whereas the solution of COBRA-IIIC /R11/ is indirectly driven by those gradients, the solution method of HOTROD /B5/ and MATTEO /F3/ rely on the basis that these gradients do not exist.

Several two-phase flow rod bundle experiments in BWR geometry have been carried out in recent years. One of the most significant phenomena observed was the fact that the gaseous phase has a tendency to move to the higher velocity regions of the bundle. This tendency has been observed for adiabatic tests (Schraub et al. /S2/, Bayoumi /B1/, Yadigaroglu and Maganas /Y1/) and for diabatic experiments

as well (Lahey et al. /L2/, Herkenrath et al./H3/). The lateral vapor drift phenomenon has been widely discussed in the open literature. For several years there was a tendency to neglect it mostly because the models incorporated into the subchannel programs then were unable to display the correct trends. The codes MATTEO /F3/ and apparently, MIXER have lateral vapor drift in their formulations. In MATTEO it is assumed that the turbulent mixing exchange also occurs as a volume-for-volume process but this is not reflected in the code formulation. Besides. MATTEO mixing model is based in adiabatic air-water mixing tests and, for this reason, tends to overestimate the rate of mixing. MIXER is a proprietary code and there is no available documentation concerning its physical models.

Unfortunately the recent trends in subchannel code development have been only in improving the solution technique. It is certainly important to account for more realistic boundary conditions that those incurred by the use of the marching-type technique. This allows a larger class of problems to be solved. However, the reliability of the results for bulk quality conditions is in question because important physical phenomena are being neglected.

1.5 Basic Assumptions

The following assumptions form the basis of the derivation of the conservation equations used in program CANAL:

(a) Thermodynamic equilibrium is assumed in the bulk boiling region.
(b) Vapor is assumed to be always saturated.
(c) Fluid physical properties (except densities) are evaluated at a single reference pressure.
(d) The fluid conditions within a given subchannel vary only

in the dominant axial flow direction.

(e) No transverse pressure gradient exits at any axial elevation in the bundle.

(f) The net mass flow circulations along closed paths around the individual fuel pins are zero.

(g) Liquid and Vapor flow at different speeds.

(h) The transverse transport of mass between neighboring subchannels by turbulent mixing occurs on a volume-for-volume basis.

Assumptions (a) and (b) are reasonable for BWR steady-state conditions and operational transients since superheating of the vapor phase is not anticipated.

Assumption (c) is appropriate BWR applications, where the inlet subcooling is low.

Assumption (d) implies that the variations of the axial components of the flow quantities in the axial direction is much larger than the variation in the transverse direction in analogy with the boundary layer approximation.

Assumption (e) eliminates the transverse momentum equation. This essentially means that all subchannels in the bundle depict the same pressure at a given axial level. This seems to be a reasonable approximation for BWR-type fuel rod bundles Because the bundles are encapsuled and the rod-to-rod spacing is large the pressure gradient across the bundle is expected to be negligible. However, it may be questionable to use this assumption when blockages appear and/or in the presence of strong power tilts across the bundle.

Assumption (f) is necessary to make the momentum equation well-posed. It guards against the possibility of unlimited circuit flow that can occur if the fluid can find a closed path in the transverse direction (see further discussion in

Section 2.7).

Assumption (h) implies that there is a net mass transfer between adjacent subchannels due to two-phase turbulent mixing. This has been experimentally observed by Gonzalez-Santalo /G4/.

Table 1.1 - Models for Two-Phase Flow and Heat Transfer

Model	Homogeneous Equilibrium	Drift Flux	Two-Fluid
Conservation Equations	Mixture Continuity Mixture Momentum Mixture Energy	Mixture Continuity Vapor Continuity Mixture Momentum Mixture Energy	Vapor Continuity Liquid Continuity Vapor Momentum Liquid Momentum Vapor Energy Liquid Energy
Imposed Restrictions	$v_\ell = v_v = v_{CM}$ $h_\ell = h_v = h_{sat}$	$v_v - v_{CM} = (\ )$ $h_v = h_{sat}$	None
Interfacial Interaction Terms	None	Mass	Mass Momentum Energy
Core and Subchannel Codes	COBRA-IIIC THINC-II TORC COBRA-IV THINC-IV	MATTEO	SCORE TRAC THERMIT
Loop Codes	RELAP RETRAN FLASH	THOR	

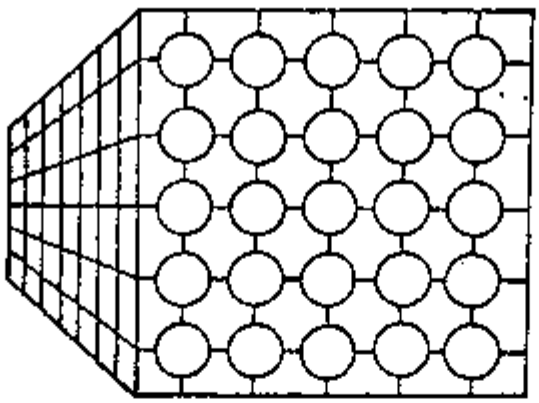

Fig. 1.1 - Coolant-centered Scheme of Defining Subchannels.

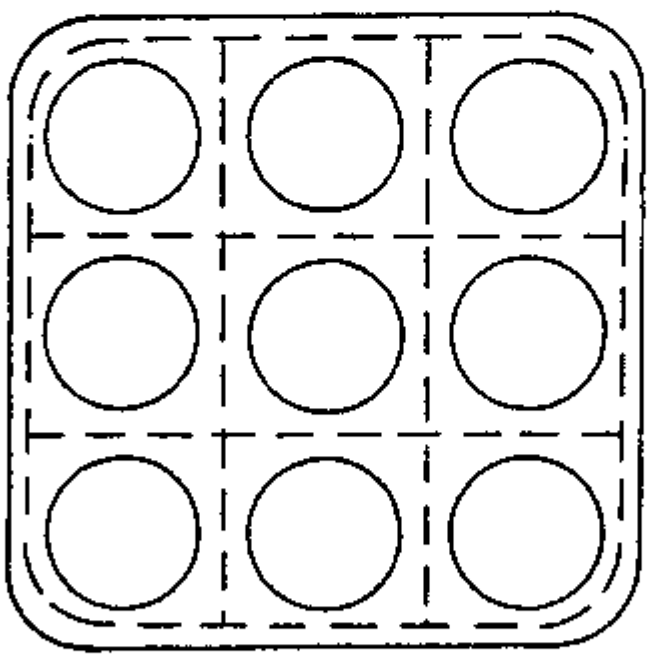

Fig. 1.2 - Rod-centered Scheme.

CHAPTER 2 - MODELS AND METHOD OF SOLUTION

2.1 Conservation Equations

The formulation of the governing equations for the problem under consideration will be based on the drift-flux approach developed by Zuber and co-workers/Z1,Z2,I1/. To accomplish this the six conservation equations of the two-fluid model will be reduced to a set of four conservation equations by eliminating one energy and one momentum equation. As a result of this process two constitutive equations must be provided to account for the relative velocity and difference in energies between the two-phases.

The following equations constitute one accepted set of the six basic conservation equations of the two-phase two-fluid model.

Conservation of Vapor Mass

$$\frac{\partial}{\partial t}(\alpha\rho_v) + \nabla.(\alpha\rho_v\vec{v}_v) = \Gamma_v \qquad (2.1)$$

Conservation of Liquid Mass

$$\frac{\partial}{\partial t}\left[(1-\alpha)\rho_\ell\right] + \nabla.\left[(1-\alpha)\rho_\ell\vec{v}_\ell\right] = -\Gamma_v \qquad (2.2)$$

Conservation of Vapor Momentum

$$\frac{\partial}{\partial t}(\alpha\rho_v\vec{v}_v) + \nabla.(\alpha\rho_v\vec{v}_v\vec{v}_v) = -\alpha\nabla P - \vec{F}_{wv} - \vec{F}_I - \alpha\rho_v\vec{g} \qquad (2.3)$$

Conservation of Liquid Momentum

$$\frac{\partial}{\partial t}\left[(1-\alpha)\rho_\ell \vec{v}_\ell\right] + \nabla\cdot\left[(1-\alpha)\rho_\ell \vec{v}_\ell \vec{v}_\ell\right]$$

$$= -(1-\alpha)\nabla P - \vec{F}_{w\ell} + \vec{F}_I - (1-\alpha)\rho_\ell \vec{g} \qquad (2.4)$$

Conservation of Vapor Energy

$$\frac{\partial}{\partial t}(\alpha\rho_v h_v) + \nabla\cdot\left[\alpha\rho_v h_v \vec{v}_v\right] = -\alpha\frac{DP}{Dt} - P\frac{\partial\alpha}{\partial t} + Q_{wv} + Q_I \qquad (2.5)$$

Conservation of Liquid Energy

$$\frac{\partial}{\partial t}\left[(1-\alpha)\rho_\ell h_\ell\right] + \nabla\cdot\left[(1-\alpha)\rho_\ell h_\ell \vec{v}_\ell\right]$$

$$= -(1-\alpha)\frac{DP}{Dt} + P\frac{\partial(1-\alpha)}{\partial t} + Q_{w\ell} - Q_I \qquad (2.6)$$

It is basically the same set of equations as presented in THERMIT/R1/ except for the energy equations which are here written in terms of enthalpies instead of internal energies.

The first and second terms on the LHS of each equation account for the storage rate and convection of mass, momentum or energy, respectively. The first term on the RHS of the momentum equations represents pressure forces acting to accelerate the fluid. On the RHS of the energy equations the first term represents work done on the fluid due to compressibility effects and the second term work done on one phase by expansion of the other phase. Γ_v, $\vec{F}_I$ and Q_I are rates of exchange of mass, momentum and energy, respectively, at the interface between the two phases. $\vec{F}_w$ and Q_w account for exchanges of momentum and energy between the two phases

and the wall. The last term on the right of the momentum equation represents gravity forces acting on the fluid.

The problem will be formulated in terms of the velocity of the center-of-volume, $\vec{j}$, and the drift velocities of vapor and liquid relative to $\vec{j}$. The reason for this choice is that it leads to simplifications in the algorithm used to solve the finite difference equations which result from the field equations.

The velocity of the center of volume is defined by

$$\vec{j} \equiv \vec{j}_v + \vec{j}_\ell \tag{2.7}$$

where,

$\vec{j}_v = \alpha\vec{v}_v$ is the vapor volumetric flux or superficial velocity of the vapor;

$\vec{j}_\ell = (1-\alpha)\vec{v}_\ell$ is the liquid volumetric flux or superficial velocity of the liquid.

In what follows the conservation equations will be formulated in terms of superficial velocities.

Consider the control volume shown in Figure 2.1. The conservation equations of the two-fluid model will now be averaged over the subchannel cross sectional area A_i. By doing this, information regarding changes of flow quantities in the horizontal plane is lost. Therefore, it should be noticed that considerable errors are introduced if gross variations are present inside the control volume.

2.1.1 Derivation of the Equation for Conservation of Vapor Mass

Equation (2.1) is rewritten here in terms of the superficial velocities,

$$\frac{\partial}{\partial t}(\alpha\rho_v) + \nabla.(\rho_v \vec{j}_v) = \Gamma_v \qquad (2.8)$$

Equation (2.8) is then integrated over the subchannel cross-sectional area, A_i

$$\int_{A_i} \frac{\partial}{\partial t}(\alpha\rho_v)dA + \int_{A_i} \nabla.(\rho_v \vec{j}_v)dA = \int_{A_i} \Gamma_v dA \qquad (2.9)$$

Using the area averaging notation introduced by Zuber, i.e.,

$$\langle\phi\rangle(z,t) = \frac{1}{A_i}\int_{A_i} \phi(x,y,z,t)dA \qquad (2.10)$$

and applying the Gauss theorem to the convective term on the left, equation (2.9) becomes

$$\frac{\partial}{\partial t}(\langle\alpha\rho_v\rangle)_i + \frac{\partial}{\partial z}(\langle\rho_v j_{vz}\rangle)_i = \langle\Gamma_v\rangle_i - \frac{1}{A_i}\sum_{k}^{N_i} W_{vik} \qquad (2.11)$$

where j_{vz} is the component of $\vec{j}_v$ in the axial direction and

$$W_{vik} = \int_{S_{ik}} \rho_v \vec{j}_v.\hat{n}_k dS \qquad (2.12)$$

$\hat{n}_k$ is a unit vector normal to the interface between adjacent subchannels i and k (see Figure 2.1). S_{ik} is a horizontal segment on that interface and it is equal to the distance between the two adjacent rods. dS is an element of length on S_{ik}. In order to interpret W_{vik} consider (x_I, y_I, z_I) as being a point on the interface between i and k. The quantity

$$\rho_v(x_I,Y_I,z_I)\vec{j}_v(x_I,y_I,z_I).\hat{n}_k dSdz$$

represents the mass flow rate of vapor from subchannel i to subchannel k at (x_I,y_I,z_I). Therefore, at a given axial plane

W_{vik} is the value of the vapor mass flow rate from subchannel i to subchannel k per unit of axial length. The summation in (2.11) is to be carried over the number of interfaces, N_i, that subchannel i shares with its neighbors.

2.1.2 Derivation of the Equation for Conservation of Liquid Mass

Starting from equation (2.2) the procedure used to derive equation (2.11) can be applied again to arrive at the following equation

$$\frac{\partial}{\partial t}\left[<(1-\alpha)\rho_\ell>\right]_i + \frac{\partial}{\partial z}(<\rho_\ell j_{\ell z}>)_i = -<\Gamma_v>_i - \frac{1}{A_i}\sum_k^{N_i} W_{\ell ik} \qquad (2.13)$$

where, similarly,

$$W_{\ell ik} = \int_{S_{ik}} \rho_\ell \vec{j}_\ell \cdot \hat{n}_k dS \qquad (2.14)$$

is the total liquid flow rate from subchannel i to subchannel k per unit of axial length. Note that the equation of continuity for the mixture vapor-liquid can be obtained by simply adding equations (2.11) and (2.13).

2.1.3 Derivation of the Equation for Conservation of Mixture Momentum in the Axial Direction

In terms of the superficial velocities the equation conservation of vapor momentum is given by

$$\frac{\partial}{\partial t}(\rho_v \vec{j}_v) + \nabla\cdot\left(\rho_v \frac{\vec{j}_v \vec{j}_v}{\alpha}\right) = -\alpha\nabla P - \vec{F}_{wv} - \vec{F}_I - \alpha\rho_v \vec{g} \qquad (2.15)$$

Integrating equation (2.15) over the subchannel cross-sectional area A_i and applying the Gauss theorem to the convective term it becomes

$$\frac{\partial}{\partial t}\left[\langle \rho_v \vec{j}_v \rangle\right]_i + \frac{\partial}{\partial z}\left[\frac{\langle \rho_v j_{vz} \vec{j}_v \rangle}{\alpha}\right]_i$$

$$= -\langle \alpha \nabla P \rangle_i - \langle \vec{F}_{wv} \rangle_i - \langle \vec{F}_x \rangle - \langle \alpha \rho_v \rangle_i \vec{g} - \frac{1}{A_i} \sum_k^{N_i} \vec{M}_{vik} S_{ik} \qquad (2.16)$$

where,

$$\vec{M}_{vik} = \frac{1}{S_{ik}} \int_{S_{ik}} \rho_v (\vec{j}_v \cdot \hat{n}_k) \frac{\vec{j}_v}{\alpha} \, dS \qquad (2.17)$$

is the segment-averaged momentum flux from subchannel i to subchannel k through the interface A_{ik}.

All the terms of equation (2.16) are now projected along the axial direction to yield the conservation of axial momentum for the vapor phase,

$$\frac{\partial}{\partial t}\left[\langle \rho_v j_{vz} \rangle\right]_i + \frac{\partial}{\partial z}\left[\langle \rho_v \frac{j_{vz}^2}{\alpha} \rangle\right]_i$$

$$= -\langle \rho \frac{\partial P}{\partial z} \rangle_i - \langle F_{wvz} \rangle_i - \langle F_{Iz} \rangle_i - \langle \alpha \rho_v \rangle_i g_z - \frac{1}{A_i} \sum_k^{N_i} \dot{M}_{vikz} S_{ik} \qquad (2.18)$$

where,

$$\dot{M}_{vikz} = \frac{1}{S_{ik}} \int_{S_{ik}} \rho_v (\vec{j}_v \cdot \hat{n}_k) \frac{j_{vz}}{\alpha} \, dS \qquad (2.19)$$

Similarly, the equation of conservation of axial momentum can be obtained for the liquid phase

$$\frac{\partial}{\partial t}\left[\langle\rho_\ell j_{\ell z}\rangle\right]_i + \frac{\partial}{\partial z}\left[\frac{\langle\rho_\ell j_{\ell z}^2\rangle}{(1-\alpha)}\right]_i = -\langle(1-\alpha)\frac{\partial P}{\partial z}\rangle_i - \langle F_{w\ell z}\rangle_i$$

$$+ \langle F_{Iz}\rangle_i - \langle(1-\alpha)\rho_\ell\rangle_i g_z - \frac{1}{A_i}\sum_k^{N_i} \dot{M}_{\ell ikz} S_{ik} \qquad (2.20)$$

with

$$\dot{M}_{\ell ikz} = \frac{1}{S_{ik}} \int_{S_{ik}} \rho_\ell (\vec{j}_\ell \cdot \hat{n}_k) \frac{j_{\ell z}}{(1-\alpha)}\, dS \qquad (2.21)$$

Equation (2.18) and (2.20) are added to yield the conservation of axial momentum equation for the mixture vapor-liquid,

$$\frac{\partial}{\partial t}\left[\langle\rho_v j_{vz}\rangle+\langle\rho_\ell j_{\ell z}\rangle\right]_i + \frac{\partial}{\partial z}\left[\langle\frac{\rho_v j_{vz}^2}{\alpha}\rangle+\langle\frac{\rho_\ell j_{\ell z}^2}{(1-\alpha)}\rangle\right]_i$$

$$= -\langle\frac{\partial P}{\partial z}\rangle_i - \langle F_{wvz}+F_{w\ell z}\rangle_i - \left[\langle\rho_v\alpha\rangle+\langle\rho_\ell(1-\alpha)\rangle\right]_i g_z$$

$$-\frac{1}{A_i}\sum_k^{N_i}\left[\dot{M}_{vikz}+\dot{M}_{\ell ikz}\right] S_{ik} \qquad (2.22)$$

where the assumption of equal pressures in both phases, i.e., $P_v=P_\ell=P$, has been used. The difference between the pressures of the two phases may be important in severe transients and propagation of disturbances. However, for the problem under consideration it has negligible effects.

2.1.4 Derivation of the Equation for Conservation of Mixture Energy

The conservation of vapor energy equation (2.5), in terms

of the superficial velocities is given by

$$\frac{\partial}{\partial t}(\alpha\rho_v h_v) + \nabla.(\rho_v \vec{j}_v h_v) = -\alpha\frac{DP}{DT} - P\frac{\partial\alpha}{\partial t} + Q_{wv} + Q_I \qquad (2.23)$$

Integrating (2.23) over the subchannel cross sectional area, A_i, and applying the Gauss theorem results

$$\frac{\partial}{\partial t}\left[<\alpha\rho_v h_v>\right]_i + \frac{\partial}{\partial z}\left[<\rho_v j_v h_v>\right]_i = -<\alpha\frac{DP}{Dt}>_i - P<\frac{\partial\alpha}{\partial t}>_i$$

$$+ <Q_{wv}>_i + <Q_I>_i - \frac{1}{A_i}\sum_k^{N_i} \dot{E}_{vik} S_{ik} \qquad (2.24)$$

where,

$$\dot{E}_{vik} = \frac{1}{S_{ik}}\int_{S_{ik}} \rho_v \vec{j}_v.\hat{n}_k h_v dS \qquad (2.25)$$

is the segment-averaged flux of energy transported by the vapor from subchannel i to subchannel k. Starting from equation (2.6) and employing the same procedure the area-averaged equation for conservation of liquid energy is obtained,

$$\frac{\partial}{\partial t}\left[<(1-\alpha)\rho_\ell h_\ell>\right]_i + \frac{\partial}{\partial z}\left[<\rho_\ell j_\ell h_\ell>\right]_i$$

$$= <(1-\alpha)\frac{DP}{Dt}>_i + <P\frac{\partial\alpha}{\partial t}>_i + <Q_{w\ell}>_i - <Q_I>_i - \frac{1}{A_i}\sum_k^{N_i} \dot{E}_{\ell ik} S_{ik} \qquad (2.26)$$

where,

$$\dot{E}_{\ell ik} = \frac{1}{S_{ik}}\int_{S_{ik}} \rho_\ell \vec{j}_\ell.\hat{n}_k h_\ell dS \qquad (2.27)$$

is the segment-averaged flux of energy transported by the liquid from subchannel i to subchannel k. The work done in the fluid due to compressibility effects is neglected for the problem at hand since severe transients are not considered. Adding equations (2.24) and (2.26) results

$$\frac{\partial}{\partial t}\left[<\alpha\rho_v h_v+(1-\alpha)\rho_\ell h_\ell>\right]_i + \frac{\partial}{\partial z}\left[<\rho_v j_v h_v+\rho_\ell j_\ell h_\ell>\right]_i$$

$$= <Q_{wv}+Q_{w\ell}>_i - \frac{1}{A_i}\sum_k^{N_i}(\dot{E}_{vik}+\dot{E}_{\ell ik})S_{ik} \qquad (2.28)$$

which is the conservation of energy equation for the mixture vapor-liquid.

Equations (2.11), (2.13), (2.22) and (2.28) constitute a set of four field equations containing seventeen unknowns:

$$\rho_v, \rho_\ell, \alpha, j_{vz}, j_{\ell z}, P, h_\ell, h_v, \Gamma_v, (F_{wv}+F_{w\ell}), (Q_{wv}+Q_{w\ell}),$$

$$W_{vik}, W_{\ell ik}, \dot{M}_{vik}, \dot{M}_{\ell ik}, \dot{E}_{vik}, \dot{E}_{\ell ik}$$

The last six unknowns reflect the transport of flow quantities across the interface of adjacent subchannels. As will be shown later F_{wv} and $F_{w\ell}$ are modeled as a single quantity, $(F_{wv}+F_{w\ell})$ and, likewise, Q_{wv} and $Q_{w\ell}$ $(Q_{wv}+Q_{w\ell})$. The remaining thirteen equations needed to make the system determined will be the subject of the next two sections.

2.2 Constitutive Equations

In this context constitutive equations mean the additional relations needed for closure of the system of conservation equations.

2.2.1 Thermal Constraint

Thermal constraints are imposed by assumptions (a) and (b) (section 1.5). Two boiling regimes must be considered: subcooled boiling and bulk boiling. For subcooled boiling conditions the vapor is saturated,

$$h_v = h_g \tag{2.29}$$

For bulk boiling conditions both phases are assumed saturated. Therefore, equation (2.29) still holds and, additionally,

$$h_\ell = h_f \tag{2.30}$$

2.2.2 Drift Velocity Correlation

As was mentioned in Section 2.1 one constitutive equation must be provided to account for the relative velocity between the two phases. In the drift-flux model this is accomplished by defining the drift velocity of the vapor phase with respect to the center-of-volume velocity of the mixture, j_z,

$$V_{vj} = \frac{j_{vz}}{\alpha} - j_z \tag{2.31}$$

It can be shown /Z2/ that the void fraction, $\langle\alpha\rangle$, will be given by

$$\langle\alpha\rangle = \frac{\langle j_{vz}\rangle}{C_o\langle j_z\rangle + \frac{\langle \alpha V_{vj}\rangle}{\langle\alpha\rangle}} \tag{2.32}$$

where C_o is the distribution parameter defined by

$$C_o = \frac{\frac{1}{A_i}\int_{A_i} \alpha j_z dA}{\left[\frac{1}{A_i}\int_{A_i} j_z dA\right]\left[\frac{1}{A_i}\int_{A_i} \alpha dA\right]} \qquad (2.33)$$

The parameter C_o takes into account the effect of the non-uniform flow and void fraction profiles accross the channel. For further discussion on C_o the reader is referred to the work of Zuber et al./Z1/.

The term

$$\frac{\langle \alpha V_{vj} \rangle}{\langle \alpha \rangle} \equiv \langle\langle V_{vj} \rangle\rangle$$

requires additional information concerning the void fraction profile in the subchannel which, a priori, is not known. $\langle\langle V_{vj} \rangle\rangle$ can be approximated by the local value, V_{vj}, for flows with relatively flat void profiles /I1/ (Appendix D).

2.2.3 Equation of State for the Vapor and Liquid

It is assumed that a relationship can be established giving the liquid density as a function of the pressure and liquid enthalpy,

$$\rho_\ell = \rho_\ell(P, h_\ell) \qquad (2.34)$$

The vapor is assumed to be always saturated. Consequently, the vapor density is a function of the pressure only,

$$\rho_v = \rho_v(P, h_g) = \rho_v(P) \qquad (2.35)$$

2.2.4 Wall Heat Flux

In the energy equation the term $\langle Q_{wv}+Q_{w\ell}\rangle_i$ (power density) denotes mechanisms of exchange of energy between the wall and the two phases. These two terms are lumped into a single one using the heat flux concept. Dissipative effects are neglected. Therefore,

$$\langle Q_{wv} + Q_{w\ell}\rangle_i = \frac{1}{V_i}\sum_{m}^{L_i} q''_{mi}(P_{Hmi}\Delta Z)$$

where q''_{mi} is the heat flux out of rod m which has a part of its perimeter, P_{Hmi}, in common with subchannel i (see Fig.2.1). V_i is an element of volume of subchannel i, $V_i=A_i\Delta Z$. The preceding equation becomes

$$\langle Q_{wv} + Q_{w\ell}\rangle_i = \frac{1}{A_i}\sum_{m}^{L_i} q''_{mi}P_{Hmi} \qquad (2.36)$$

The summation is performed over the total number of rods, L_i, which have a common interface with subchannel i.

For steady-state problems the heat flux is, of course, a known quantity. For transient cases the heat transfer coefficient and hence the heat flux is computed by the Chen's correlation (see Appendix B),

$$q''_{mi} = h_{fc}\left[T_{wmi} - T_{\ell i}\right] + h_{nb}\left[T_{wmi}-T_s\right] \qquad (2.37)$$

The liquid temperature $T_{\ell i}$ is related to the liquid enthalpy by $C_{pl}(T_s-T_{\ell i}) = h_s-h_{\ell i}$. T_{wmi} is evaluated by employing a convenient fuel pin heat conduction model (see Section 2.8). For bulk boiling conditions $T_{\ell i}=T_s$ and the heat flux is given by

$$q''_{mi} = (h_{fc}+h_{nb})\left[T_{wmi}-T_s\right] \qquad (2.38)$$

2.2.5 Wall Friction

In the conservation of axial momentum equation (2.22) the term $\langle F_{wvz}+F_{w\ell z}\rangle_i$ represents a force per unit volume acting on the fluid due to friction against the wall. This term is modeled by the standard scheme of considering a wall shear stress, τ_w, acting on the mixture vapor-liquid,

$$\langle F_{wvz} + F_{w\ell z}\rangle_i = \frac{1}{V_i}\tau_w(P_{Fi}\Delta Z) = \frac{1}{A_i}\tau_w P_{Fi} \qquad (2.39)$$

The wall shear stress is expressed in terms of a friction factor f_{tp},

$$\tau_w = f_{tp}\frac{G_i^2}{2\rho_\ell} \qquad (2.40)$$

where

$$G_i = \langle\rho_v j_v\rangle_i + \langle\rho_\ell j_\ell\rangle_i \quad , \qquad (2.41)$$

That is, the classical approach of assuming the flow to be all liquid with f_{tp} correction for two-phase effects. The two-phase flow friction factor, f_{tp}, is the product of a single-phase friction factor coefficient, f_{sp}, and a two-phase multiplier, $\phi^2_{\ell o}$,

$$f_{tp} = f_{sp}\phi^2_{\ell o} \qquad (2.42)$$

For rod bundles Marinelli and Pastori /M1/ recommend a Blasius type correlation for f_{sp},

$$f_{sp} = a\ Re^{-b} \qquad (2.43)$$

Constants a and b depend on several geometrical quantities such as the P/D ratio the gap spacing between subchannels and the roughness of the fuel rod surface. In case of smooth bundles Marinelli and Pastori recommend a=0.32 and b=0.25. The most popular correlations for $\phi^2_{\ell o}$ are those of Martinelli-Nelson /M2/ and Thom /T1/. However, both do not include mass velocity effects and tend to overestimate the pressure drop

considerably for high mass velocities /M1/. Baroczy /B2/ attempted to correct for the effect of mass velocities by producing graphical correlations for $\phi^2_{\ell o}$. His curves, however, show a complex pattern hard to fit with analytical expressions. Jones /J1/ developed simple curve fittings for the Martinelli-Nelson correlation including mass velocity effects. Jones correlation which is adopted here is

$$\phi^2_{\ell o} = \mathcal{F}(G,P)\left\{1.2\left[\left(\frac{\rho_f}{\rho_g}\right) - 1.\right]x^{.824} + 1.\right\} \qquad (2.44)$$

where

$$\mathcal{F}(G,P) = 1.43 + \left(\frac{G}{G_o} - 1.\right)(.07 - 7.35\times10^{-8}P) \qquad \text{if } G<G_o$$

$$= 1.43 + \left(\frac{G_o}{G} - 1.\right)(.17 - 6\times10^{-8}P) \qquad \text{if } G\geq G_o \qquad (2.45)$$

with G_o=950 Kg/m^{2}sec.

2.2.6 Evaluation of the Vapor Source Term

In equation (2.11) Γ_v represents the rate at which mass is being exchanged between the two phases, i. e., Γ_v is the mass of vapor being produced per unit of volume per unit of time. The vapor source term will naturally depend on the boiling regime. Only subcooled boiling and bulk boiling conditions are considered.

Subcooled Flow Boiling Region

Fig.2.2 shows schematically a typical void fraction profile in a heated tube. It can be seen that the subcooled regime can be divided into two distinct regions. Region I is often called the highly subcooled boiling region or region of wall voidage, meaning that the boiling process starts but the bubbles adhere to the wall. Downstream the bubbles grow in size under the competing effects of bubble coalescence

and condensation until a point is reached where the bubbles detach from the wall and are ejected into the subcooled flowing liquid. The point of the first bubble detachment marks the start of Region II called low subcooled region or region of detached voidage. Appreciable voids can occur in Region II. For practical purposes the voids in Region I can be neglected.

To compute the vapor source term $\langle \Gamma_v \rangle_i$ the energy equation (2.28) is arbitrarily split into two equations: one that governs the enthalpy rise of the liquid and other that evaluates $\langle \Gamma_v \rangle_i$.
Two equalities are assumed:

$$\langle \Gamma_v \rangle_i h_{fg} = \frac{1}{A_i} \sum_{m}^{L_i} (q''_{mi})_{evap} P_{Hmi} - \frac{\partial}{\partial t} \left[\langle \alpha \rho_v h_v \rangle \right]_i \qquad (2.46)$$

(computes the vapor source term), where $(q''_{mi})_{evap}$ is the portion of the heat flux from rod m to subchannel i that goes to vapor formation, and

$$\frac{\partial}{\partial t} \left[\langle (1-\alpha) \rho_\ell h_\ell \rangle \right]_i + \frac{\partial}{\partial z} \left[\langle \rho_v j_v h_v + \rho_\ell h_\ell j_\ell \rangle \right]_i$$

$$= \frac{1}{A_i} \sum_{m}^{L_i} \left[q''_{mi} - (q''_{mi})_{evap} \right] P_{Hmi} - \sum_{k}^{N_i} (\dot{E}_{vik} + \dot{E}_{\ell ik}) \frac{S_{ik}}{A_i} \qquad (2.47)$$

(computes the liquid enthalpy rise). The problem here is how to determine $(q''_{mi})_{evap}$.

Bowring /B8/ suggests that in the low subcooling region the heat flux at the wall surface can be split into three components:

$$q'' = q''_{sp} + q''_{a} + q''_{evap} \tag{2.48}$$

where the subscripts m and i were dropped to simplify the notation. Here q''_{sp} is the component associated with single-phase convection to the liquid and q''_{a} is due to bubble agitation. The second and third terms on the right of equation (2.47) are usually grouped into a single one, q''_{b}, defined as the fraction of the heat flux associated with the boiling process. i.e.,

$$q''_{b} = q''_{a} + q''_{evap} \tag{2.49}$$

The single phase convection component, q''_{sp}, is assumed to depend linearly on the liquid enthalpy /L4/,

$$\begin{aligned} q''_{sp} &= q''\left(\frac{h_f - h_\ell}{h_f - h_{\ell d}}\right) && \text{if} \quad h_{\ell d} \leq h_\ell < h_f \\ &= 0. && \text{if} \quad h_\ell > h_f \end{aligned} \tag{2.50}$$

Therefore,

$$\begin{aligned} q_b &= 0. && \text{if} \quad h_\ell < h_{\ell d} \\ &= q'' - q''_{sp} && \text{if} \quad h_\ell \geq h_{\ell d} \end{aligned} \tag{2.51}$$

where $h_{\ell d}$ is liquid enthalpy at which the bubbles start to detach from the wall. Among the several bubble detachment criteria available in the literature the most accurate have been found to be those of Levy /L7/ and Saha /S1/. The latter is adopted here because of its computational simplicity. It is as follows:

$$\left[h_f-(h_\ell)_d\right] = 0.0022\,\frac{q''D_h C_{p\ell}}{k_\ell} \quad \text{if} \quad Pe < 70000$$

$$= 154.\,\frac{q''}{G} \quad \text{if} \quad Pe \geq 70000 \qquad (2.52)$$

Saha showed empirically that for low mass flow rates (Peclet number < 70000) the point of bubble detachment is determined by local thermal conditions whereas at high mass flow rates (Pe>70000) it depends upon local hydrodynamic conditions

Finally, a relationship between q''_{evap} and q''_b is needed in order to find q''_{evap}. Bowring defines the parameter ϵ as the ratio

$$\epsilon = \frac{q_a}{q''_{evap}} = \frac{\rho_f}{\rho_g}\left(\frac{C_{pf}}{h_{fg}}\right)\tau \qquad (2.53)$$

where τ is and effective temperature rise of the liquid that is replaced by the bubble. Assuming $\tau = T_f - T_\ell$ /R4/ results for ϵ

$$\epsilon = \frac{\rho_f}{\rho_g}\,\frac{h_f-h_\ell}{h_{fg}} \qquad (2.54)$$

The expression for q''_{evap} is then

$$q''_{evap} = \frac{q''_b}{1+\epsilon} \qquad (2.55)$$

Bulk Boiling Region

As contrasted to the subcooled region here the consevation of energy equation is redundant since, by assumption (a) in Section 1.5, the liquid is saturated in the bulk boiling regime. Thus $h_\ell = h_f$ and the energy equation (2.28) becomes

$$h_g\left[\frac{\partial}{\partial t}\langle\alpha\rho_v\rangle+\frac{\partial}{\partial z}\langle\rho_v j_v\rangle\right]_i + h_f\left[\frac{\partial}{\partial t}\langle(1-\alpha)\rho_\ell\rangle+\frac{\partial}{\partial z}\langle\rho_\ell j_\ell\rangle\right]_i \qquad (2.56)$$

$$+\left[\langle\alpha\rho_v\rangle\frac{\partial h_g}{\partial t}+\langle(1-\alpha)\rho_\ell\rangle\frac{\partial h_f}{\partial t}\right]_i = \frac{1}{A_i}\sum_m^{L_i} q''_{mi}P_{Hmi} - \sum_k^{N_i}(\dot{E}_{vik}+\dot{E}_{\ell ik})\frac{1}{A_i}S_{ik}$$

The first two terms on the left of equation (2.56) can be expressed in another form by using the continuity equations for the vapor and liquid phases. The following equation results

$$h_g\left[\langle\Gamma_v\rangle_i-\frac{1}{A_i}\sum_k^{N_i} W_{vik}\right] + h_f\left[-\langle\Gamma_v\rangle_i-\frac{1}{A_i}\sum_k^{N_i} W_{\ell ik}\right] \qquad (2.57)$$

$$+\left[\langle\alpha\rho_v\rangle\frac{\partial h_g}{\partial t}+\langle(1-\alpha)\rho_\ell\rangle\frac{\partial h_f}{\partial t}\right] = \frac{1}{A_i}\sum_m^{L_i} q''_{mi}P_{Hmi} - \frac{1}{A_i}\sum_m^{N_i}(\dot{E}_{vik}+\dot{E}_{\ell ik})$$

By rearranging equation (2.57) an expression is found for the vapor source,

$$\langle\Gamma_{vi}\rangle = \frac{1}{h_{fg}}\left\{\frac{1}{A_i}\sum_m^{L_i} q''_{mi}P_{Hm} - \frac{1}{A_i}\sum_k^{N_i}(\dot{E}_{vik}+\dot{E}_{\ell ik})S_{ik} + \frac{h_g}{A_i}\sum_k^{N_i} W_{vik}\right.$$

$$\left. + \frac{h_f}{A_i}\sum_k^{N_i} W_{\ell ik} - \left[\langle\alpha\rho_v\rangle\frac{\partial h_g}{\partial t} + \langle(1-\alpha)\rho_\ell\rangle\frac{\partial h_\ell}{\partial t}\right]_i\right\} \qquad (2.58)$$

2.3 Exchange of Mass, Momentum and Energy between Adjacent Subchannels

2.3.1 Exchange of Mass

2.3.1.1 General Approach

In Section 2.3 the net vapor and liquid mass flow rates from subchannel i to subchannel k per unit of axial length were defined by equations (2.12) and (2.14) as follows

$$W_{vik} = \int_{S_{ik}} \rho_v \vec{j}_v . \hat{n}_k dS \tag{2.12}$$

and

$$W_{\ell ik} = \int_{S_{ik}} \rho_\ell \vec{j}_\ell . \hat{n}_k dS \tag{2.14}$$

The sum of these two terms represent the total net mass flow rate from subchannel i to subchannel k per unit of axial length,

$$W_{ik} = W_{vik} + W_{\ell ik} \tag{2.59}$$

The total mass flow rate leaving subchannel i is defined by

$$W_i = \sum_{k}^{N_i} W_{ik} \tag{2.60}$$

It should be recalled that the exchange of mass between subchannels is assumed to occur in the absence of transverse pressure gradients. It is always possible to determine W_i and W_{ik} such that the pressure drop is the same for all subchannels. However, there is an infinite number of combi-

nations of W_{vik} and $W_{\ell ik}$ which will produce equal pressure drop in all subchannels because the pressure drop depends not only on the mass flow rate but also on the flowing quality and physical properties of the liquid and the vapor. In this section a method based on experimental evidence is presented to uniquely determine W_{vik} and $W_{\ell ik}$.

Both W_{vik} and $W_{\ell ik}$ are split into a turbulent mixing component and a diversion flow component,

$$W_{vik} = (W_{vik})_{mix} + (W_{vik})_{div} \tag{2.61}$$

and

$$W_{\ell ik} = (W_{\ell ik})_{mix} + (W_{\ell ik})_{div} \tag{2.62}$$

Therefore, there are four unknowns to be determined: $(W_{vik})_{mix}$, $(W_{vik})_{div}$, $(W_{\ell ik})_{mix}$ and $(W_{\ell ik})_{div}$.

Evaluation of $(W_{vik})_{mix}$

Assumptions (b) and (e) in Section 1.5 imply that at a given axial level the vapor density is constant over the subchannel cross section, $\rho_v(x,y,z)=\rho_g(z)$. Therefore, equation (2.12) becomes

$$W_{vik} = \rho_g \int_{S_{ik}} \vec{j}_v \cdot \hat{n}_k dS \tag{2.63}$$

and the turbulent mixing component of W_{vik} can be approximated by

$$(W_{vik})_{mix} = \rho_g \int_{S_{ik}} (\vec{j} \cdot \hat{n}_k)_{mix} dS = \rho_g \tilde{u}_{ik} (\alpha_i - \alpha_k) S_{ik} \tag{2.64}$$

where $\tilde{u}_{ik}$ is the turbulent component of the vapor velocity in the transverse direction. This quantity is evaluated using the model described in Section 2.3.1.2. Equation (2.64) implies that the vapor exchange between neighboring subchannels is zero when $\alpha_i=\alpha_k$. However, in adiabatic and diabatic tests with two-phase mixtures it has been observed that the void fraction distribution at the exit of the channel is not uniform /S2,L2,B1,Y1,H2/. These experiments indicate that the vapor is preferentially transported into regions where the velocities are higher. This tendency seems stronger when the vapor is the dispersed phase. As proposed by Gonzalez-Santalo /G4/ this phenomenon can be modeled by using the concept of fully developed void fraction distribution. This is the condition for which the mixing flow between adjacent subchannels is zero. In this approach equation (2.64) is altered to become

$$(W_{vik})_{mix} = \rho_g \tilde{u}_{ik}\left[(\alpha_i-\alpha_k) - (\alpha_i-\alpha_k)_{FD}\right]S_{ik} \qquad (2.65)$$

where $(\alpha_i-\alpha_k)_{FD}$ is the void fraction difference between subchannels i and k corresponding to the fully developed condition.

Based on the experimental evidence mentioned above the following expression is assumed for the fully-developed void fraction distribution,

$$(\alpha_i-\alpha_k)_{FD} = K_a\frac{(G_i-G_k)_{FD}}{G_{av}} \qquad (2.66)$$

where $G_{av}=(G_i+G_k)/2$ and $(G_i-G_k)_{FD}$ denotes the fully-developed mass velocity distribution between subchannels i and k. K_a is an empirical constant of proportionality. Equation (2.66) simply expresses the observed fact that the vapor tends to

move to regions of higher velocities. $(G_i-G_k)_{FD}$ can be assumed, to a first approximation, equal to the existing mass velocity difference, i.e., $(G_i-G_k)_{FD}=(G_i-G_k)$ /L5/.

Evaluation of $(W_{\ell ik})_{mix}$

It should be recalled at this point that the process of exchange of mass by turbulent mixing between subchannels is considered here to occur on a volume-to-volume basis. Therefore, the net liquid flow rate from subchannel i to subchannel k due to turbulent mixing must satisfy the equation

$$\frac{(W_{\ell ik})_{mix}}{\bar{\rho}_\ell} = - \frac{(W_{vik})_{mix}}{\rho_g}$$

or

$$(W_{\ell ik})_{mix} = - \frac{\bar{\rho}_\ell}{\rho_g}(W_{vik})_{mix} \qquad (2.67)$$

where $\bar{\rho}_\ell$ is the liquid density at the interface approximated by

$$\bar{\rho}_\ell = 0.5(\rho_{\ell i} + \rho_{\ell k}) \qquad (2.68)$$

Evaluation of $(W_{vik})_{div}$ and $(W_{\ell ik})_{div}$

The total net mass flow rate from subchannel i to subchannel k due to diversion crossflow is defined by

$$(W_{ik})_{div} = (W_{vik})_{div} + (W_{\ell ik})_{div}$$

or

$$(W_{ik})_{div} = W_{ik} - (W_{vik})_{mix} - (W_{\ell ik})_{mix} \qquad (2.69)$$

$(W_{vik})_{div}$ is simply the product of the vapor density and the volume of vapor exchanged,

$$(W_{vik})_{div} = \rho_g \alpha_d \left[(W_{ik})_{div} / (\rho_g \alpha_d + \rho_{\ell d}(1-\alpha_d)) \right] \qquad (2.70)$$

where α_d is the void fraction of the donor subchannel. Note that the quantity between brackets is the total (liquid + vapor) volumetric crossflow rate by diversion crossflow per unit of axial length. Finally,

$$(W_{\ell ik})_{div} = (W_{ik})_{div} - (W_{vik})_{div} \qquad (2.71)$$

2.3.1.2 Reduction of the General Approach to Single-Phase and Two-Phase Flow Predictions

Single-Phase

For single-phase situations the preceding formulation reduces to

$$W_{vik} = 0.$$

and

$$W_{\ell ik} = (W_{\ell ik})_{div} = W_{ik}$$

That is, the liquid is exchanged by diversion crossflow only. Thus turbulent mixing affects the momentum and energy exchange but not the mass exchange.

The turbulent transverse velocity $\tilde{u}_{ik}$ is found by using the so called mixing constant β which relates the mixing crossflow rate to the axial flow rate through the expression

$$(\beta_{ik})_{sp} = \frac{(W_{ik})_{mix}}{\bar{G}_{av} S_{ik}} = \frac{\tilde{u}_{ik}}{j_{av}} \qquad (2.72)$$

Where $\bar{G}_{av} = 0.5(G_i + G_k)$ and, likewise, $j_{av} = 0.5(j_i + j_k)$. The basis for the development of this expression is discussed in

reviews by Rogers and Todreas /R2/ and Lahey and Schraub /L1/. The expression for $(\beta_{ik})_{sp}$ is obtained from Rogers and Rosehart correlation /R3/ which was developed based on a number of mixing experiments in simple geometries and rod bundle geometries. It is expressed by

$$(\beta_{ik})_{sp} = \frac{1}{2}\left[1 + \left(\frac{D_{ek}}{D_{ei}}\right)^{1.5}\right] Re^{-0.1}\lambda_{ik} \qquad (2.73)$$

This correlation is recommended for smooth bundles and P/D ratios in the range from 1.08 to 1.4 (for typical BWR fuel rod bundles P/D=1.25). λ_{ik} denotes a dimensionless mixing parameter defined by

$$\lambda_{ik} = K' \frac{D_{FS}}{\Delta y_{ik}} \qquad (2.74)$$

Δy_{ik} is mixing length between subchannels i and k. For rod bundle geometries Rogers and Rosehart found that the normalized distance $\Delta y_{ik}/D_{FS}$ depended only on the ratio (S_{ik}/D_{FS}) with the functional dependence of λ_{ik} expressed by

$$\lambda_{ik} = K\left(\frac{S_{ik}}{D_{FS}}\right)^{r} \qquad (2.75)$$

with K=0.0058 and r=-1.46 obtained by least square curve fits.

Two-Phase

Several experiments /B1,G4,R9/ have indicated that turbulent mixing is enhanced when two phases are present and depends strongly on the flow regime. Fig.2.4 shows the results of experiments by Rowe and Angle /R8/ and illustrates the behavior of a mixing parameter as a function of quality.

Mixing in the bubble and churn-turbulent flow regimes is substantially higher than single-phase mixing. Besides it appears to reach a peak around the slug-annular flow regime transition and then, after the peak, recedes to a value slightly below that of the single-phase mixing. This dependence of turbulent mixing on flow regime will be simulated in a "two-phase mixing multiplier", θ, defined by

$$(\beta_{ik})_{tp} = \theta (\beta_{ik})_{sp} \tag{2.76}$$

Following Beus /B4/ θ will be modeled as linearly dependent on the flow quality until the slug-annular transition where it reaches its peak value, θ_M. Referring to Fig.2.4 θ can be expressed in Region A as

$$\theta = 1 + \frac{\theta_M - 1}{x_M} x \qquad (x<x_M) \tag{2.77}$$

After the peak a hyperbolic curve is constructed such that it passes through the point (x_M, θ_M) and approaches the line $\theta=1$. assymptotically, i.e., it is assumed that the transverse turbulent velocities of single-phase liquid and single-phase vapor are the same. Therefore, in Region B., the expression for θ is

$$\theta = 1.+ (\theta_M-1) \frac{\left(1 - \frac{x_o}{x_M}\right)}{\left(\frac{x}{x_M} - \frac{x_o}{x_M}\right)} \quad , \qquad x \geq x_M \tag{2.78}$$

The ratio $\left(\frac{x_o}{x_M}\right)$ is an empirical coefficient which was found to depend on the Reynolds number /B4/. By least square fitting to the experimental data Beus obtained

$$\left(\frac{x_o}{x_M}\right) = 0.57\ Re^{.0417} \tag{2.79}$$

In order to determine x_M it is necessary to find out under what flow conditions the slug-annular transition occurs. Several flow regime maps are available in the literature /B3, D2,G5/. The slug-annular transition criteria of Wallis /W1/ is probably one of the simplest and falls close to the peak data points. Wallis correlation states that the transition occurs at

$$j_v^* = A_1 + A_2 j_\ell^* \tag{2.80}$$

where A_1=0.4, A_2=0.6. Equation (2.80) can be solved for the flow quality x_M to yield

$$x_M = \frac{\rho_v j_v}{G} = \frac{A_1\sqrt{\rho_\ell g D_e(\rho_\ell-\rho_v)} + A_2 G}{G\left[\sqrt{\rho_\ell/\rho_g} + A_2\right]} \tag{2.81}$$

The peak value θ_M should be a function of the pressure, mass velocity and geometrical configuration but due to lack of experimental evidence it is difficult to establish a functional dependence of θ_M on those variables. In his derivation Beus found that the peak value increases linearly with the mass velocity but this is not supported by the work of Rowe and Angle /R8/ which showed the peak value as a decreasing function of the mass velocity (see Fig 2.3). As a first approximation θ_M is taken here as independent of the mass velocity. This should be satisfactory if the mass velocity does not change substantially across the bundle.

In short $(W_{vik})_{mix}$ is obtained from equation (2.65) where $\tilde{u}_{ik}$ is found from equations (2.72) and (2.76). Then $(W_{\ell ik})_{mix}$ is computed from (2.67) and finally $(W_{vik})_{div}$ and $(W_{\ell ik})_{div}$

from (2.70) and (2.71) respectively.

2.3.2 Exchange of Momentum between Subchannels

The momentum fluxes carried by the vapor from subchannel i to subchannel k as expressed by equations (2.19) and (2.21) are

$$\dot{M}_{vik} = \frac{1}{S_{ik}} \int_{S_{ik}} \rho_v (\vec{j}_v . \hat{n}_k) \frac{j_{vz}}{\alpha} \, dS \tag{2.19}$$

and

$$\dot{M}_{\ell ik} = \frac{1}{S_{ik}} \int_{S_{ik}} \rho_\ell (\vec{j}_\ell . \hat{n}_k) \frac{j_{\ell z}}{(1-\alpha)} \, dS \tag{2.21}$$

respectively. Both $\dot{M}_{vik}$ and $\dot{M}_{\ell ik}$ are split into turbulent mixing and diversion flow components,

$$\dot{M}_{vik} = (\dot{M}_{vik})_{mix} + (\dot{M}_{vik})_{div} \tag{2.82}$$

and

$$\dot{M}_{\ell ik} = (\dot{M}_{\ell ik})_{mix} + (\dot{M}_{\ell ik})_{div} \tag{2.83}$$

Turbulent Mixing Components

The mixing component of $\dot{M}_{vik}$ is given by

$$(\dot{M}_{vik})_{mix} = \frac{1}{S_{ik}} \int_{S_{ik}} \rho_v (\vec{j}_v . \hat{n}_k)_{mix} \frac{j_{vz}}{\alpha} \, dS \tag{2.84}$$

In order to approximate the integral the average values of (j_{vz}/α) in the adjacent subchannels i and k are used since the change of (j_{vz}/α) along S_{ik} is not known. Thus equation

(2.04) becomes

$$(\dot{M}_{vik})_{mix} = \rho_g \tilde{u}_{ik}\left[\alpha_i\left(\frac{j_{vzi}}{\alpha_i}\right) - \alpha_k\left(\frac{j_{vzk}}{\alpha_k}\right)\right]$$

$$= \rho_g \tilde{u}_{ik}(j_{vzi} - j_{vzk}) \qquad (2.85)$$

Similarly for the liquid,

$$(\dot{M}_{\ell ik})_{mix} = \tilde{u}_{ik}(\rho_{\ell i} j_{\ell zi} - \rho_{\ell k} j_{\ell zk}) \qquad (2.86)$$

Now define

$$(\dot{M}_{ik})_{mix} = (\dot{M}_{vik})_{mix} + (\dot{M}_{\ell ik})_{mix} \qquad (2.87)$$

It can be easily verified that

$$(\dot{M}_{ik})_{mix} = \tilde{u}_{ik}(G_i - G_k) \qquad (2.88)$$

Diversion Flow Components

The diversion flow component of $\dot{M}_{vik}$ is given by

$$(\dot{M}_{vik})_{div} = \frac{1}{S_{ik}}\int_{S_{ik}} \rho_v (\vec{j}_v \cdot \hat{n}_k)_{div} \frac{j_{vz}}{\alpha}\, dS \qquad (2.89)$$

and is approximated by using the donor-cell formulation, that is,

$$(\dot{M}_{vik})_{div} = \frac{1}{S_{ik}}(W_{vik})_{div}\left(\frac{j_{vz}}{\alpha}\right)_d \qquad (2.90)$$

where d indicates the donor subchannel. Similarly for the liquid,

$$(\dot{M}_{\ell ik})_{div} = \frac{1}{S_{ik}} (W_{\ell ik})_{div} \left(\frac{j_{\ell z}}{1-\alpha}\right)_d \tag{2.91}$$

2.3.3 Exchange of Energy

The fluxes of energy transported by the vapor and by the liquid from subchannel i to subchannel k as expressed by equations (2.25) and (2.27) are

$$\dot{E}_{vik} = \frac{1}{S_{ik}} \int_{S_{ik}} \rho_v (\vec{j}_v \cdot \hat{n}_k) h_v dS \tag{2.25}$$

and

$$\dot{E}_{\ell ik} = \frac{1}{S_{ik}} \int_{S_{ik}} \rho_\ell (\vec{j}_\ell \cdot \hat{n}_k) h_\ell dS \tag{2.27}$$

respectively. As was done with the momentum fluxes in the preceding section both $\dot{E}_{vik}$ and $\dot{E}_{\ell ik}$ are split into turbulent mixing and diversion flow components,

$$\dot{E}_{vik} = (\dot{E}_{vik})_{mix} + (\dot{E}_{vik})_{div} \tag{2.92}$$

and

$$\dot{E}_{\ell ik} = (\dot{E}_{\ell ik})_{mix} + (\dot{E}_{\ell ik})_{div} \tag{2.93}$$

The components on the right of equations (2.92) and (2.93) are found by the same procedure used to evaluate the components of $\dot{M}_{vik}$ and $\dot{M}_{\ell ik}$ in the preceding section. It results

$$(\dot{E}_{vik})_{mix} = \rho_g \tilde{u}_{ik} h_g (\alpha_i - \alpha_k) \tag{2.94}$$

$$(\dot{E}_{\ell ik})_{mix} = \tilde{u}_{ik}\left[\rho_{\ell i} h_{\ell i}(1-\alpha_i) - \rho_{\ell k} h_{\ell k}(1-\alpha_k)\right] \tag{2.95}$$

$$(\dot{E}_{vik})_{div} = \frac{1}{S_{ik}}(W_{vik})_{div}\, h_g \tag{2.96}$$

$$(\dot{E}_{\ell ik})_{div} = \frac{1}{S_{ik}}(W_{vik})_{div}\, h_{\ell d} \tag{2.97}$$

2.4 Closure

Subcooled Boiling

As stated in Section 2.1.4 seventeen equations are needed for closure of the system. However in the subcooled boiling regime three additional unknowns, q''_{sp}, q''_a and q''_{evap}, were introduced when the heat flux, q'', was split into three components. Therefore, twenty equations are needed to close the system in the subcooled region. They are the following

Field Equations	Constitutive Equations	
2.11	2.29	2.61
2.13	2.31	2.62
2.22	2.34	2.82
2.47	2.35	2.83
	2.36	2.92
	2.39	2.93
	2.46	
	2.48, 2.50, 2.55	heat flux partition

Bulk Boiling

For bulk boiling conditions the energy equation is redundant since the liquid is assumed saturated. Therefore, the number of field equations is reduced by one while the number of constitutive equations increases by one. The seventeen equations are the following

Field Equations	Constitutive Equations	
2.11	2.29	2.58
2.13	2.30	2.61
2.22	2.31	2.62
	2.34	2.82
	2.35	2.83
	2.36	2.92
	2.39	2.93

2.5 Finite Difference Form of the Conservation Equations

To establish the finite difference form of the conservation equations each subchannel is divided along its length so a spatial mesh is obtained in which axial node 1 is at the inlet of the channel and axial node J at the exit. All the variables are defined at the interfaces between the axial nodes as shown in Fig.2.1. The finite difference scheme depends on the method of solution which will be the subject of the next section. In the finite difference equations that follow all unknown variables are written at the new time step to insure implicity. The subscript j refers to the axial node while the superscript - denote the old time step value.

Conservation of Vapor Mass

$$\frac{1}{\Delta t}(\alpha_i\rho_{vi}-\bar{\alpha}_i\bar{\rho}_{vi})_j + \frac{1}{\Delta z}\left[(\rho_{vi}j_{vi})_j-(\rho_{vi}j_{vi})_{j-1}\right]$$

$$= \Gamma_{vi,j} - \frac{1}{A_i}\sum_k^{N_i} W_{vik,j} \tag{2.98}$$

Conservation of Liquid Mass

$$\frac{1}{\Delta t}\left[(1-\alpha_i)\rho_{\ell i}-(1-\bar{\alpha}_i)\bar{\rho}_{\ell i}\right]_j + \frac{1}{\Delta z}\left[(\rho_{\ell i}j_{\ell i})_j-(\rho_{\ell i}j_{\ell i})_{j-1}\right]$$

$$= -\Gamma_{vi,j} - \frac{1}{A_i}\sum_k^{N_i} W_{\ell ik,j} \tag{2.99}$$

Conservation of Axial Momentum for the Mixture

$$\frac{1}{\Delta t}\left[(\rho_{vi}j_{vi}+\rho_{\ell i}j_{\ell i}) - (\bar{\rho}_{vi}\bar{j}_{vi}+\bar{\rho}_{\ell i}\bar{j}_{\ell i})\right]_j$$

$$+ \frac{1}{\Delta z}\left\{\left[\frac{\rho_{vi}(j_{vi})^2}{\alpha_i} + \frac{\rho_{\ell i}(j_{\ell i})^2}{(1-\alpha_i)}\right]_j - \left[\frac{\rho_{vi}(j_{vi})^2}{\alpha_i} + \frac{\rho_{\ell i}(j_{\ell i})^2}{(1-\alpha_i)}\right]_{j-1}\right\}$$

$$= \frac{1}{\Delta z}(P_{j-1}-P_j) - \frac{1}{A_i}(\tau_{wi,j})P_{Fi} - \left[\rho_{vi}\alpha_i+\rho_{\ell i}(1-\alpha_i)\right]_j g_z$$

$$- \frac{1}{A_i}\sum_k^{N_i}\left[\dot{M}_{vik}+\dot{M}_{\ell ik}\right]_j S_{ik} \tag{2.100}$$

Conservation of Energy for the Liquid in the Subcooled Region

$$\frac{1}{\Delta t}\left[(1-\alpha_i)\rho_{\ell i}h_{\ell i} - (1-\alpha_i^-)\rho_{\ell i}^- h_{\ell i}^-\right]_j$$

$$+ \frac{1}{\Delta z}\left[(\rho_{vi}j_{vi}h_g)_j - (\rho_{vi}j_{vi}h_g)_{j-1} + (\rho_{\ell i}j_{\ell i}h_{\ell i})_j - (\rho_{\ell i}j_{\ell i}h_{\ell i})_{j-1}\right]$$

$$= \frac{1}{A_i}\sum_m^{L_i}\left[q''_{mi} - (q''_{mi})_{evap}\right]_j P_{Hmi} - \frac{1}{A_i}\sum_k^{N_i}\left[\dot{E}_{vik} + \dot{E}_{\ell ik}\right]_j S_{ik} \qquad (2.101)$$

2.6 Method of Solution

AS shown in Section 2.6 the difference technique represents a fully implicit differencing of the partial differential equations. One method of solving the set of algebraic finite difference equations is the successive substitution technique. In this method the equations are solved simultaneously at all axial intervals. However, due to the fully implicit differencing, this would imply increased computational costs and add on the code complexity. In order to keep computational costs low a marching technique is employed. Relative to the successive substitution scheme the main disadvantage is that marching methods are based on the premise that the flow is always from the inlet to the outlet. However, only BWR operational transients will be subject of simulation here and reverse flow situations are not anticipated throughout the study.

The method of solution closely follows a strategy outline by Forti and Gonzalez-Santalo /F2/. First equation (2.98) is multiplied by $1/(\rho_{vij})$ and equation (2.99) by $1/(\rho_{\ell ij})$. The resulting equations are added to yield

$$\frac{\Delta z}{\Delta t}\left[1-\frac{\bar{\rho}_{\ell i}}{\rho_{\ell i}}+\bar{\alpha}_i\left(\frac{\bar{\rho}_{\ell i}}{\rho_{\ell i}}-\frac{\bar{\rho}_{vi}}{\rho_{vi}}\right)\right]_j+j_{i,j}-\frac{(\rho_{\ell i}j_{\ell i})_{j-1}}{\rho_{\ell i,j}}-\frac{(\rho_{vi}j_{vi})_{j-1}}{\rho_{vi,j}}$$

$$=\Delta z\left(\frac{1}{\rho_{vi}}-\frac{1}{\rho_{\ell i}}\right)_j\Gamma_{vi,j}-\frac{\Delta z}{\bar{A}_i}\sum_k\left[\frac{W_{\ell ik}}{\rho_{\ell i}}+\frac{W_{vik}}{\rho_{vi}}\right]_j \qquad (2.102)$$

In the finite difference equation for the vapor mass (2.98) $\alpha_{i,j}$ is replaced by its value given by (2.32), i.e.,

$$\alpha_{i,j}=\left[\frac{j_{vi}}{C_o j_i+V_{vj}}\right]_j \qquad (2.103)$$

Substituting (2.103) into (2.98) results

$$-\frac{1}{\Delta t}(\bar{\rho}_{vi}\bar{\alpha}_i)_j+\left[\rho_{vi}\left(\frac{1}{\Delta t}\frac{1}{C_o j_i+V_{vj}}+\frac{1}{\Delta z}\right)j_{vi}\right]_j-\frac{(\rho_{vi}j_{vi})_{j-1}}{\Delta z}$$

$$=\Gamma_{vi,j}-\frac{1}{\bar{A}_i}\sum_k W_{vik,j} \qquad (2.104)$$

Equation (2.100) is rearranged to give the pressure drop between two consecutive axial nodes,

$$(P_{j-1} - P_j) = \frac{\Delta z}{\Delta t}\left[(\rho_{vi}j_{vi}+\rho_{\ell i}j_{\ell i}) - (\bar{\rho}_{vi}\bar{j}_{vi}+\bar{\rho}_{\ell i}\bar{j}_{\ell i})\right]_j$$

$$+ \left[\frac{\rho_{vi}(j_{vi})^2}{\alpha_i} + \frac{\rho_i(j_{\ell i})^2}{(1-\alpha_i)}\right]_j - \left[\frac{\rho_{vi}(j_{vi})^2}{\alpha_i} + \frac{\rho_{\ell i}(j_{\ell i})^2}{(1-\alpha_i)}\right]_{j-1}$$

$$+ \frac{\Delta z}{A_i}\tau_{wi,j}P_{Fi} + \left[\rho_{vi}\alpha_i+\rho_{\ell i}(1-\alpha_i)\right]_j g_z\Delta z$$

$$+ \frac{\Delta z}{A_i}\sum_k^{N_i}\left[\dot{M}_{vik}+\dot{M}_{\ell ik}\right]S_{ik} \qquad (2.105)$$

The second, third and fourth terms on the right of (2.105) are commonly identified, respectively, as acceleration, friction and gravity pressure drop. The first term accounts for the momentum storage rate while the fifth represents the momentum exchanged between subchannels. The densities ρ_{vij} and $\rho_{\ell ij}$ are assumed equal to the values at the preceding interval. For high pressures and small node spacing Δz these assumptions should introduce little error and avoid iterative schemes to find the densities.

The system to be solved consists of four algebraic equations (2.102), (2.104), (2.105) and (2.101) and five unknowns: $j_{vi,j}$, $j_{\ell i,j}$, P_j, $h_{\ell i,j}$ and W_i (recall that W_{vik}, $W_{\ell ik}$, $\dot{M}_{vik}$, $\dot{M}_{\ell ik}$, $\dot{E}_{vik}$ and $\dot{E}_{\ell ik}$ are dependent on these five variables). The fifth equation is given by the condition of no transverse pressure gradient. This means that at a given axial plane j the total mass crossflow rate for each subchannel $W_{i,j}$ is dependent on the pressure drop,

$$W_{i,j} = \sum_{k}^{N_i} W_{ik,j} = f(P_{j-1}-P_j) \qquad (2.106)$$

Where $W_{ik,j}=W_{vik,j}+W_{\ell ik,j}$. The total mass crossflow rate $W_{i,j}$ is found iteratively by requiring that all subchannels achieve the same planar pressure. In the numerical scheme the pressure drops in the subchannels should not differ from each other by more than a prespecified convergence criterion. To completely solve the problem it is necessary to find the inter-subchannel crossflow rate W_{ik}. This is done as follows.

In a bundle containing N subchannels there are N equations of the type

$$W_{i,j} = \sum_{k}^{N_i} W_{ik,j} \qquad (2.107)$$

However it can be easily verified that the resulting equation for the N^{th} subchannel is just a linear combination of the remaining N-1 equations. Therefore, only N-1 equations represented by (2.107) are linearly independent. It can also be shown /W3/ that in a rod bundle with N subchannels the number of interfaces between adjacent subchannels, i.e., the number of W_{ik} unknowns, is given by (N+L-1) where L is the number of independent loops in the subchannel lattice. The concept of loops is illustrated in Fig.2.5 which shows a four-rod bundle with 180° symmetry. Below all the possible loop configurations are drawn.

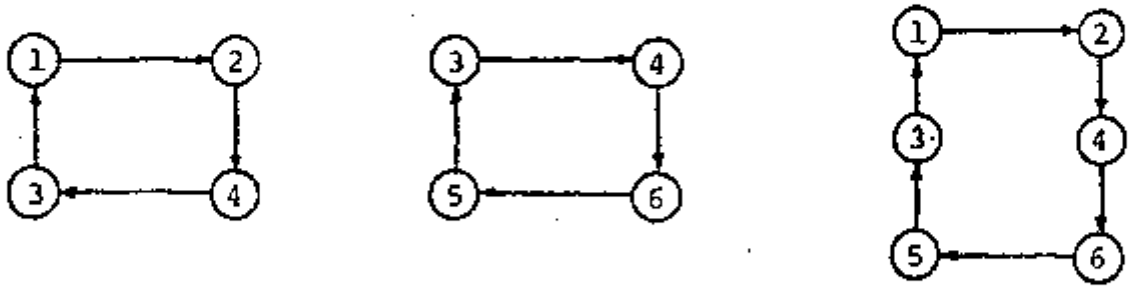

It is easy to see that only two of the three loops are independent. For example, loop C can be viewed as a combination of loops A and B. For each independent loop it is assumed that the flow does not circulate around that loop, i.e.,

$$\sum_{\text{loop}} W_{ik,j} = 0 \qquad (2.108)$$

This guards against the possibility of unlimited circulation flow around the fuel rods. Without this assumption the circulation flow could assume any value and, hence, the number of solutions to the set of equations would be infinite. Another way of avoiding this problem by Beus et al /B5/ by writing a pseudo momentum equation in the transverse direction. By doing this, however, cases may occur where the circulating flow is unavoidable. Equation (2.108) provides the L additional relations required to solve W_{ik}.

2.7 Thermal Coupling between Fuel and Coolant

The temperature distribution in the fuel rod is computed by a collocation method applied to the heat conduction problem in cylindrical coordinates. The method uses backward finite differencing in the time variable and treats the spatial dependence analytically (see Appendix A).

As was mentioned before the thermal coupling between fuel and coolant is accomplished by using the concept of heat flux. To detect critical heat flux conditions (CHF) only the single-phase and nucleate boiling regions of the flow boiling curve need to be considered. These can be accurately modeled by the Chen's correlation /C6/. The solution is numerically advanced in time by assuming that the heat transfer coefficient is not strongly dependent on fluid temperature, T_B. Thus the heat transfer coefficient is treated explicitly in the

numerical expression for the heat flux

$$(q'')^{+} = h_{fc}^{-}(T_w^{+}-T_B^{-}) + h_{nb}^{-}(T_w^{+}-T_S^{-}) \qquad (2.109)$$

This is a reasonable approximation for operational transients where the heat capacity of the fluid is large enough that small changes in the heat fluxes lead to small changes in the fluid thermal conditions. The temperature distribution of each fuel rod is computed at all axial steps at every time step.

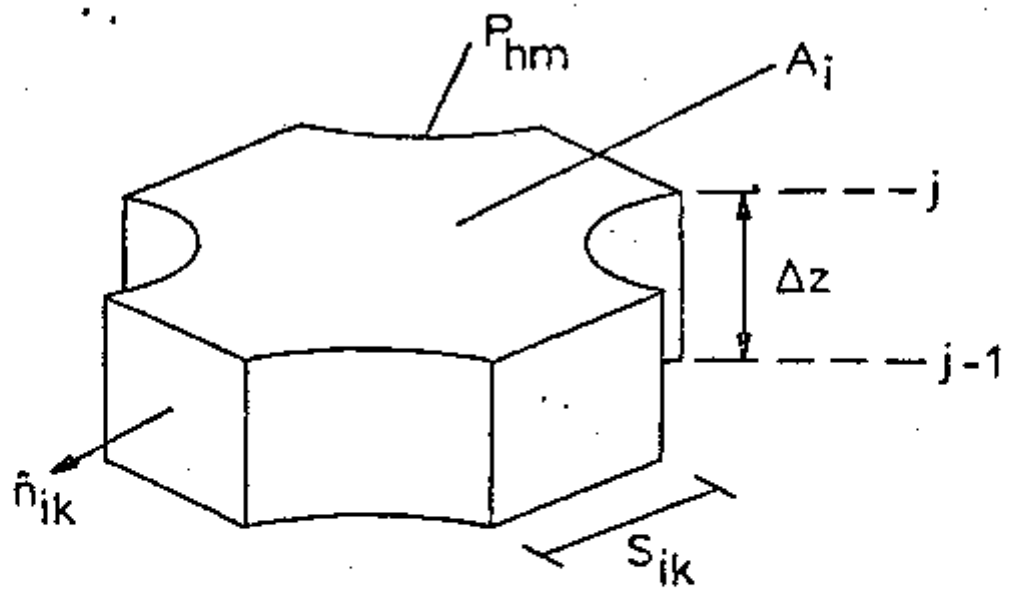

Fig. 2.1 - Control Volume Used in the Averaging Procedure

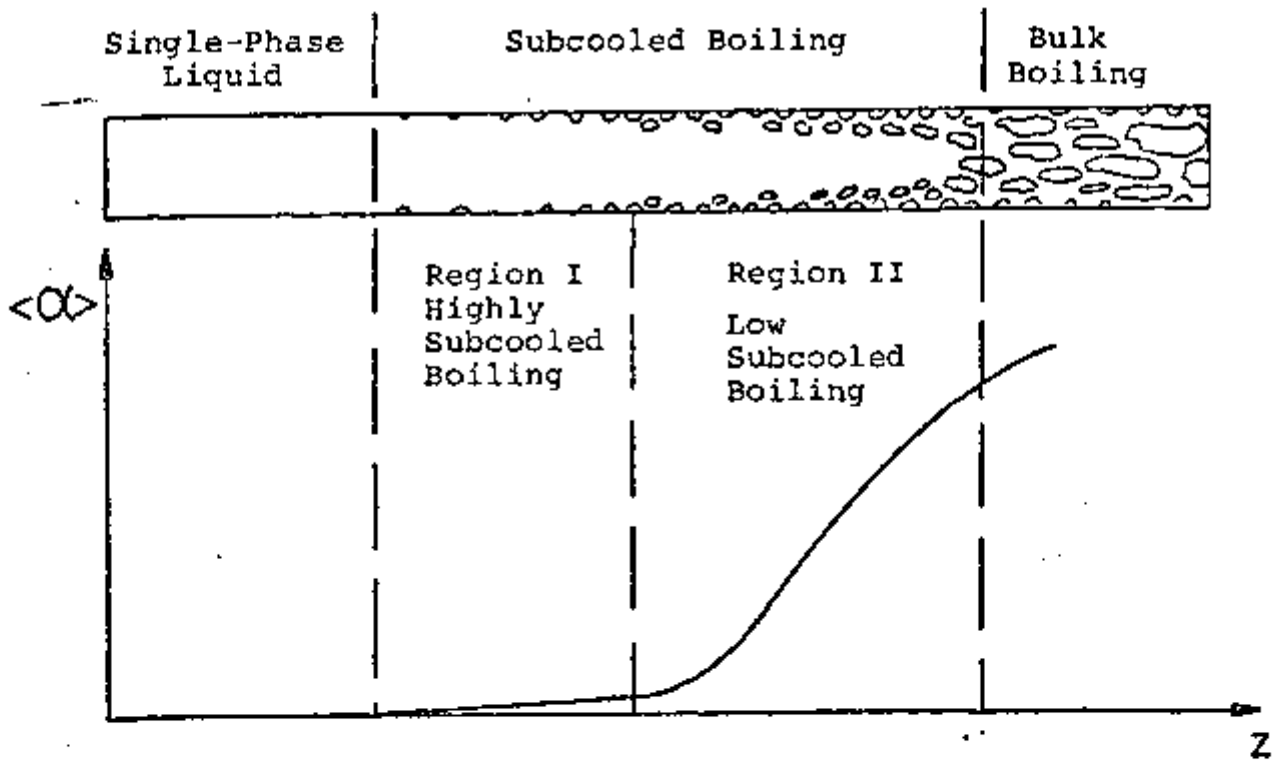

Fig. 2.2 - Void Profile in Subcooled Boiling

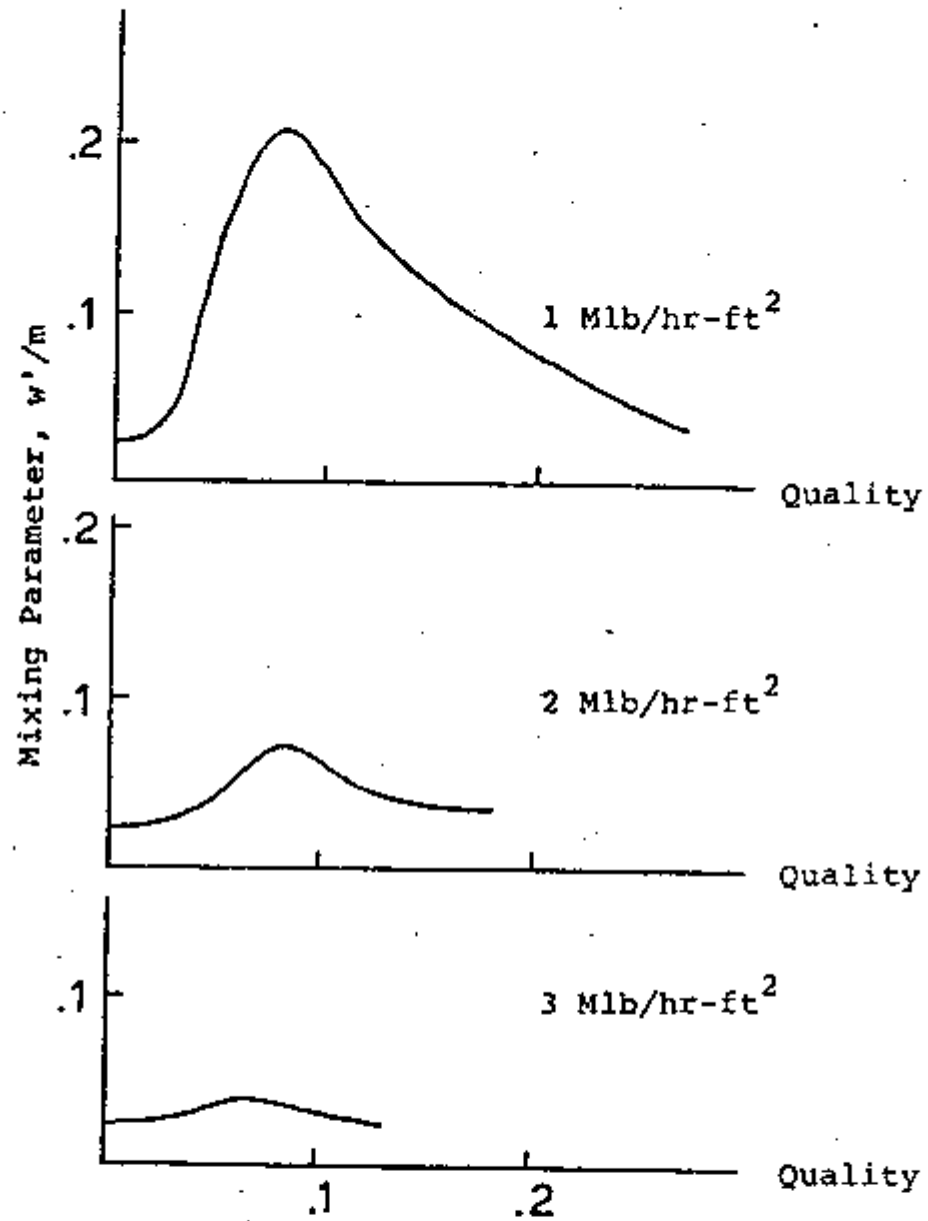

Fig. 2.3 - Variation of Mixing with Steam Quality at 750 psia and 0.085 in. Gap Spacing/R9/.

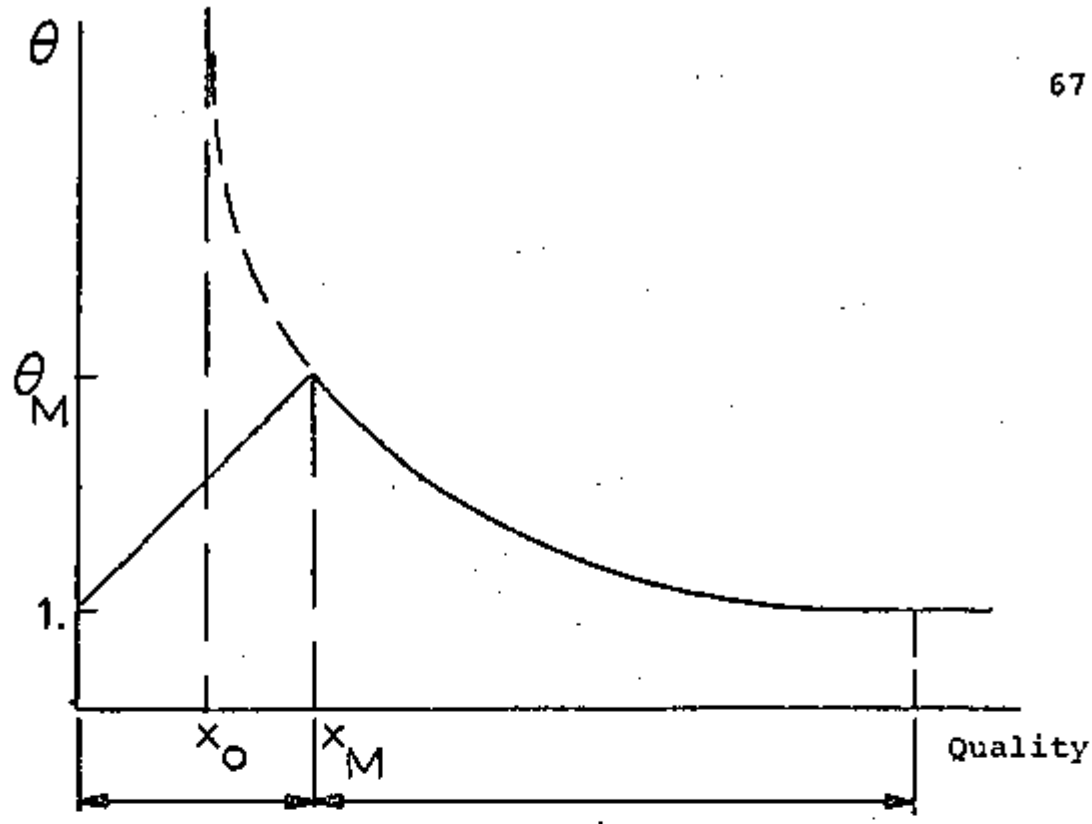

Fig. 2.4 - Variation of the Two-Phase Mixing Parameter with Quality.

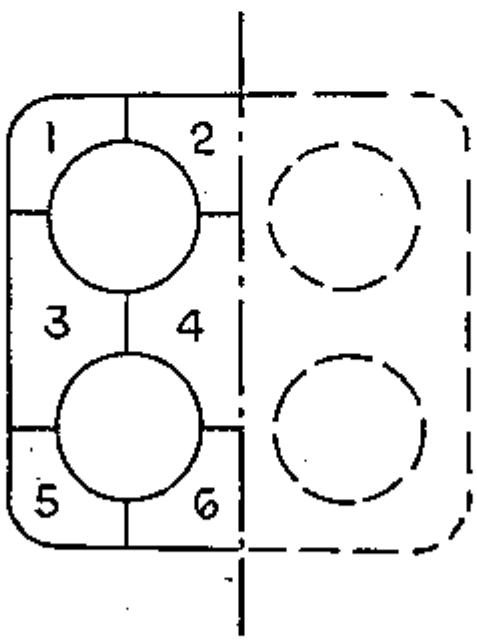

Fig. 2.5 - 4x4 Rod Bundle with 180° Symmetry.

CHAPTER 3 - RESULTS AND DISCUSSION

In order to validate the physical models presented in the previous chapter a comparison between the code results and experimental findings is performed and discussed in this chapter. This is limited to experiments where detailed information concerning subchannel flow quantities is available. Large bundles have been tested in the past but only global quantities were measured. In this study comparisons will be performed for steady-state conditions. At this time no information is available for subchannel quantities under non-stationary conditions. The experiments chosen are those where the geometric and hydraulic parameters were typical of BWR design. The comparisons are mainly performed on the basis of the following data:

- Nine-Rod GE Test Bundle /L2,L3/ .
- Sixteen-Rod ISPRA Test Bundle /H2,H3/
- Nine-Rod Studsvik Test Bundle /G6,U1/

It is fortunate that several commonly used subchannel codes have been tested against the aforementioned experimental evidence. Therefore, it is possible not only to show how the code CANAL compares against the experiments but also how it performs in comparison to other codes.

In these experiments the following flow quantities were measured: subchannel exit mass velocity, subchannel exit quality and pressure drop along the heated length. These measurements provide to some extent sufficient information for the verification of the physical models. However, the mixing model could be substantially improved if measurements of the subchannel void fractions were available. This would also permit a check on the hypothesis of functional dependence between the void fraction distribution and the mass velocity

distribution.

A comment is necessary here on the choice of the empirical parameters of the mixing model, K_a and θ_M (Section 2.5.1). Through numerical experiments it was found that the calculated results have little sensivity to K_a as long as this parameter is in the range from 1.2 to 1.6. In this range the best agreements with all experimental findings were observed. To simulate the three experiments already mentioned a constant value K_a=1.4 was arbitrarily chosen. The results showed a moderate sensitivity to θ_M. The choice of this second parameter will be discussed in the following section in the framework of each experiments. At this points it suffices to say that for each experiment a constant value of θ_M was assumed.

3.1 Nine-Rod GE Test Bundle /L2,L3/

3.1.1 Bundle and Test Description

In 1969 test conditions of typical BWR operation situations were investigated at GE /L2/ with electrically heated 3x3 rod bundles for both uniform and non-uniform radial power distributions and for adiabatic conditions. Simultaneous measurements of exit mass velocity and exit quality were performed for individual subchannels using the isokinetic sampling technique. The GE data were the first published for square-array arrangements. For this reason it is particularly important for the development of CANAL to assess the analytical predictions against these experimental findings.

The nine-rod bundle test section is shown in Fig.3.1 and its geometric and hydraulic data are summarized in Table 3.1. Three types of experiments were conducted:

(1) Isothermal tests in order to determine the liquid flow split between subchannels. The corresponding test

conditions are shown in Table 3.2. (These tests were called Series 1 by GE)

(2) Tests where all rods were uniformly heated in the radial and axial directions. The test conditions are shown in Table 3.3. (These tests were called Series 2 by GE)

(3) Tests where the rods were non-uniformly heated radially but uniformly heated axially. The radial peaking pattern is shown in Fig.3.2 whereas the corresponding test conditions are reported in Table 3.4. (GE Series 3)

3.1.2 Results and Comparisons for the Isothermal Test Data (GE Series 1)

The experimental and calculated results for the isothermal tests are shown in Table 3.5 and Fig.3.3. Included are results obtained with COBRA-IV /W4/. Lahey et al. estimated an error band of 3% in the measurements of subchannel mass velocities. The comparison of the CANAL results with the measured data shows good agreement. In all cases the calculated mass velocities for the side and center subchannels were within 4% of the measured values. The largest difference occurred for the corner subchannel of test point 1B. Comparison with the COBRA-IV results indicates that the two codes are equivalent in terms of accuracy for this test. It can be stated that the assumption of no transverse pressure gradient is obviously valid for the isothermal test conditions.

3.1.3 Results and Comparisons for the Two-Phase Test with Radially Uniform Heating (GE Series 2)

This was the first experiment to reveal the phenomenom of lateral drift of the vapor phase to regions of higher velocities under diabatic conditions. The experimental data shown in Table 3.6 indicate that the exit quality of the center subchannel is always the highest among the three types

of subchannels, the side subchannel behaves approximately as the bundle average and the exit quality of the corner subchannel is lower than the bundle average. The most reasonable explanation for this trend of the data is the tendency of the steam to move preferentially to the center of the rod bundle and/or the presence of a thick liquid cold film on the unheated bundle wall.

The results of CANAL for GE Series 2 are also shown in Table 3.6. In all the runs the empirical mixing parameter was set as θ_M=5. This means that at the slug-annular flow regime transition the turbulent exchange of mass between adjacent subchannels is enhanced by a factor of θ_M=5. with respect to the single-phase value. In general CANAL compares very well against the measured data and its mixing model does a good work in establishing the correct trend of the exit quality distribution. The exceptions are those runs with low bundle average quality, 2B2, 2E1 and 2G1, where the exit quality of the corner subchannel is overpredicted.

Enhanced Mixing

The experimental data clearly reveals the phenomenon of enhanced two-phase mixing. Fig.3.4 shows the change of the normalized mass velocities of the three subchannels as a function of the bundle average quality for runs 2E1, 2E2 and 2E3. It can be observed that the measured velocity distribution depicts a more uniform profile in the vicinity of x=10%, that is, about the slug-annular flow regime transition. This effect is attributed to an enhacement of turbulent mixing around this transition. As shown in Fig.3.4 CANAL predicts this trend as the flow regime evolves from bubbly to slug flow but it overpredicts mixing for run 2E3 whose exit conditions corresponds to the annular flow regime.

The experimental results for the three runs 2G have

similar behavior as that shown in Fig.3.4 for the three runs 2E. They indicate that for these experiments the turbulent mixing rate is probable more intense not at but before the slug-annular transition. This comes from the following argument. In all the experiments the flow quantities are measured at the exit of the subchannels. For example the exit conditions for run 2E2 are characteristic of the transition slug-annular where the maximum in turbulent mixing is assumed to occur in the mixing model formulation. This implies that for run 2E2 the bubbly and/or slug flow regimes should prevail along most of the bundle length (this is more evident for the corner subchannel where the exit quality is low). Therefore the turbulent exchange of mass, momentum and energy between subchannels is more intense probably under slug regime conditions. However, from the available experimental evidence it is difficult to establish a precise criterion for the occurrence of the maximum in turbulent mixing. Using the slug-annular flow regime transition is convenient and appears to be a good approximation as the calculated results show.

Heat Flux

From runs 2C, 2E and 2G it is possible to obtain other trends of the experimental data. This is done by plotting the exit quality of each individual subchannel against the bundle average quality while holding the average mass velocity constant and varying the heat flux. Figures 3.5 to 3.7 show the effect of the heat flux on the exit subchannel qualities. It is observed that for bundle average quality above 6% the corner and side subchannels run cooler while the center subchannel becomes hotter as the heat flux is increased. At average exit qualities below 6% the trend is reversed. In fact, the trend in this range may be similar to that at higher qualities because the the uncertainty in the quality measurements is estimated to be ±2%(±0.02). The calculated results

also shown in Figures 3.5 to 3.7 indicate that CANAL does not model satisfactorily the effect of the heat flux on the subchannel qualities. It is more than probable that these observed trends are due to subcooled boiling effects since the heat flux plays a major role in the void detachment phenomenon. This illustrated in Fig.3.8 where the estimated behavior of the corner subchannel quality along the bundle length is plotted for runs 2E2 and 2G2. These runs were chosen because the average exit conditions are about the same. For simplicity it is assumed that the quality in linearly dependent on z (the dependence is not exactly linear because of the transverse mass flow). The subcooled quality, x_d, corresponding to the void detachment point is lower for run 2G2 than for 2E2 since heat flux is higher for the first. It can also be noticed that for run 2E2 the portion of the subchannel length under boiling conditions is larger than that of run 2G2.

Fig.3.8 is also another indication that the mixing model of CANAL is underestimating the rate of turbulent mixing for bubbly conditions since CANAL is overpredicting the corner subchannel quality for both runs and bubbly conditions are certainly predominant in these two cases.

Mixing Parameter, θ_M

The effect of the mixing parameter θ_M on the flow quantities of the corner subchannel for runs 2E1, 2E2 and 2E3 is shown in Figures 3.9 and 3.10. Increasing θ_M tends to drive more vapor to the center subchannel and more liquid to the corner subchannel with little change in the mass velocities of the side and center subchannels. It must be noted that most of the flow is in the side and center subchannels. Therefore, even substantial changes in the flow of the corner subchannel affect very little the flow in the two other subchannels. Decreasing θ_M has the opposite effect.

Other Codes

Comparison of COBRA-IV /W4/ results with the observed trends, also presented in Table 3.6, shows a strong overprediction of the corner subchannel exit quality and, accordingly, an underprediction of the corner subchannel mass velocity. The exit quality of the center subchannel is also underpredicted to some extent. COBRA-IV fails to predict the experimental trends due to an inherent deficiency in the mixing model of the COBRA codes for two-phase conditions. Even if the mixing parameter, β, in COBRA is set to a very large value it would result in a quality distribution which approaches a uniform profile, i.e., the exit qualities of the three subchannels will be nearly identical. These experiments reveal that the formulation of the mixing model in COBRA is incomplete and β cannot be taken constant throughout the bundle but its dependence on flow regime, mass flow rate and gap spacing must be accounted for. The same coments apply to other subchannel codes using mixing models similar to that of COBRA. For instance, the results of THINC-II and THINC-IV for tests 2E1, 2E2 and 2E3 shown in Figures 3.11 and 3.12 support again these findings.

3.1.4 Results and Comparisons for the Two-Phase Test with Non-Uniform Heating (GE Series 3)

As Fig.3.2 shows the radial peaking factor pattern for this series is nearly diagonally symmetric with the hot corner rod power being approximately twice that of the cold rod power. Unfortunately, no mass and energy balance can be checked for these runs bacause, as shown in Table 3.7, GE sampled only five of the subchannels. If diagonal symmetry is assumed there are ten distinct subchannels in the bundle. It should be recalled that with the exception of the local peaking factor pattern the test conditions for runs 3B2, 3D1, 3E1 and 3E2 are nearly identical to those of runs 2B2, 2D1, 2E1 and

2E2 respectively. This makes it easy to refer back to the radially uniform heated cases discussed in the preceding section.

In order to reveal the trends of quality and mass velocity distributions the measured exit flow quantities of the non-uniform heating case are compared to those of the uniform heating case. That is, the behavior of the hot and cold corner subchannel in Series 3 is compared to the behavior of the corner subchannel is Series 2 and, likewise, the cold and hot side subchannels are compared to the side subchannel. For all cases, relative to the uniform heating runs, the following conclusions can be drawn:

(1) the exit quality of the hot corner subchannel is higher;
(2) the exit quality of the cold corner subchannel is not very much affected and does not show a definite trend;
(3) the exit quality of the hot side subchannel is higher;
(4) the exit quality of the cold side subchannel is lower;
(5) the exit quality of the hot center subchannel is higher;
(6) the exit mass velocity of the hot corner subchannel is lower;
(7) the exit mass velocity of the cold corner subchannel is lower;
(8) the exit mass velocity of the hot side subchannel is lower;
(9) the exit mass velocity of the cold side subchannel is higher;
(10) the exit mass velocity of the hot center subchannel is lower.

These comparisons are shown schematically below (refer to Table 3.7)

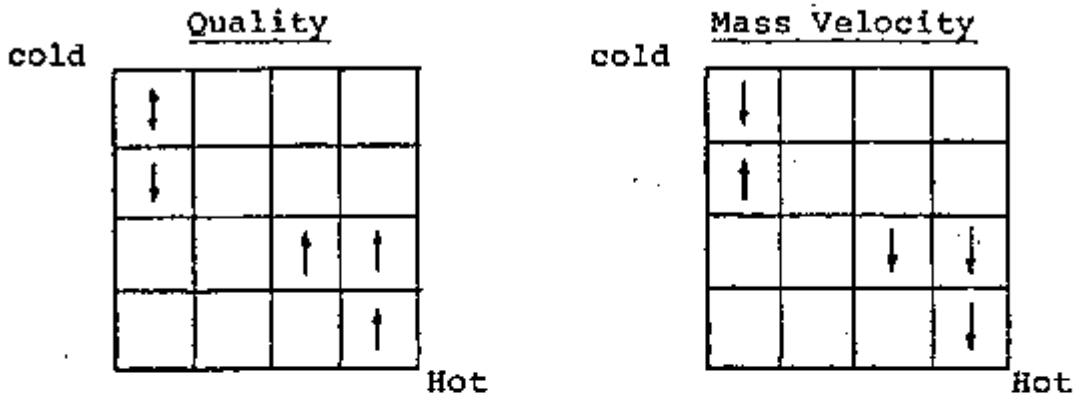

Again, in the hot side of the bundle the phenomenon of vapor lateral drift to the higher velocity regions is observed, i.e.,

(11) the hot center subchannel runs at the highest exit quality;

(12) the hot corner subchannel runs at higher-than-average exit quality;

(13) the exit quality of the hot side subchannel is always higher than that of the hot corner subchannel.

Table 3.7 summarized the comparisons of CANAL results against the experimental findings. Again for all runs the empirical mixing parameter was fixed at θ_M=5. Satisfactory agreement has been achieved in general. Qualitatively CANAL is not able to predict trend (7) for runs 3D1, 3E1 and 3E2 and, as was the case with GE Series 2, CANAL is underestimating the effect of lateral vapor drift to the hot center subchannel for the low exit quality runs 3B2 and 3E1. Quantitatively the following comments can be made:

(a) The qualities of the hot corner, side and center subchannels are considerably underpredicted (differences between 0.04 and 0.08 in terms of quality) for run 3E2 while the mass velocities of the hot side and hot center subchannels are overpredicted (14% to 20%) for runs 3E1 and 3E2. It should be recalled the for runs 3E1 and 3E2 the heat flux at the hot rod surface is much higher than that of runs 2E1 and 2E2. Because of the importance of

heat flux on the subcooled boiling regime it seems that subcooled boiling has pronounced effects as the conditions change from radially unifrom to radially non-uniform heating. Again these results indicate that CANAL needs some improvement in modeling turbulent mixing under subcooled boiling.

(b) The mass velocity of the cold corner subchannel is overpredicted (7% to 30%) while the mass velocity of the cold side subchannel is underpredicted (-15% to -8%). The reason for these differences is not clear. It would be helpful to know the exit flow quantities of the cold center subchannel which unfortunately was not sampled.

One of the main problems in modeling this experiment is the higher degree of complexity of the power tilt flow and boiling regimes in adjacent subchannels may be very distinct in some cases. For this reason it is not clear yet what is the best scheme of averaging the flow quantities in neighboring subchannels in order to simulate the flow conditions at the interface between those subchannels.

The results of COBRA-IV are also shown in Table 3.7. It can be noticed that COBRA-IV is not able of predicting several of the previously mentioned experimental trends. Particularly COBRA-IV fails again in simulating the trend in exit quality distribution on the hot side of the bundle because of the already mentioned deficiency in its mixing model. For all cases COBRA-IV strongly underpredicts the mass velocity on the cold side subchannel for no apparent reason.

An overall conclusive statement cannot be reached on the basis of built-in models in today's subchannel codes. However, the combination of CANAL mixing model with the assumption of zero transverse pressure gradient seems to be acceptable for the GE experiments.

3.2 Nine-Rod Studsvik Bundle Experiment with Power Tilt /G6,U1/

3.2.1 Description of the Bundle and Test Conditions

At Studsvik (Sweden) measurements of mass velocity, quality and enthalpy were performed in a nine-rod square array rod bundle with very high radial power gradient. Fig.3.13 shows the nine-rod bundle test section. The rods are of three types positioned in such way that the rods of the same type are positioned in one row. The power generated was zero in the rods of the first row, 30 percent of the total power in the second row and 70 percent in the third. The outlet of the test section was equipped with flow split devices arranged such that always two subchannels were sampled together according to the following scheme:

Split Channel	Subchannel
1	7 + 8
2	5 + 6
3	3 + 4
4	1 + 2

Thus no individual subchannel quantities were measured during these tests. The bundle contains four spacers typical of BWR design. Their axial position is depicted in Fig.3.14. The subchannel spacer loss coefficients and subchannel flow areas as given in /G6/ are

Subchannel	Spacer coefficient (velocity heads)	Flow Areas $x10^{-6} m^2$
1	1.22	62.9
2	2.03	100.7
3	2.08	99.6
4	1.53	150.2
5	2.13	98.4

Subchannel	Spacer coefficient (velocity heads)	Flow Areas $x10^{-6}m^2$
6	1.58	147.8
7	1.27	61.7
8	2.13	98.4

The test conditions for the seven cases run are summarized in Table 3.8.

3.2.2 Results and Comparisons

A unique feature of the Studsvik bundle test is the strong radial power tilt. This complicates the modeling of the mixing phenomenon because flow and boiling regimes may be very distinct accros the bundle even for adjacent subchannels due to the occurence of various boiling modes at the same axial position. For example, along most of the channel length subchannels 1 and 2 are subcooled while subchannels 7 and 8 are saturated as indicated by the experiment.

A collection of results of various subchannel codes was assembled /U1/ using this experiment as a benchmark test. Nine institutions participated in this exercise with the following codes, most of them being of proprietary character:

1) HAMBO
2) COBRA-IIIC — Belgonucleaire, Bruxelles, Belgium
3) SDS — AB Atomenergi, Studsvik, Sweden
4) COBRA-II — Royal Inst.of Technology, Stockholm, Sweden
5) Matteo — Consorzio Nuclital, Italy
6) THERMOHYDRAULIK
7) VIPER old
8) VIPER new — KWU, Erlangen, Germany
9) MIXER 2 — KWU, Frankfurt, Germany

10) COLA I } - Institute for Space Aviation and Nuclear
11) COLA IIS } Engineering, Tu Braunschweig, Germany
12) FLICA - Centre d'Etude Nucleaire, Grenoble, France
13) SDS - Research Establishment Riso, Denmark
14) TORC - Combustion Engineering, U.S.A.

The results of the most popular codes together with those from CANAL and the measured data for cases 1 through 4 are summarized in Tables 3.9 to 3.16. It should be mentioned that cases 1 through 4 were given the highest priority in the report specifying the benchmark exercise /U1/. The coverage of all seven cases is not necessary here. The remaining three cases present the same trends as obseverd in the first four cases.

In order to compare the calculated results with the experiment the average quality of each split channel is obtained from the individually predicted subchannel qualities according to

$$x_j^s = \frac{x_e G_e A_e + x_m G_m A_m}{G_e A_e + G_m A_m} \qquad (3.1)$$

and the split channel mass velocity from

$$G_j^s = \frac{G_e A_e + G_m A_m}{A_e + A_m} \qquad (3.2)$$

where $j=1,\ldots,4$
$m=10-2j$
$e=9-2j$,

as prescribed by Ulrych and Kemner /U1/ for the participants of this benchmark test.

Figures 3.15 to 3.22 show the differences between the calculated results and the experimental data. The mixing parameter was set as θ_M=4. Comparing the experimental findings with CANAL results the following remarks can be made with respect to exit quality and exit mass velocity predictions in the split channels:

(1) The exit quality of split channels 1, 2 and 4 are well predicted for all cases.
(2) The exit quality of split channel 3 is consistently overpredicted by CANAL more so in case 1 where the difference is 4%.
(3) The exit mass velocities of all split channels are well predicted for all cases except for split channel 4 in case 3.

In general CANAL results in good agreement with the experimental findings. The interchange of mass, momentum and energy between split channels 3 and 4 seems to be the cause of the larger deviations observed for case 3. Varying the mixing parameter, θ_M, affects very little the trends in split channels 3 and 4 since channel 4 is in subcooled conditions along its whole length (except for case 1) as illustrated in Fig.3.23. Consequently, there is little exchange of vapor between these two split channels.

The major conclusions in comparing the results of the other codes against the experimental data are

(1) In general the codes are conservative for split channel 1 overpredicting its exit quality.
(2) There is a considerable scatter of the calculated results on the prediction of the exit mass velocity of split channel 4. Again, it appears that this arises from the difficulty in modeling the exchange of flow quantities between split channels which operate under different flow and boiling regimes.

The best predictions come from institutions that either performed the experiments (SDS-Studsvik) or are closest to BWR bundle design (MIXER 2 - KWU). The discrepancies between two results of the same code, SDS, operated at two differnt laboratories seem to support this point of view since they deviate from each other by a large margin.

The results of COBRA-II are closer to the experimental data than those of COBRA-IIIC. However no information was given on the choice of the mixing parameter. Besides it is more than possible that these codes underwent substantial changes in some of their physical models at the various institutions. Therefore, it is not obvious that these codes are still identical to the publicly available versions.

Fig.3.24 shows the comparisons between calculated and measured pressure drops. CANAL predictions are in very good agreement with the measured data.

Unfortunately, Studsvik did not supply an error analysis for the measured quantities. It is estimated that the error bands of GE and Studsvik experiments are about the same since both used similar sampling techniques.

The Studsvik experiment is certainly an important step for the verification process of subchannel codes. In order to supply final conclusive evidence, however, it is necessary to measure individual subchannel quantities. It is hoped that Studsvik will undertake this experiment.

3.3 Sixteen-Rod ISPRA Test Bundle /H3/

3.3.1 Description of the Bundle and Test Conditions

Experiments based on the subchannel isokinetic sampling technique have been recently conducted at Ispra (Italy) using

an electrically-heated 16-rod test section simulating a typical BWR geometry. The main purpose of this test was to check the trends observed in the GE experiments. As will be shown in the next section the ISPRA test confirmed the trend in exit quality distrubition observed in the GE Series 2 test.

Simultaneous measurements of mass flow and enthalpy were made at the end of the bundle active length in four characteristic subchannels of the 16-rod lattice. Figure 3.25 shows the bundle cross section. The subchannels sampled are shown in dark. The geometric and hydraulic parameters as given in /H2/ are summarized in Table 3.17. Seven grid spacers were 0.5m separated along the heated length; the upper spacer is located 0.36m upstream of the heated length end. The estimated values of the spacer loss coefficients (in terms of velocity head in the free flow area) are as follows /H2/:

Subchannel	Spacer Coefficient
1	0.82
2	1.70
3	0.86
4	0.61
5	0.62
6	0.62

The power was uniform both radially and axially. The subchannel measurements were carried out over the range of conditions as shown in Table 3.18. A maximum error of $\pm$ 3% was estimated /H3/ for both subchannel flow and quality.

3.3.2 Results and Comparisons

From a qualitative point of view the experimental results obtained at ISPRA show the same trend as those obtained at GE for the uniform heat flux case. A quantitative comparison is

difficult because of the differences in bundle design and experimental conditions. For example, GE used "pin"-type spacers which should have little effect on the flow conditions whereas ISPRA employed "grid" spacers. In Figures 3.26 to 3.29 the experimental findings of GE runs 2E1, 2E2 and 2E3 ($\bar{G}$=1.47x10^3 Kg/m^{2}S) and those of Ispra test B ($\bar{G}$=1.5x10^3 Kg/m^{2}S) are plotted. It can be noticed that the trends in quality and mass velocity distribution are similar for both experiments. Again the phenomenon of vapor lateral drift is clearly manifested. The corner subchannel exit quality turns out to be lower than the bundle average value in spite of the low exit mass velicity measured in this subchannel. The side subchannel behaves close to the bundle average value while the two sampled center subchannel run at exit qualities and exit mass velocities slightly higher than the bundle average values. The exit mass velocity of the corner subchannel in the Ispra test is much lower than that of GE. One of the possible reasons is the different type of spacer employed. In the Ispra test the corner subchannel presents a much stronger restriction to the flow (larger spacer coefficient) than the side and center subchannel spacers.

Mass and energy balances cannot be strictly performed for the Ispra test because only four of the six characteristic subchannels were sampled. However the exit mass velocity and exit quality of subchannel 6 (refer to Fig.3.25.) are expected to be close to the values of subchannel 4 and/or 5. Likewise, subchannels 1 and 3 behave similarly.

Figures 3.30 to 3.36 show the measured data for each subchannel together with the calculated results of COBRA-IIIC and CANAL.

In general CANAL results are in good agreement with the experimental findings (for this test the best agreement was found for θ_M=5.). The following remarks can be made about

the predictions:

(1) The exit quality of each sampled channel is very well predicted for all cases. The calculated results are always within the uncertainty range of the measured data.
(2) CANAL is not able to predict the trend of subchannel 2 exit mass velocity which decreases as the average bundle quality decreases. A similar trend was observed in the GE experiments with uniform heating (see Fig.3.4) for qualities above 10%.
(3) The exit mass velocity of subchannel 1 is underpredicted.
(4) For all practical purposes CANAL yielded the same values of mass velocity for the center subchannel 4,5 and 6. CANAL does not predict the trend of the exit mass velocity of subchannel 4 which for high flow rates increases as the bundle average exit quality increases.

The experimental data are shown in the form of locuses because there are an infinite number of combinations of inlet subcooling and heat flux that can yield the same average exit quality for a given bundle average flow rate. It is unfortunate that the data are presented in this form because it is not possible to verify all important trends and compare them to those observed in the GE experiments. For example, the effect of enhancement of two-phase flow mixing is apparent in the corner subchannel as shown in Figures 3.30 and 3.31 but this is not clear for other subchannels. Also the effect of heat flux and subcooled boiling on the flow quantities cannot be investigated. These types of trends would be helpful in assessing future improvements in the mixing models. It is hoped that the forthcoming main report on these experiments will contain more details about the aforementioned issues. Further efforts to analyze these experiments are recommended.

The agreement of COBRA-IIIC results (β=0.02) /H3/ with the measured data is also acceptable except for the corner

subchannel exit quality which is appreciable overpredicted. Again the mixing model of COBRA is not able to simulate the process of vapor exchange between subchannels adequately. COBRA-IIIC also predicts identical values of exit mass velocity for subchannels 4 and 5.

3.4 Mass Flow Decay Transient

In contrast to the steady-state condition there are no individually measured subchannel quantities available in transient situations. Therefore, the results that follow are only of scoping character in order to show some basic transient features of CANAL.

The mass flow transient was performed using the GE 3x3 bundle geometry (Fig.3.1) with radially uniform heating. The initial test conditions are the following:

System Pressure	1000 psi
Inlet Subcooling	50 BTU/lb
Average Mass Velocity	$1.x10^6$ lb/hr-ft^2
Power	1. MW

The numerical parameters are

Number of axial steps	20
Time increment	0.05 sec
Turbulent Mixing Parameter, θ_M	5.

Fig.3.38 shows the deviation of the subchannel exit quality from the bundle average exit quality as function of time for a 50% flow reduction in 0.5 sec. It is observed that the transient is practically over about t=1.2 sec. It is interesting to notice that the center subchannel becomes even more hot relative to the bundle average value compared to its initial value whereas the corner subchannel exit quality lags more and more behind the bundle average value. This causes

the mass velocity distribution to become more uniform as shown in Fig.3.37. The side subchannel which has been observed to follow about the bundle average in steady-state follows this trend approximately also for the mass flow decay transient. Fig.3.38 also shows the behavior of the critical heat flux ratio (CHFR) as function of time with the critical heat flux computed by Barnett and CISE correlations (Appendix C). Critical heat flux condition is estimated by the Barnett correlation at t=0.85 sec.

Table 3.1 - Geometric and Hydraulic Parameters of the Nine-Rod GE Test Bundle

Number of Rods	9
Rod Diameter, in	.564
Radius of Corner Subchannel, in	.40
Rod-to-Rod Clearance, in	.174
Rod-to-Wall Clearance, in	.138
Hydraulic Diameter (Total Bundle), in	.474
Heated Length, in	72
Total Flow Area, in^2	2.978

Subchannel	Flow Area, in^2
1	0.0796
2	0.1851
3	0.2947

Table 3.2 - Experimental Test Conditions For the 9-Rod GE Isothermal Data (p=1000psia)

Test Point	Bundle Average Mass Flux (10^{-6} lb/ft^2-hr)	Inlet Subcooling (BTU/lb)
1B	0.480	504.6
1C	0.990	504.6
1D	1.510	504.6
1E	1.970	504.6

Table 3.3 - Experimental Test Conditions For Uniform Radial Peaking Runs (P=1000psia)

Test Point	Bundle Average Mass Flux (10^{-6}lb/ft^2-hr)	Power (KW)	Inlet Subcooling (BTU/lb)
2B2	0.530	532.	149.9
2B3	0.535	532.	108.7
2B4	0.535	532.	52.8
2C1	1.060	532.	57.2
2C2	1.068	532.	35.1
2D1	0.540	1064.	259.2
2D3	0.540	1064.	124.4
2E1	1.080	1064.	142.9
2E2	1.080	1064.	96.7
2E3	1.060	1064.	29.1
2G1	1.070	1596.	225.9
2G2	1.080	1596.	189.8
2G3	1.070	1596.	146.7

Table 3.4 - Test Conditions For Non-Uniform Radial peaking Runs (P=1000psia)

Test Point	Average Mass Flux (10^{-6}lb/ft^2-hr)	Power (KW)	Inlet Subcooling (BTU/lb)
3D1	0.545	1064.	273.0
3E1	1.080	1064.	142.9
3E2	1.060	994.	92.4

Table 3.5 - Comparison of Experiments and Calculations For Single-Phase Data

Test Point		G_1(corner)	G_2(side)	G_3(center)
		(10^{-6}lb/hr-ft^2)		
	Data	.311	.462	.526
1B	COBRA-IV	.318	.456	.560
	CANAL	.352	.454	.546
	Data	.701	.939	1.150
1C	COBRA-IV	.661	.941	1.123
	CANAL	.738	.944	1.115
	Data	1.095	1.441	1.690
1D	COBRA-IV	1.014	1.435	1.710
	CANAL	1.141	1.445	1.691
	Data	1.620	1.910	2.190
1E	COBRA-IV	1.578	1.911	2.150
	CANAL	1.498	1.888	2.200

Table 3.6 - Meassured and Predicted Results for GE Test Data with Radially Uniform Heating

Test Point		Bundle Average		Corner Subchannel		Side Subchannel		Center Subchannel	
		$\bar{G}$ (Mlb/hr-ft^2)	$\bar{X}$	G_1 (Mlb/hr-ft^2)	X_1	G_2 (Mlb/hr-ft^2)	X_2	G_3 (Mlb/hr-ft^2)	X_3
	Data	0.540	0.110	0.425	0.083	0.560	0.105	0.556	0.117
2D1	COBRA-IV			0.393	0.127	0.516	0.105	0.611	0.112
	CANAL			0.429	0.092	0.527	0.104	0.583	0.120
	Data	0.540	0.318	0.490	0.260	0.532	0.330	0.563	0.364
2D2	COBRA-IV			0.396	0.331	0.520	0.306	0.604	0.327
	CANAL			0.465	0.227	0.533	0.297	0.568	0.362
	Data	1.080	0.035	0.950	0.004	1.102	0.026	1.162	0.051
2E1	COBRA-IV			0.786	0.046	1.031	0.032	1.221	0.035
	CANAL			0.816	0.038	1.065	0.031	1.167	0.038
	Data	1.080	0.106	1.046	0.049	1.078	0.097	1.180	0.105
2E2	COBRA-IV			0.790	0.115	1.040	0.101	1.209	0.109
	CANAL			0.922	0.077	1.058	0.099	1.150	0.119
	Data	1.060	0.215	0.965	0.160	1.081	0.185	1.126	0.249
2E3	COBRA-IV			0.784	0.221	1.020	0.208	1.185	0.220
	CANAL			0.913	0.149	1.034	0.198	1.132	0.247

Table 3.6 continued

Test Point		Bundle Average		Corner Subchannel		Side Subchannel		Center Subchannel	
		$\bar{G}$ (Mlb/hr-ft^2)	$\bar{X}$	G_1 (Mlb/hr-ft^2)	X_1	G_2 (Mlb/hr-ft^2)	X_2	G_3 (Mlb/hr-ft^2)	X_3
	Data	1.070	0.038	0.882	0.032	0.968	0.044	1.142	0.043
2G1	COBRA-IV			0.766	0.054	1.024	0.035	1.211	0.038
	CANAL			0.796	0.045	1.049	0.033	1.165	0.041
	Data	1.080	0.090	1.000	0.020	1.111	0.068	1.130	0.110
2G2	COBRA-IV			0.777	0.104	1.042	0.084	1.209	0.093
	CANAL			0.888	0.074	1.065	0.085	1.151	0.098
	Data	1.070	0.160	0.865	0.074	1.132	0.127	1.160	0.176
2G3	COBRA-IV			0.781	0.172	1.035	0.151	1.191	0.166
	CANAL			0.938	0.117	1.048	0.151	1.132	0.179
	Data	1.060	0.042	0.965	0.029	1.066	0.018	1.077	0.059
2C1	COBRA-IV			0.783	0.047	1.011	0.040	1.197	0.042
	CANAL			0.845	0.034	1.035	0.039	1.150	0.046
	Data	1.068	0.075	0.968	0.063	1.028	0.075	1.144	0.100
2C2	COBRA-IV			0.789	0.079	1.021	0.072	1.202	0.076
	CANAL			0.896	0.053	1.042	0.069	1.151	0.085

Table 3.6 continued

Test Point		Bundle Average		Corner Subchannel		Side Subchannel		Center Subchannel	
		$\bar{G}$ (Mlb/hr-ft^2)	$\bar{X}$	G_1 (Mlb/hr-ft^2)	X_1	G_2 (Mlb/hr-ft^2)	X	G_3 (Mlb/hr-ft^2)	X
	Data	0.530	0.029	0.372	0.003	0.521	0.014	0.540	0.030
2B2	COBRA-IV			0.426	0.039	0.493	0.027	0.605	0.028
	CANAL			0.399	0.035	0.508	0.025	0.592	0.031
	Data	0.535	0.090	0.550	0.072	0.530	0.076	0.521	0.104
2B3	COBRA-IV			0.396	0.097	0.508	0.087	0.605	0.091
	CANAL			0.429	0.068	0.518	0.084	0.585	0.100
	Data	0.535	0.176	0.524	0.133	0.517	0.180	0.560	0.220
2B4	COBRA-IV			0.394	0.183	0.511	0.171	0.606	0.179
	CANAL			0.465	0.118	0.522	0.160	0.570	0.206

Table 3.7 - Measured and Predicted Results for GE Test Data with Radially Non-uniform Heating

Test Point		Bundle Average		Hot Corner Subchannel		Cold Corner Subchannel		Hot side Subchannel		Cold side Subchannel		Hot Center Subchannel	
		G^*	$\bar{x}$	G_1	X_1	G_{16}	X_{16}	G_2	X_2	G_{12}	X_{12}	G_6	X_6
	Data	0.535	0.032	0.400	0.080	0.320	0.009	0.507	0.042	0.505	-0.043	0.555	0.108
3B2	COBRA-IV			0.489	0.089	0.137	-0.007	0.645	0.065	0.195	-0.007	0.769	0.052
	CANAL			0.410	0.064	0.342	-0.003	0.514	0.061	0.463	-0.008	0.603	0.057
	Data	0.545	0.084	0.322	0.123	0.335	0.024			0.628	-0.037		
3D1	COBRA-IV			0.344	0.220	0.274	0.017			0.419	0.024		
	CANAL			0.398	0.117	0.474	0.016	0.479	0.131	0.579	0.024	0.548	0.133
	Data	1.080	0.035	0.794	0.105	0.925	0.002			1.430	-0.036	0.852	0.161
3E1	COBRA-IV			0.641	0.126	0.854	-0.016			1.109	-0.012	1.100	0.075
	CANAL			0.695	0.078	1.199	-0.031	0.857	0.082	1.323	-0.022	1.000	0.079
	Data	1.060	0.100	0.800	0.160	0.940	0.075	0.755	0.167	1.475	0.034	0.890	0.227
3E2	COBRA-IV			0.628	0.198	0.983	0.039	0.856	0.163	1.218	0.044	1.011	0.153
	CANAL			0.791	0.105	1.151	0.032	0.908	0.128	1.254	0.055	1.012	0.141

* Mass velocities in Mlb/hr-ft^2

Table 3.8 - Test Conditions for the Studsvik Bundle

Case	Average Mass Velocity Kg/m^2S	Electric Power KW	Inlet Subcooling C
1	907.	380.	9.30
2	897.	384.	16.2
3	908.	381.	31.0
4	1209.	422.	11.1
5	1239.	421.	31.6
6	2064.	498.	10.3
7	2013.	501.	20.6

Pressure : 70. bar

Table 3.9 - Steam Quality in Each Split Channel - Comparison Between Experiment and Various Subchannel Codes for Case 1 of the Studsvik Test

Split Channel	Data	SDS[1]	SDS[2]	HAMBO	MIXER2	COBRA-II	COBRA-IIIC	FLICA	CANAL
1	26.7	27.6	36.5	29.7	28.0	30.4	29.3	36.0	27.2
2	22.7	20.8	27.5	22.6	21.9	23.4	22.3	30.4	22.1
3	10.2	11.1	9.0	8.9	9.9	9.1	8.3	8.8	14.7
4	1.8	3.4	1.0	2.2	3.2	2.7	1.9	0.2	0.0

Table 3.10 - Mass Velocity (Kg/m^2S) in Each Split Channel - Comparison Between Experiment and Various Subchannel Code for Case 1 of the Studsvik Test

Split Channel	Data	SDS[1]	SDS[2]	HAMBO	MIXER2	COBRA-II	COBRA-IIIC	FLICA	CANAL
1	678.	631.	595.	661.	632.	612.	689.	541.	661.
2	812.	800.	734.	794.	784.	760.	837.	652.	756.
3	951.	1009.	1033.	1024.	1018.	1044.	1058.	1045.	980.
4	1204.	1117.	1279.	1140.	1189.	1208.	996.	1382.	1328.

1) Studsvik; 2) Risö

P = 70.3 bar; G_{av} = 907. Kg/m^2S; ΔT_{sub} = 9.3 C; Power = 380. KW

Table 3.11 - Steam Quality in Each Split Channel - Comparison Between Experiment and Various Subchannel Codes for Case 2 of the Studsvik Test

Split Channel	Data	SDS[1]	SDS[2]	HAMBO	MIXER2	COBRA-II	COBRA-IIIC	FLICA	CANAL
1	26.9	25.3	34.1	26.8	24.8	27.4	26.9	31.4	25.2
2	22.1	19.2	25.8	19.9	19.5	20.6	19.4	26.3	19.9
3	7.1	8.5	6.6	6.2	7.5	6.7	5.4	5.4	11.5
4	-1.8	-0.2	0.2	-0.5	0.3	0.3	-1.2	-3.1	-1.7

Table 3.12 - Mass Velocity (Kg/m^2S) in Each Split Channel - Comparison Between Experiment and Various Subchannel Code for Case 2 of the Studsvik Test

Split Channel	DATA	SDS[1]	SDS[2]	HAMBO	MIXER2	COBRA-II	COBRA-IIIC	FLICA	CANAL
1	584.	631.	591.	654.	624.	607.	699.	552.	602.
2	780.	778.	753.	785.	763.	747.	849.	662.	748.
3	1003.	1005.	1050.	1024.	996.	1013.	1035.	1080.	997.
4	1216.	1174.	1224.	1111.	1212.	1229.	953.	1341.	1239.

1) Studsvik 2) Risö

P = 70.0 bar; G_{av} = 897. Kg/m^2S; ΔT_{sub} = 18.2 C; Power = 384. KW

Table 3.13 - Steam Quality in Each Split Channel - Comparison Between Experiment and Various Subchannel Codes for Case 3 of the Studsvik Test

Split Channel	Data	SDS[1]	SDS[2]	HAMBO	MIXER2	COBRA-II	COBRA-IIIC	FLICA	CANAL
1	21.7	20.0	32.4	21.1	18.2	21.4	20.5	27.0	18.4
2	16.7	15.5	25.0	14.6	14.6	14.8	18.7	22.0	13.9
3	2.2	3.3	3.0	1.8	4.0	1.9	1.2	1.6	4.6
4	-5.8	-5.9	0.1	-4.8	-6.4	0.	-5.6	-6.4	-6.2

Table 3.14 - Mass Velocity (Kg/m^2S) in Each Split Channel - Comparison Between Experiment and Various Subchannel Code for Case 3 of the Studsvik Test

Split Channel	DATA	SDS[1]	SDS[2]	HAMBO	MIXER2	COBRA-II	COBRA-IIIC	FLICA	CANAL
1	668.	655.	599.	675.	679.	648.	756.	573.	630.
2	745.	780.	711.	808.	799.	788.	903.	686.	773.
3	1033.	1057.	1147.	1054.	1050.	1075.	1002.	1123.	1078.
4	1201.	1128.	1141.	1066.	1078.	1089.	921.	1199.	1072.

1) Studsvik 2) Risö

P = 70.8 bar; G_{av} = 908. Kg/m^2S; ΔT_{sub} = 31. C; Power = 381 KW

Table 3.15 - Steam Quality in Each Split Channel - Comparison Between Experiment and Various Subchannel Codes for Case 4 of the Studsvik Test

Split Channel	DATA	SDS[1]	SDS[2]	HAMBO	MIXER2	COBRA-II	COBRA-IIIC	FLICA	CANAL
1	23.1	23.5	29.9	24.4	22.4	24.8	26.1	29.2	21.3
2	20.5	18.1	22.5	18.2	18.0	18.8	19.6	24.7	17.3
3	7.6	8.2	6.5	6.2	7.3	6.5	5.4	24.8	11.2
4	-1.1	0.6	0.4	0.6	0.8	1.2	-0.7	-0.9	-1.3

Table 3.16 - Mass Velocity (Kg/m^2S) in Each Split Channel - Comparison Between Experiment and Various Subchannel Code for Case 4 of the Studsvik Test

Split Channel	DATA	SDS[1]	SDS[2]	HAMBO	MIXER2	COBRA-II	COBRA-IIIC	FLICA	CANAL
1	800.	781.	771.	852.	831.	965.	858.	736.	795.
2	1009.	999.	943.	1027.	1008.	998.	1043.	876.	980.
3	1303.	1323.	1389.	1375.	1335.	1378.	1369	1366.	1296.
4	1767.	1770.	1764.	1579.	1686.	1697.	1558.	1882.	1802.

1) Studsvik; 2) Riso"

P = 70.9 bar; $G_{av}^{\circledcirc}$ = 1209. Kg/m^2S; ΔT_{sub} = 11.1 C; Power = 422. KW

Table 3.17 - Geometric and Hydraulic Parameters of the 16-Rod Ispra Test Bundle

Number of Rods	16
Rod Diameter, m	.015
Rod Pitch, m	.0195
Rod-to-Wall Clearance, m	.00337
Heated Length, m	3.66
Radius of Corner Subchannel, m	0.0521

Subchannel	Flow Area $10^6 m^2$	Hydraulic Diameter m
corner	59.82	0.00789
side	127.80	0.01193
center	195.78	0.01662

Table 3.18 - Range of Operating Conditions For The 16-Rod Ispra Tests

Pressure, bar	70
Mass Velocity, Kg/m^2-S	1000, 1500, 2000
Inlet Quality	-0.04
Bundle Power	320 - 2100 KW
Average Exit Quality	0.02 - 0.31

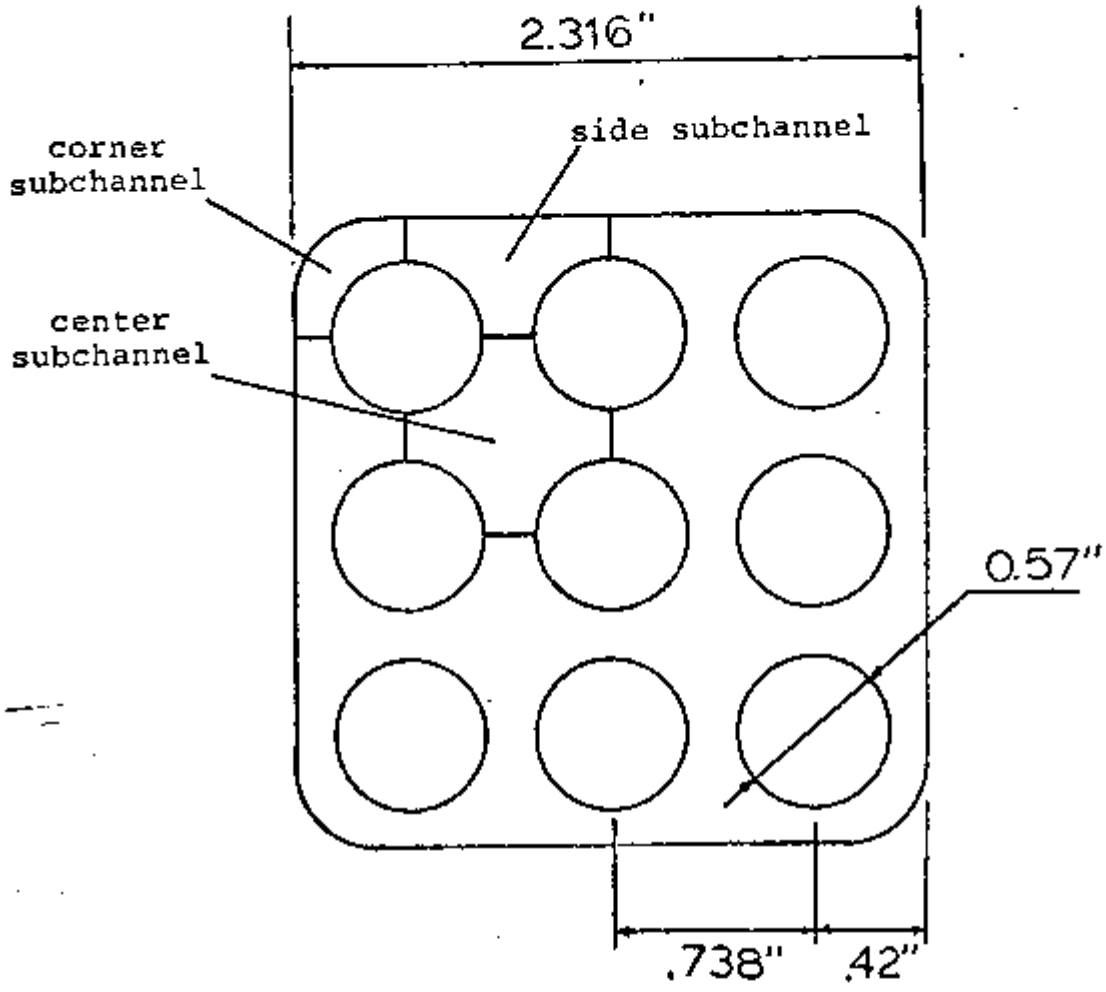

Fig. 3.1 - Geometry of the GE Nine-Rod Bundle

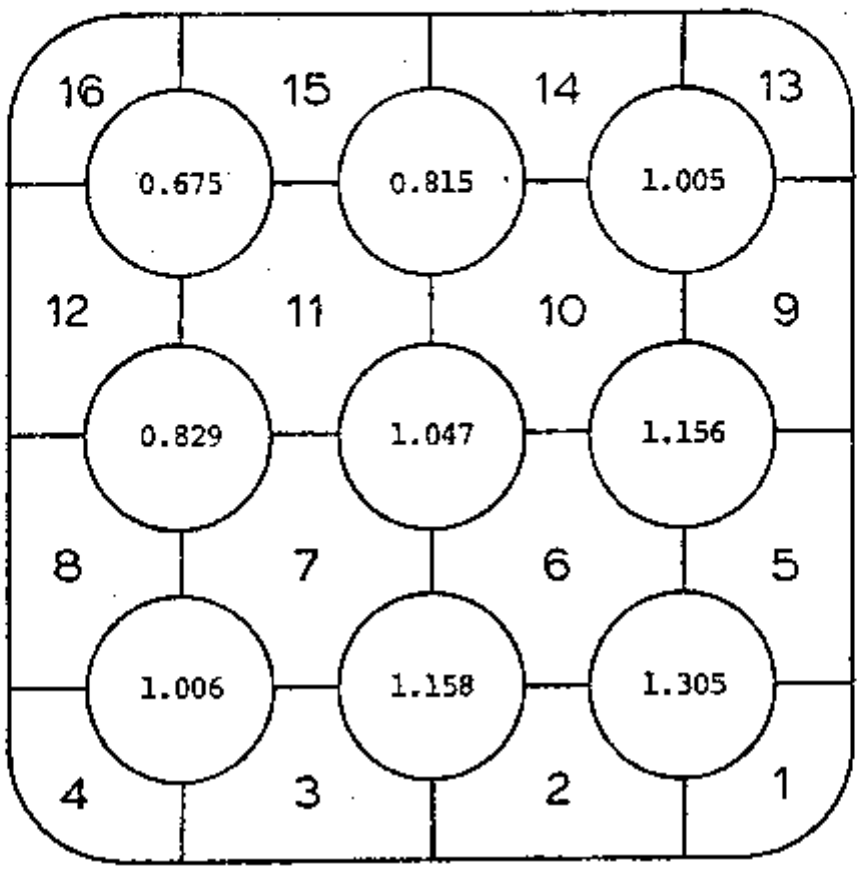

Fig. 3.2 - Radial Peaking Pattern for the GE Nine-Rod Bundle

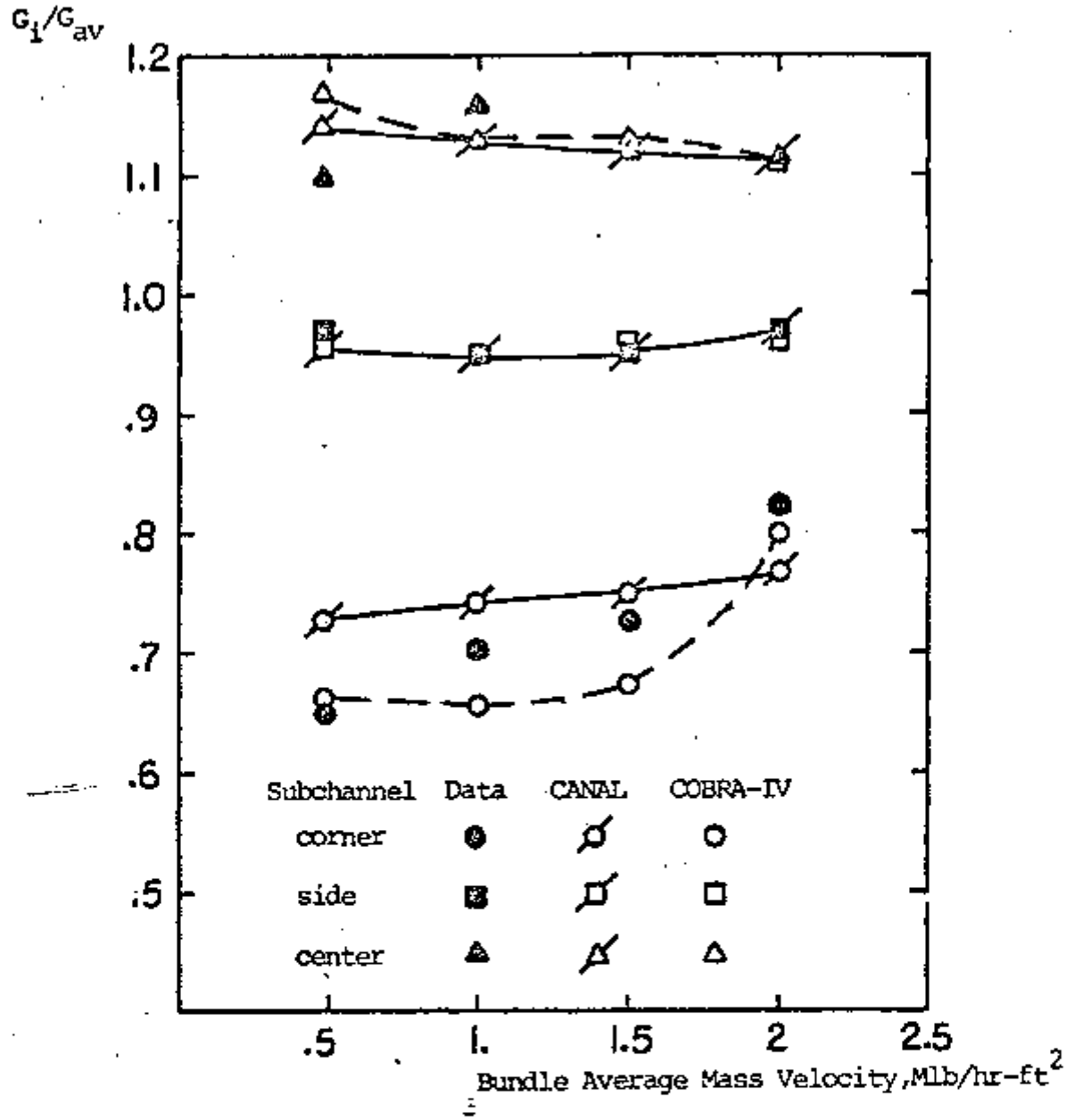

Fig. 3.3 - Comparison between Measured and Predicted Mass Velocity Distribution for the GE Single-Phase Tests.

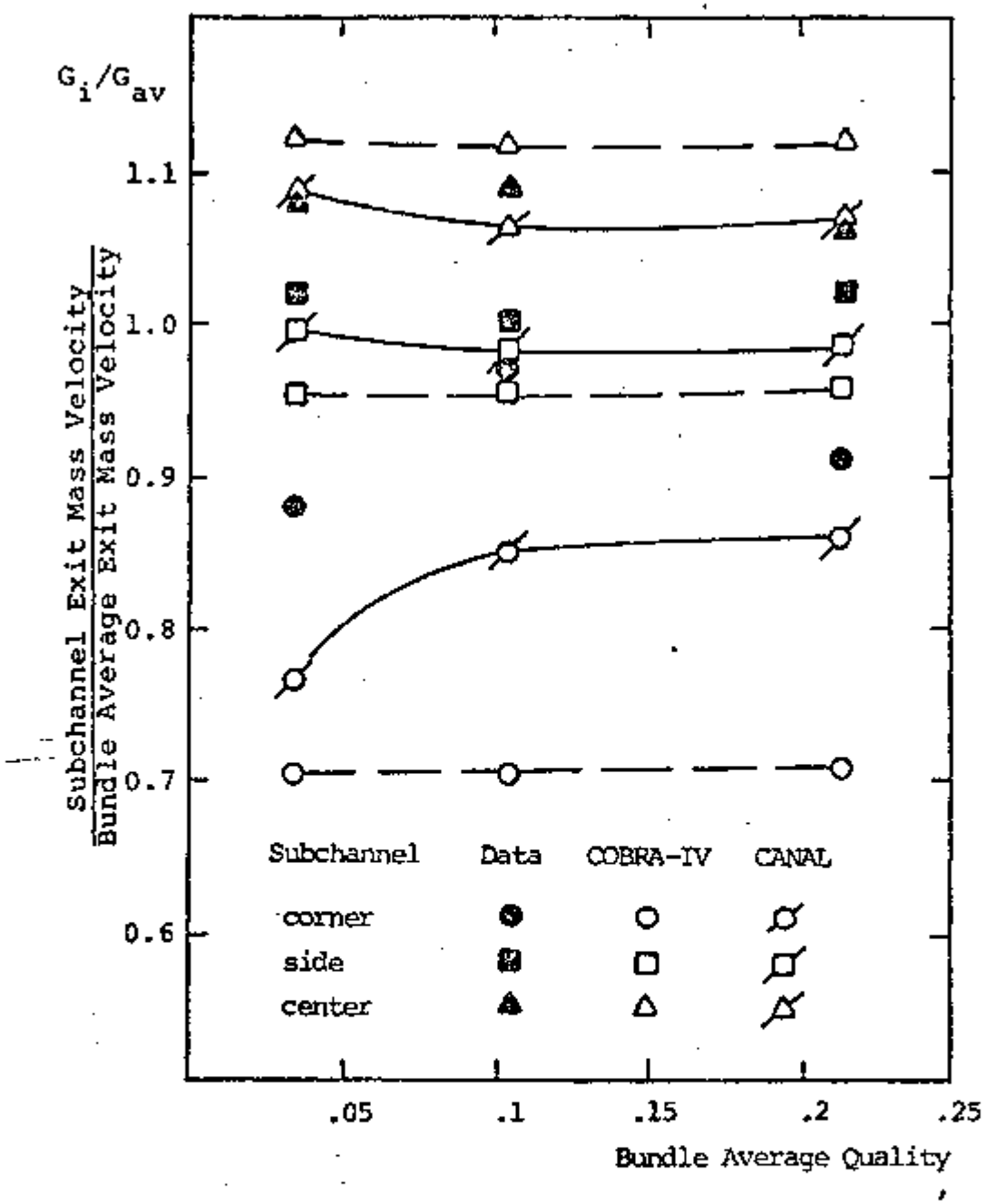

Fig. 3.4 - Comparison between Measured and Predicted Subchannel Exit Mass Velocity Distribution for GE Runs 2E1, 2E2 and 2E3.

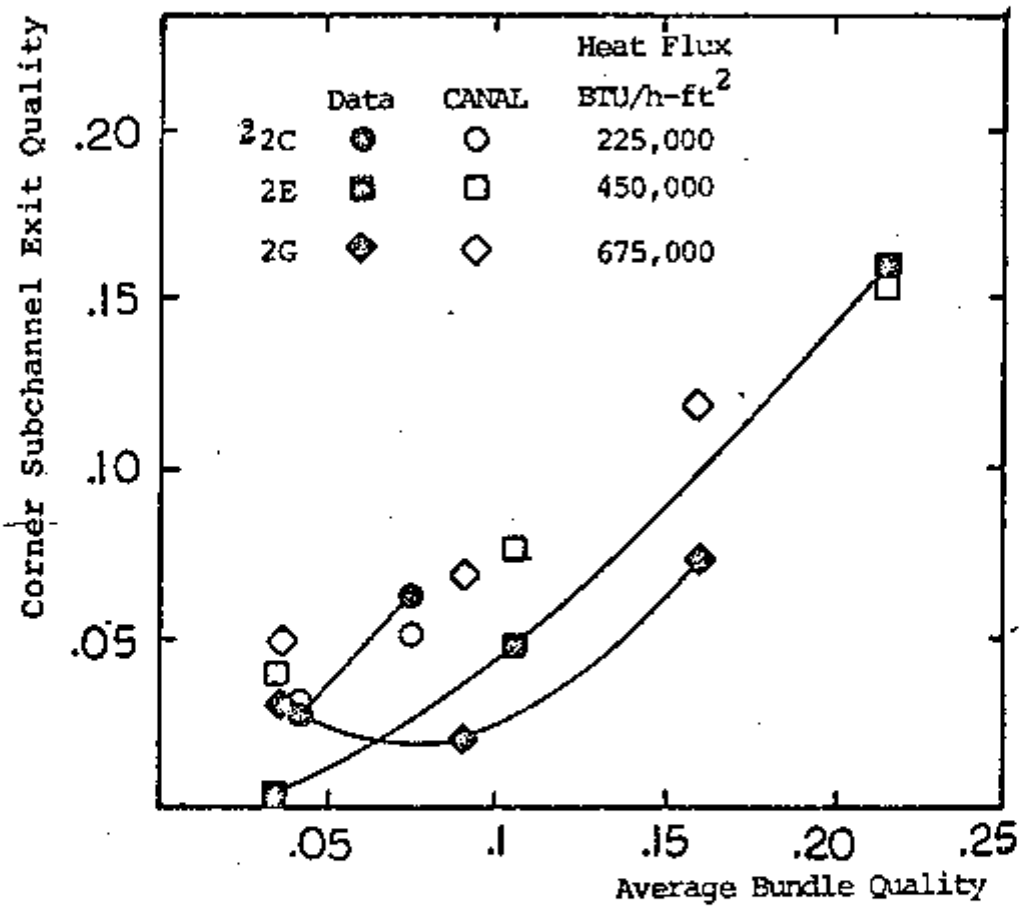

Fig. 3.5 - Effect of Heat Flux on the Corner Subchannel Exit Quality.

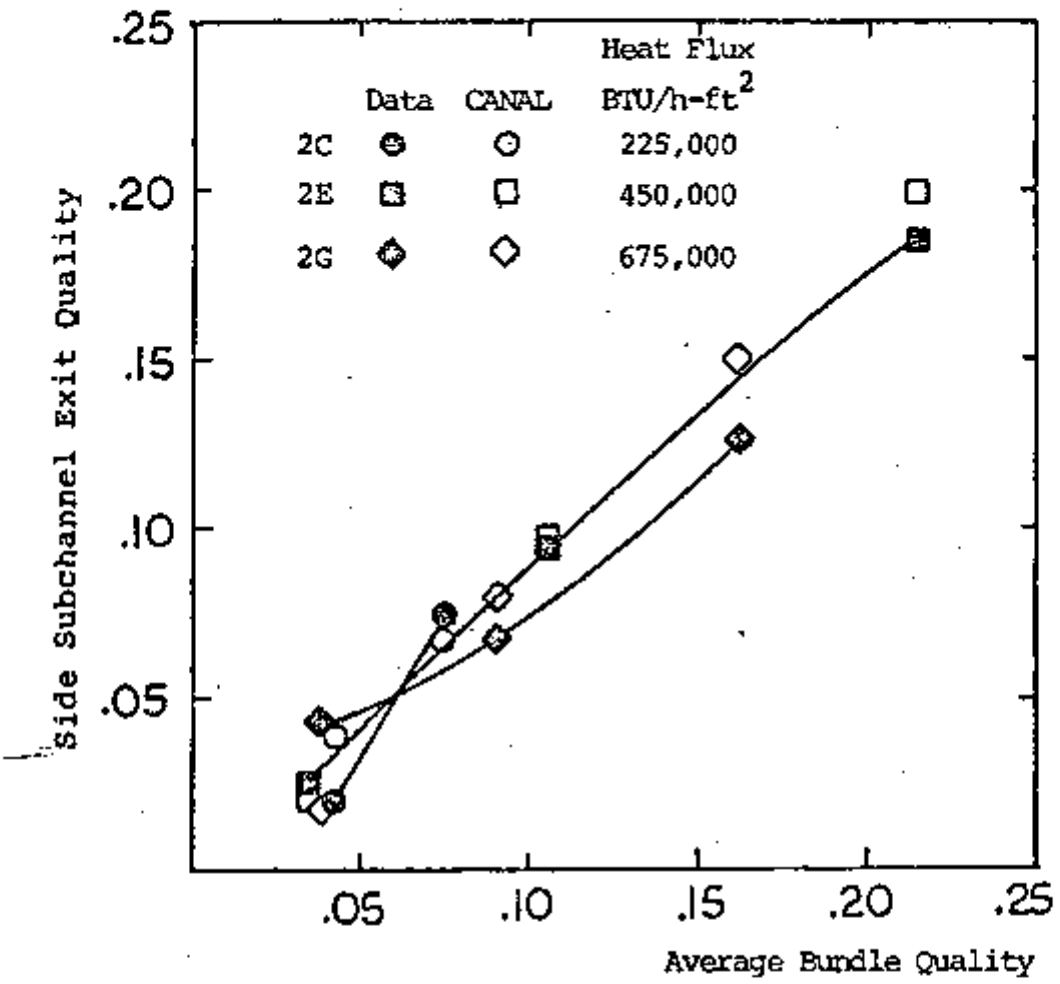

Fig. 3.6 - Effect of the Heat Flux on the Side Subchannel Exit Quality.

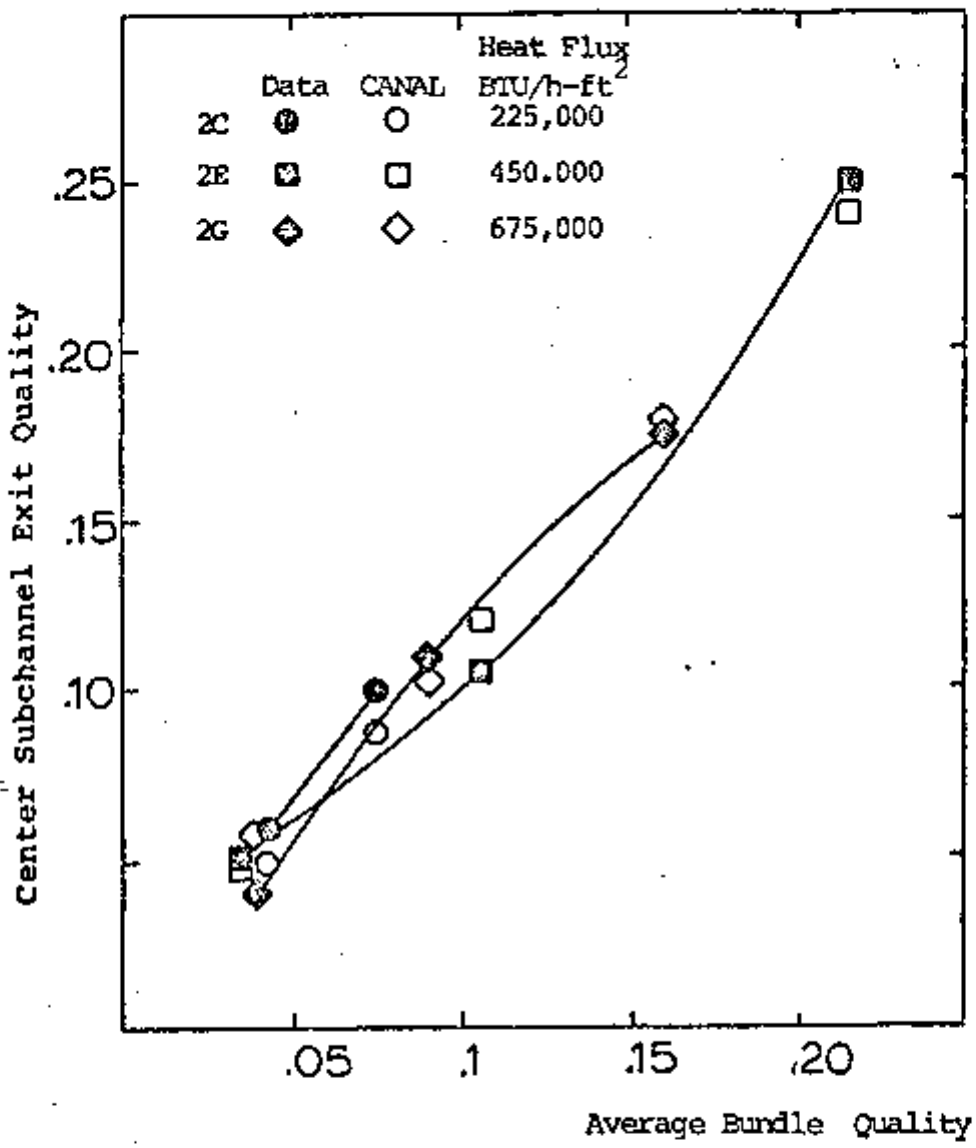

Fig. 3.7 - Effect of the Heat Flux on the Center Subchannel Exit Quality.

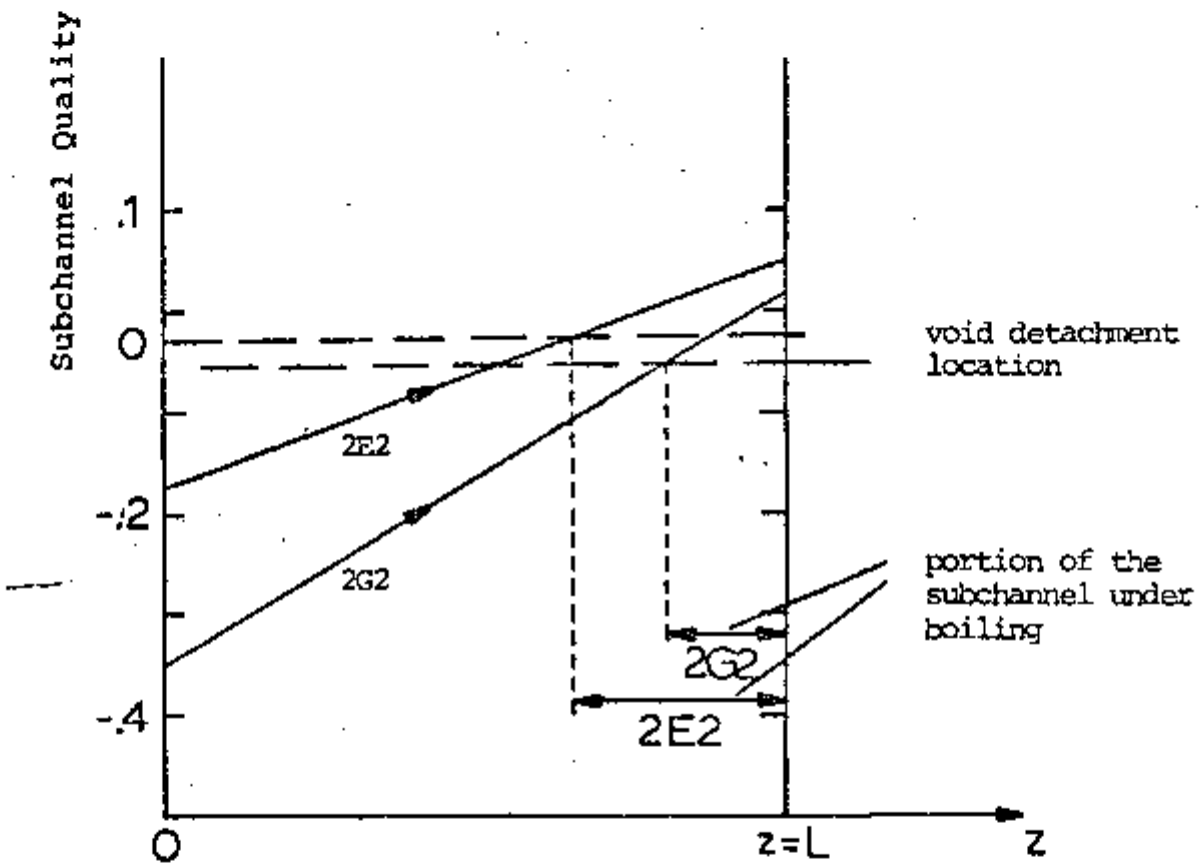

Fig. 3.8 - Estimated Behavior of the Corner Subchannel Exit Quality along the Bundle Length for GE Runs 2E2 and 2G2.

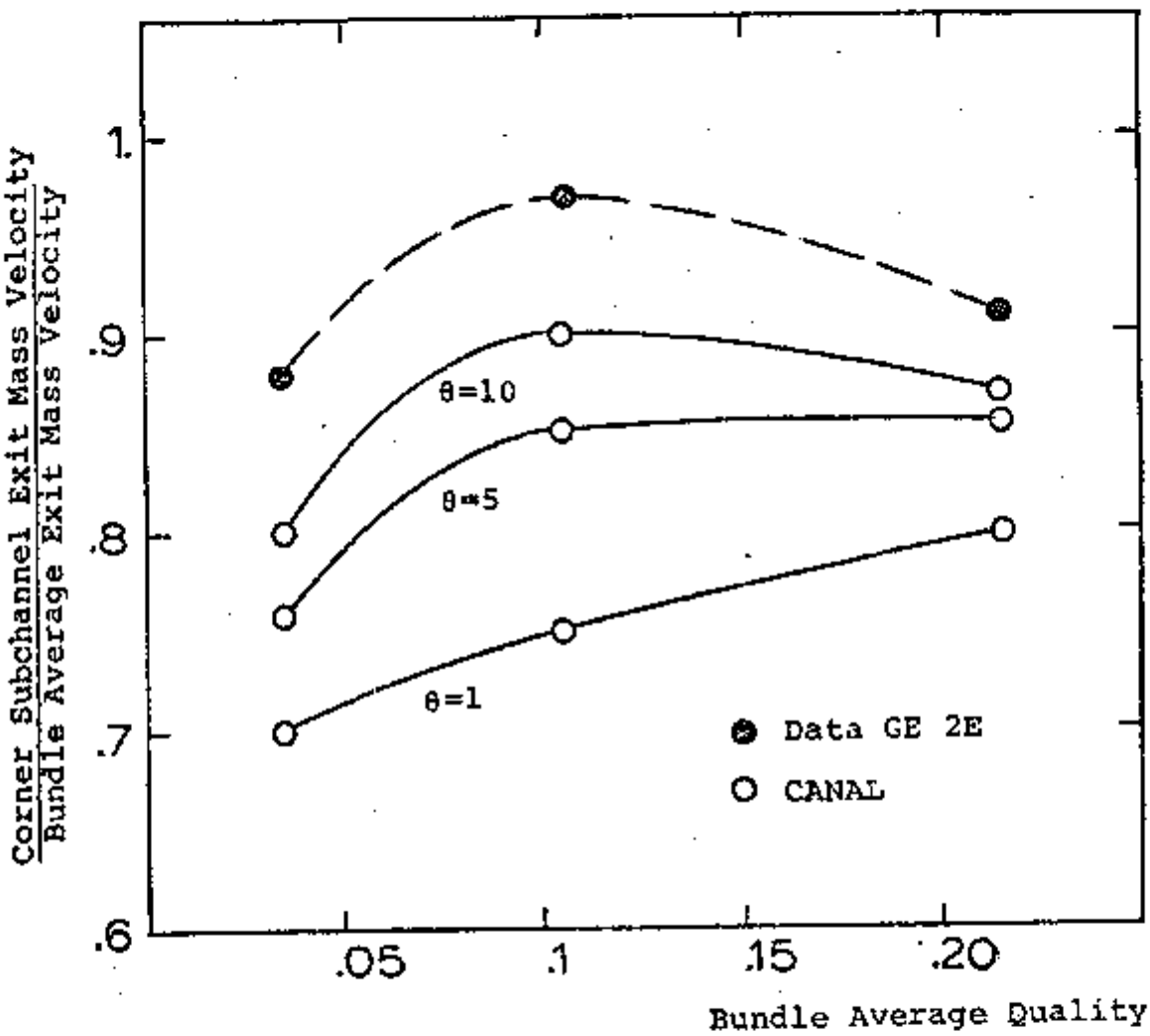

Fig. 3.9 - Effect of the Mixing Parameter on the Exit Mass Velocity of the Corner Subchannel.

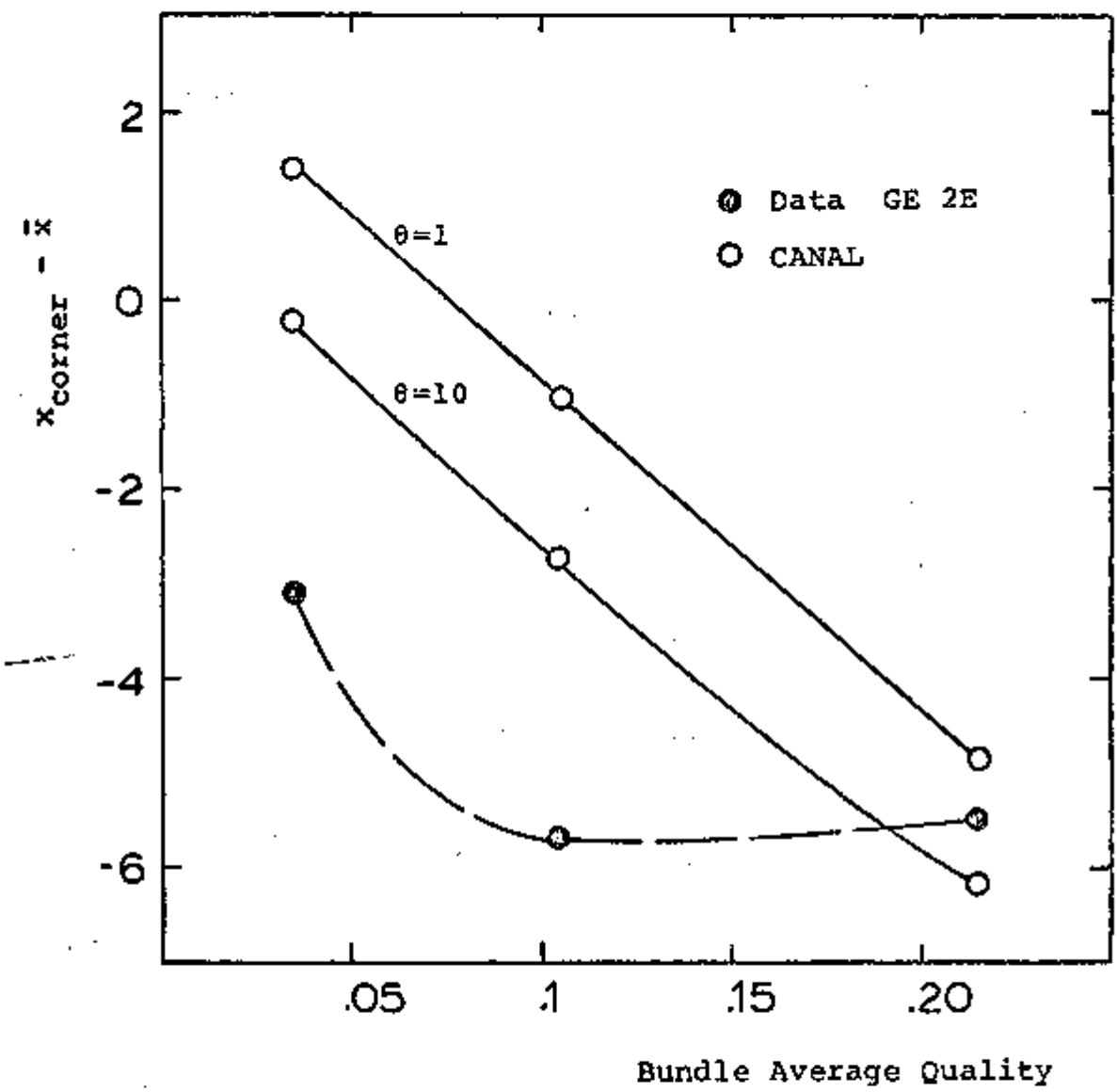

Fig. 3.10 - Effect of the Mixing Parameter θ_M on the Calculated Exit Quality of the Corner Subchannel.

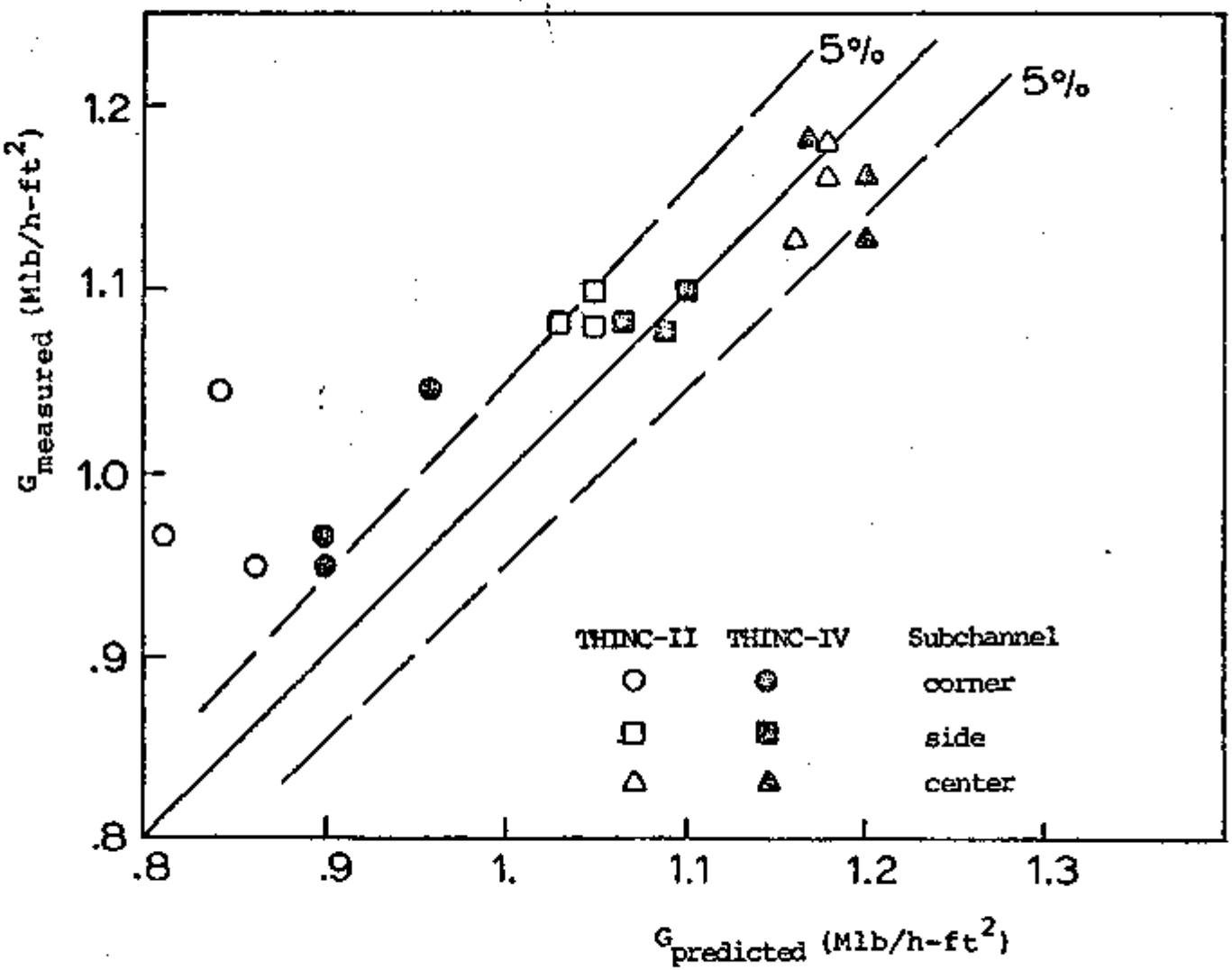

Fig. 3.11 - THINC-II and THINC-IV Results for GE Runs 2E1, 2E2 and 2E3. Mass Velocities.

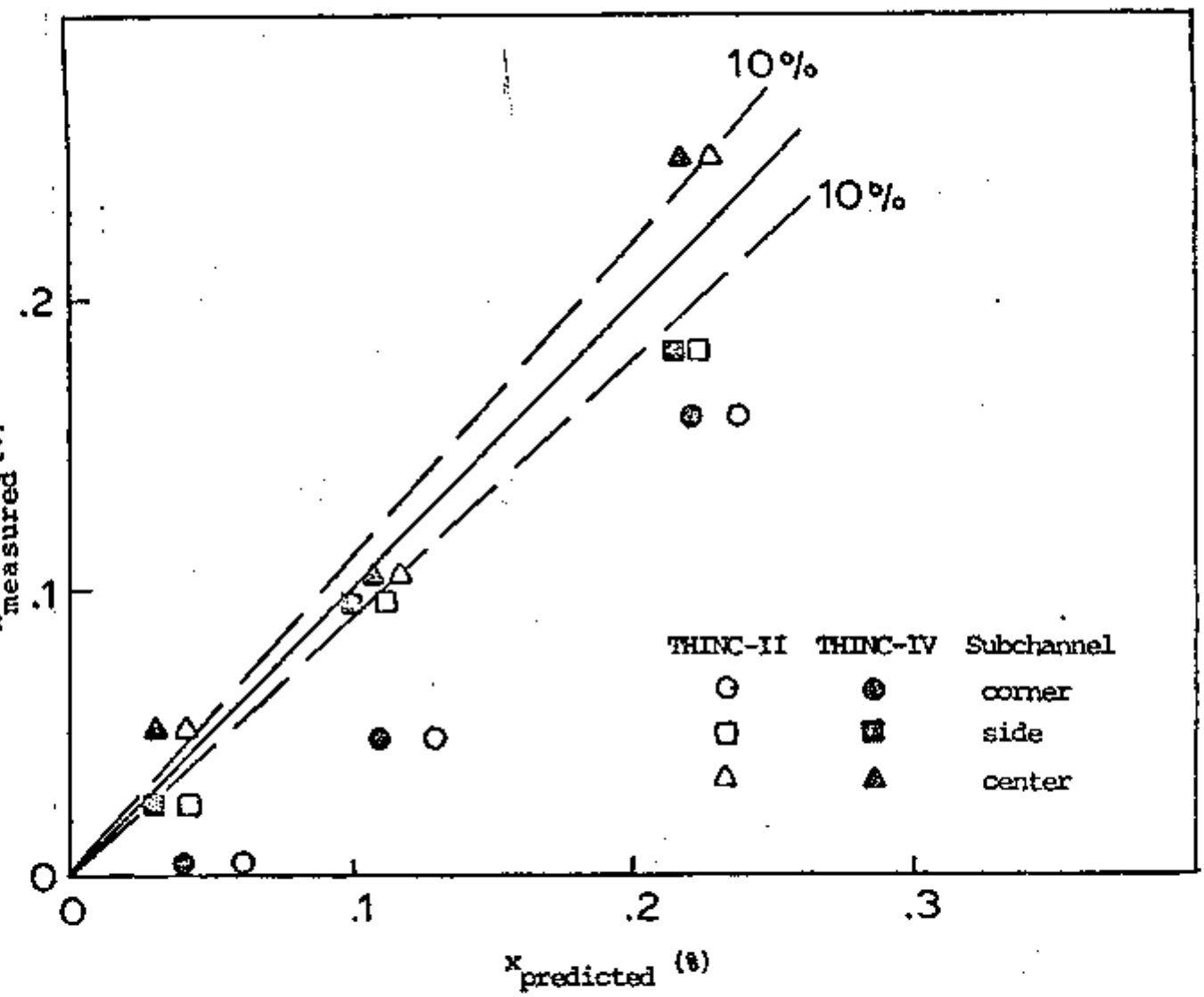

Fig. 3.12 - THINC-II and THINC-IV Results for GE Runs 2E1, 2E2 and 2E3. Qualities.

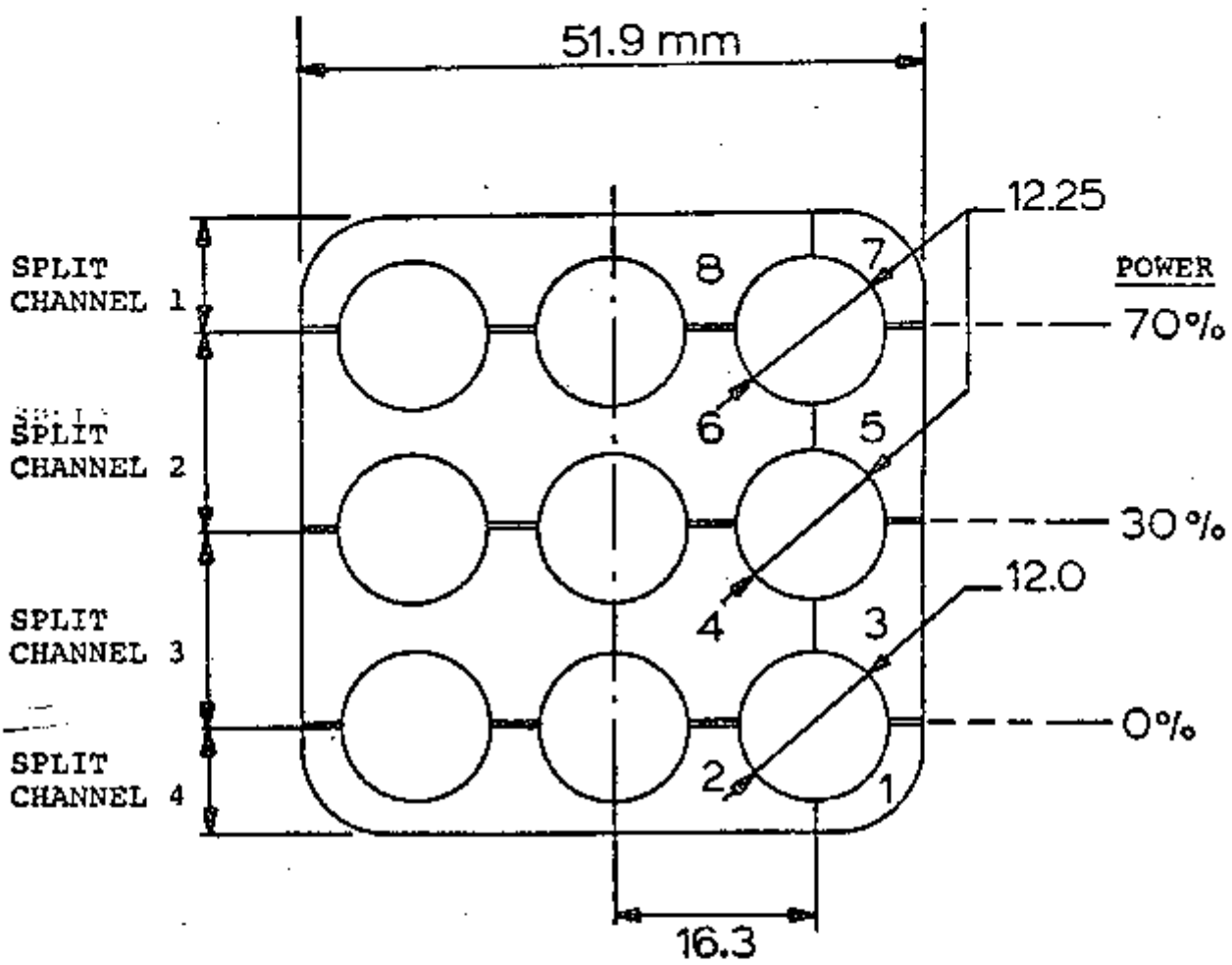

Fig. 3.13 - Geometry of the Studsvik Nine-Rod Bundle

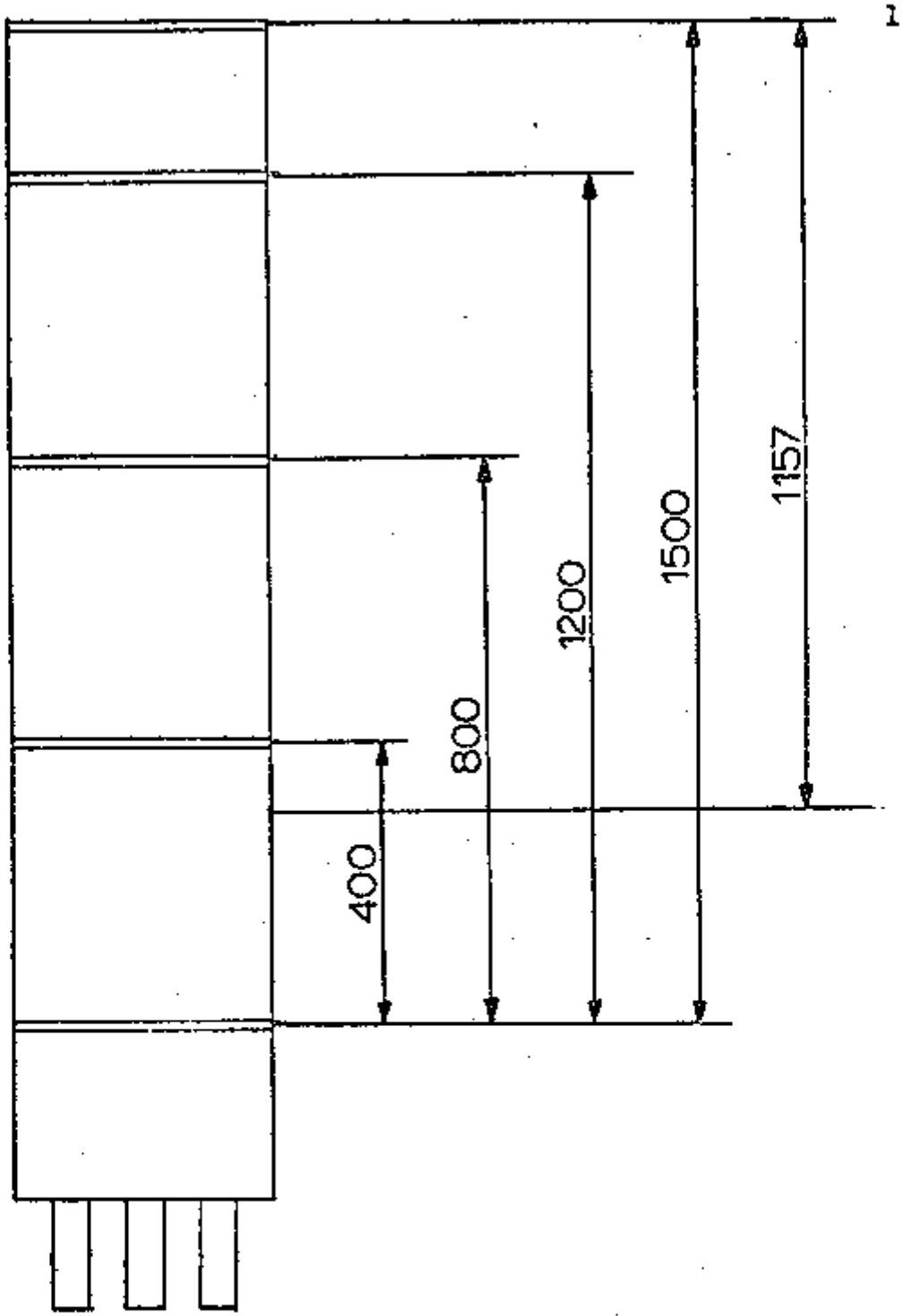

Fig. 3.14 - Axial Location of the Spacers in the Studsvik Nine-Rod Bundle

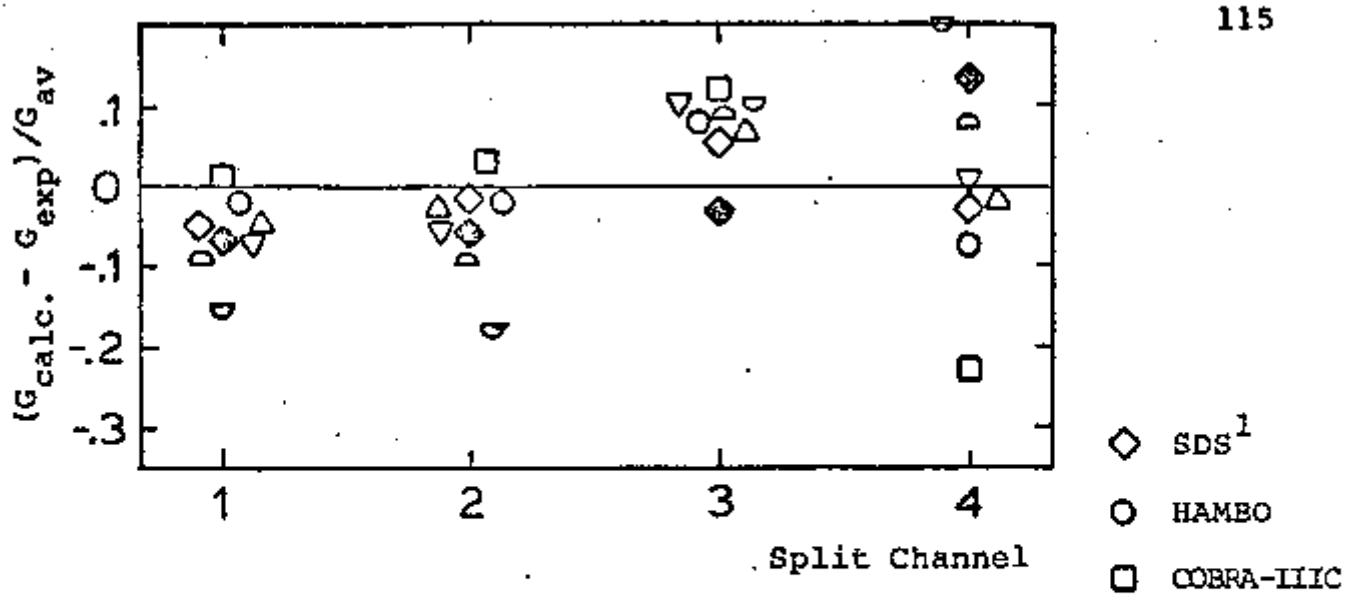

Fig 3.15 - Comparison between Measured and Predicted Split Channel Exit Mass Velocities for Case 1 of the Studsvik Test

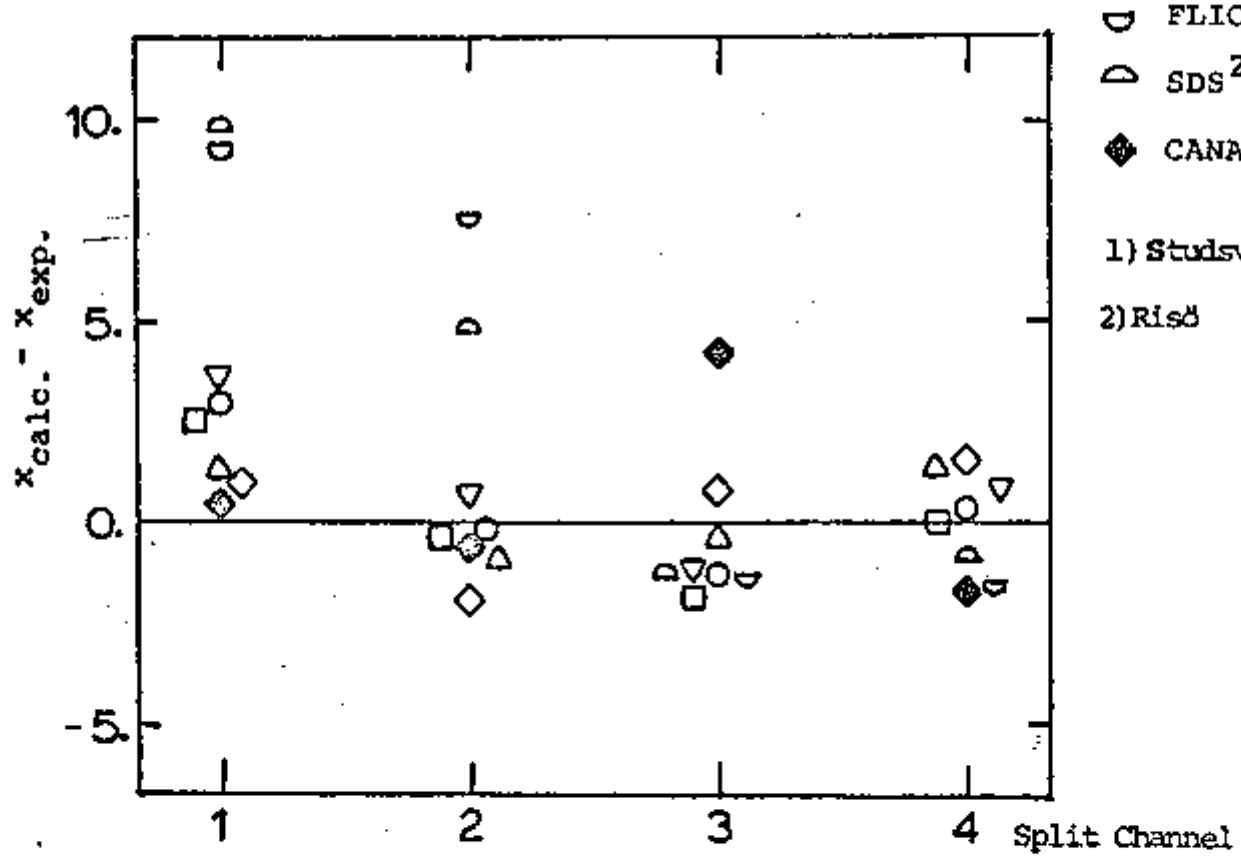

Fig. 3.16 - Comparison between Measured and Predicted Split Channel Exit Qualities for Case 1 of the Studsvik Test

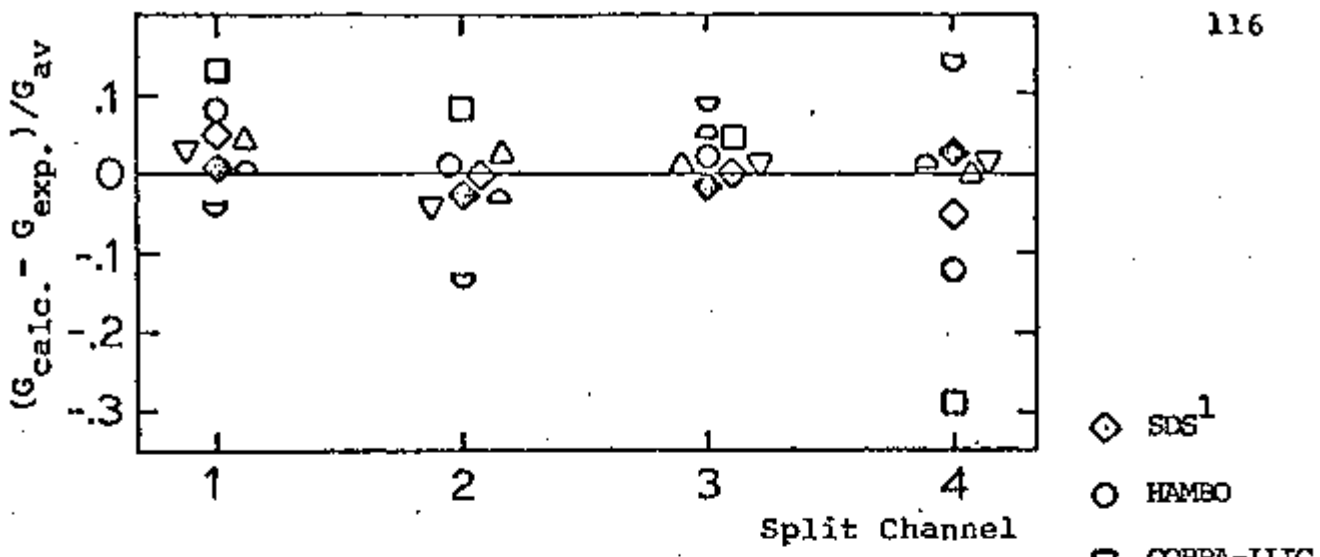

Fig. 3.17 - Comparison between Measured and Predicted split Channel Exit Mass Velocities for Case 2 of the Studsvik Test

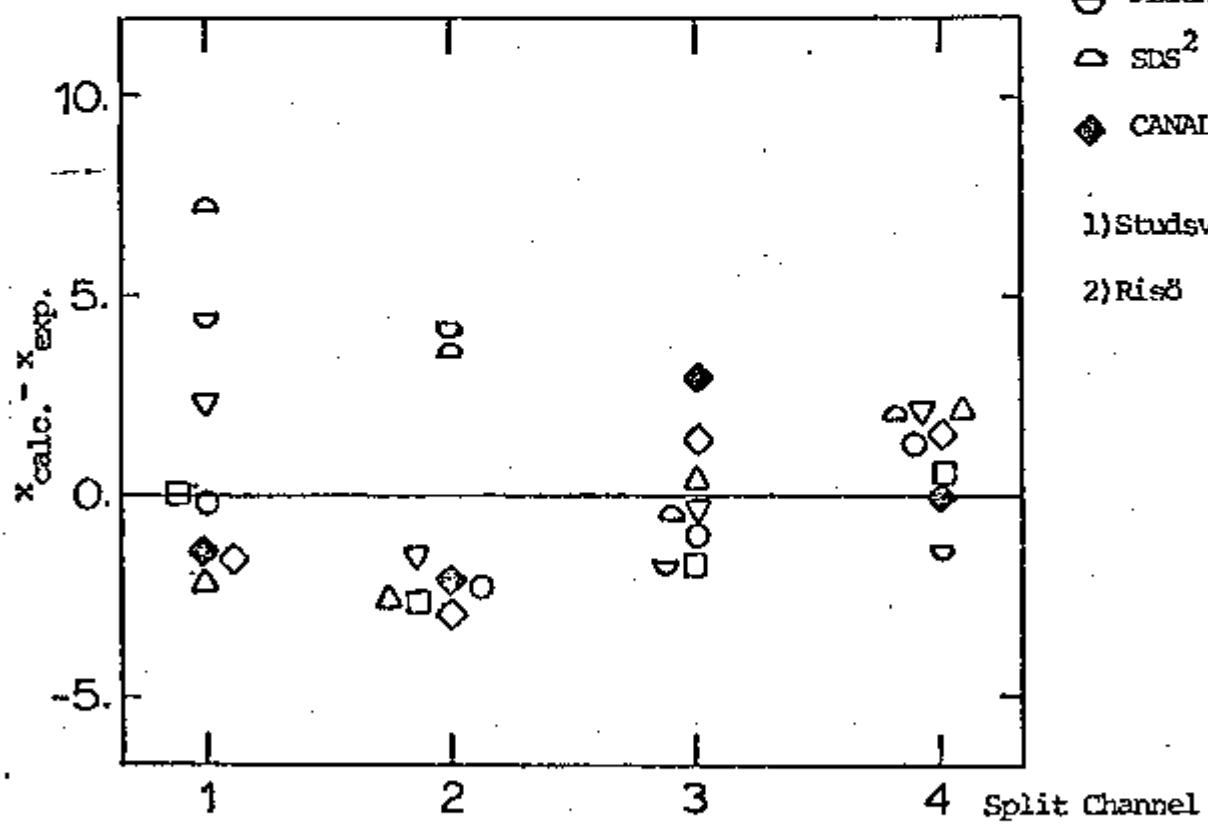

Fig. 3.18 - Comparison between Measured and Predicted Split Channel Exit Qualities for Case 2 of the Studsvik Test

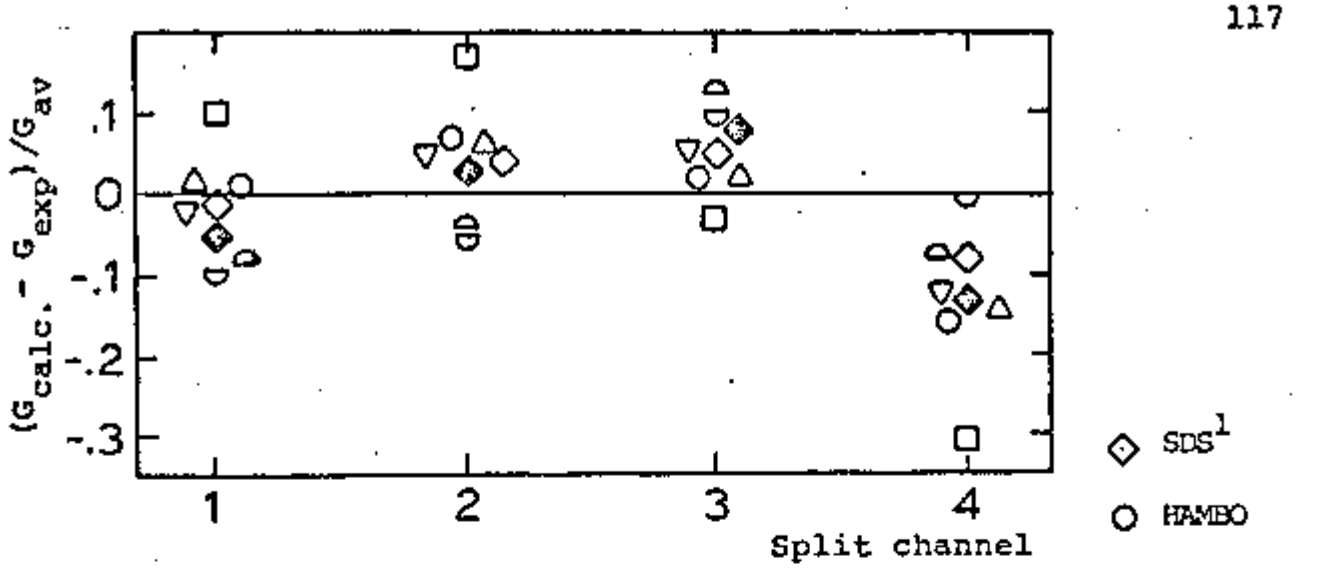

Fig. 3.19 - Comparison between Measured and Predicted Split Channel Exit Mass Velocities for Case 3 of the Studsvik Test

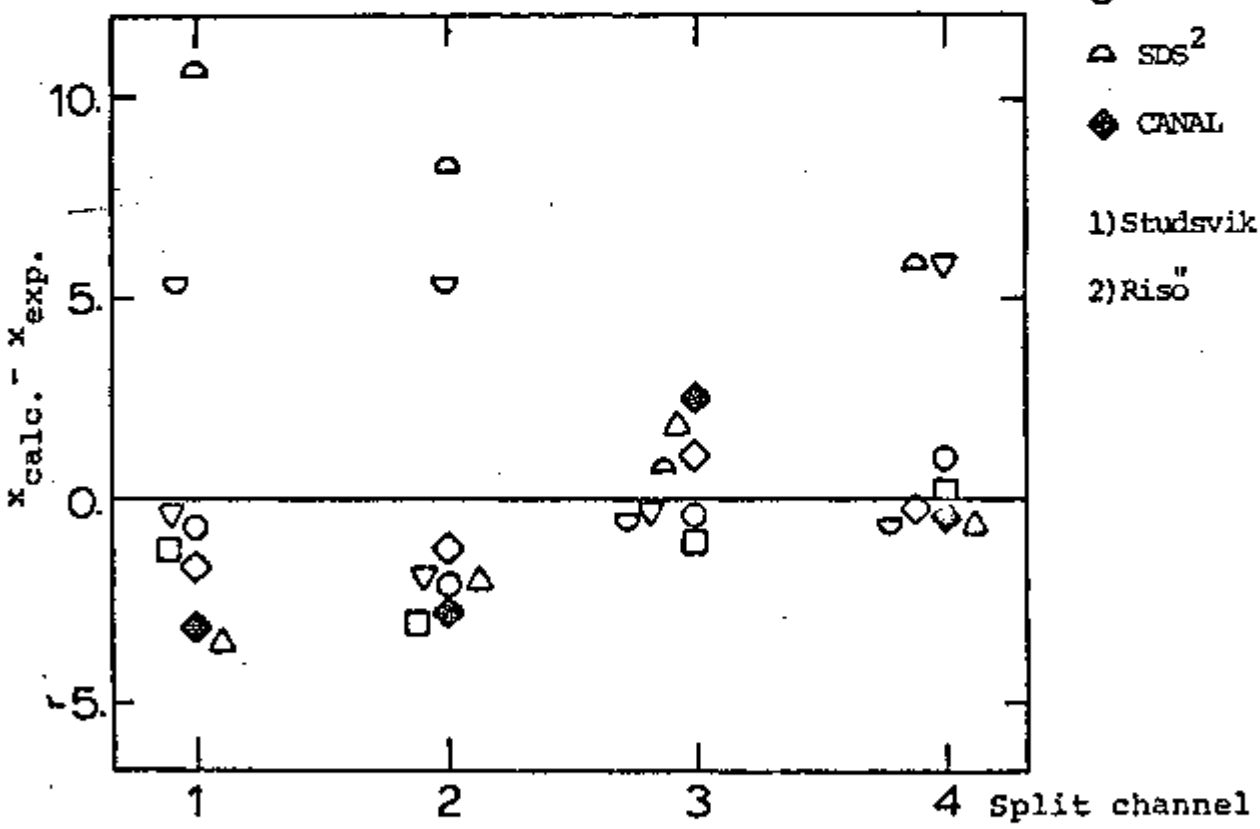

Fig. 3.20 - Comparison between Measured and Predicted Split Channel Exit Qualities for Case 3 of the Studsvik Test

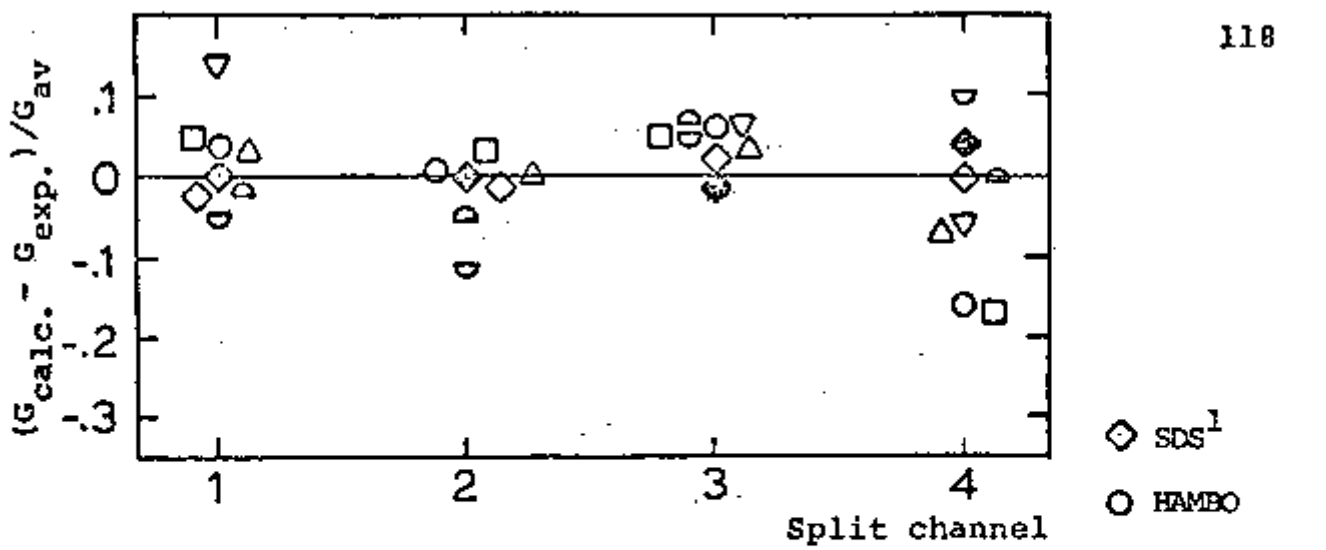

Fig. 3.21 - Comparison between Measured and Predicted Split Channel Exit Mass Velocities for Case 4 of the Studsvik Test

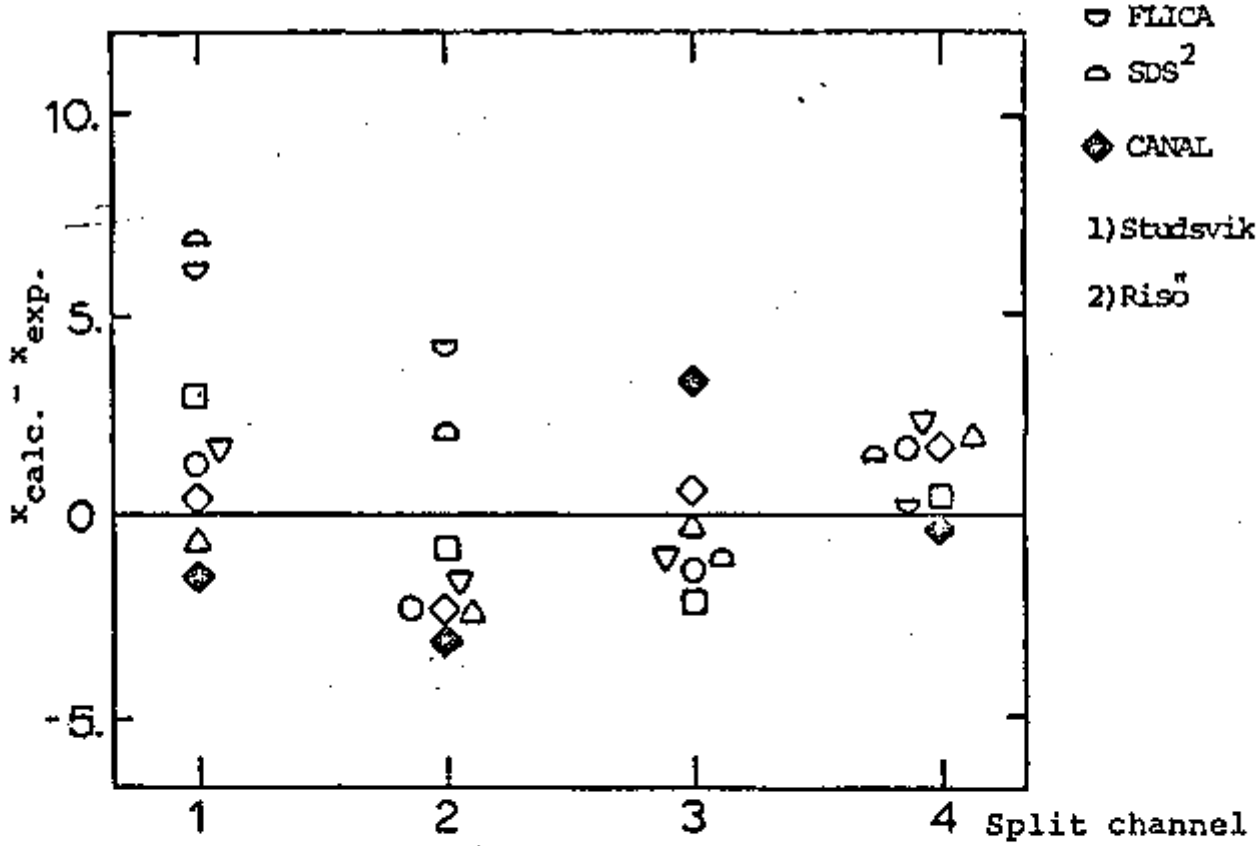

Fig. 3.22 - Comparison between Measured and Predicted Split Channel Exit Qualities for Case 4 of the Studsvik Test

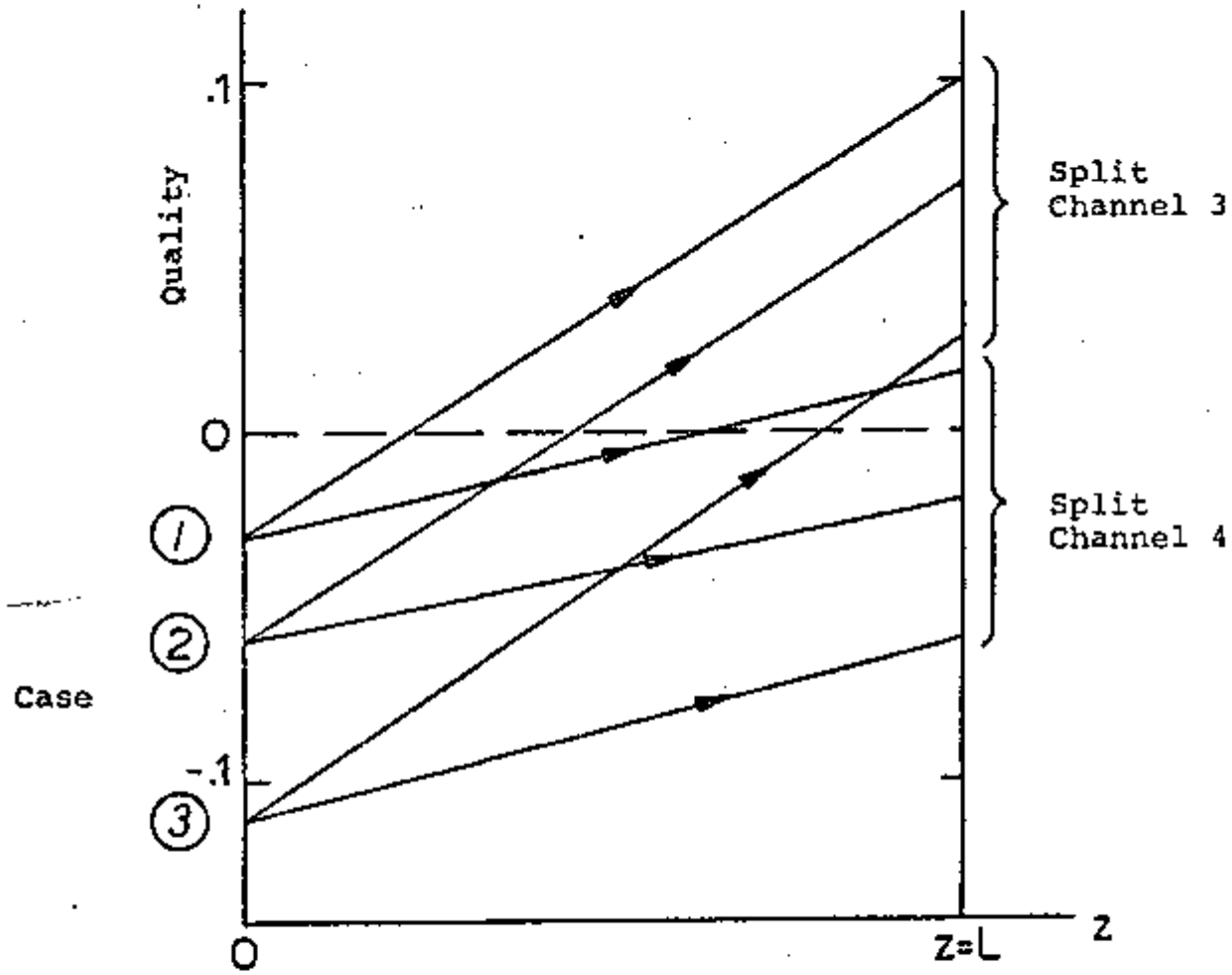

Fig. 3.23 - Estimated Behavior of the Quality along the Bundle Length for Split Channels 3 and 4 of the Studsvik Test.

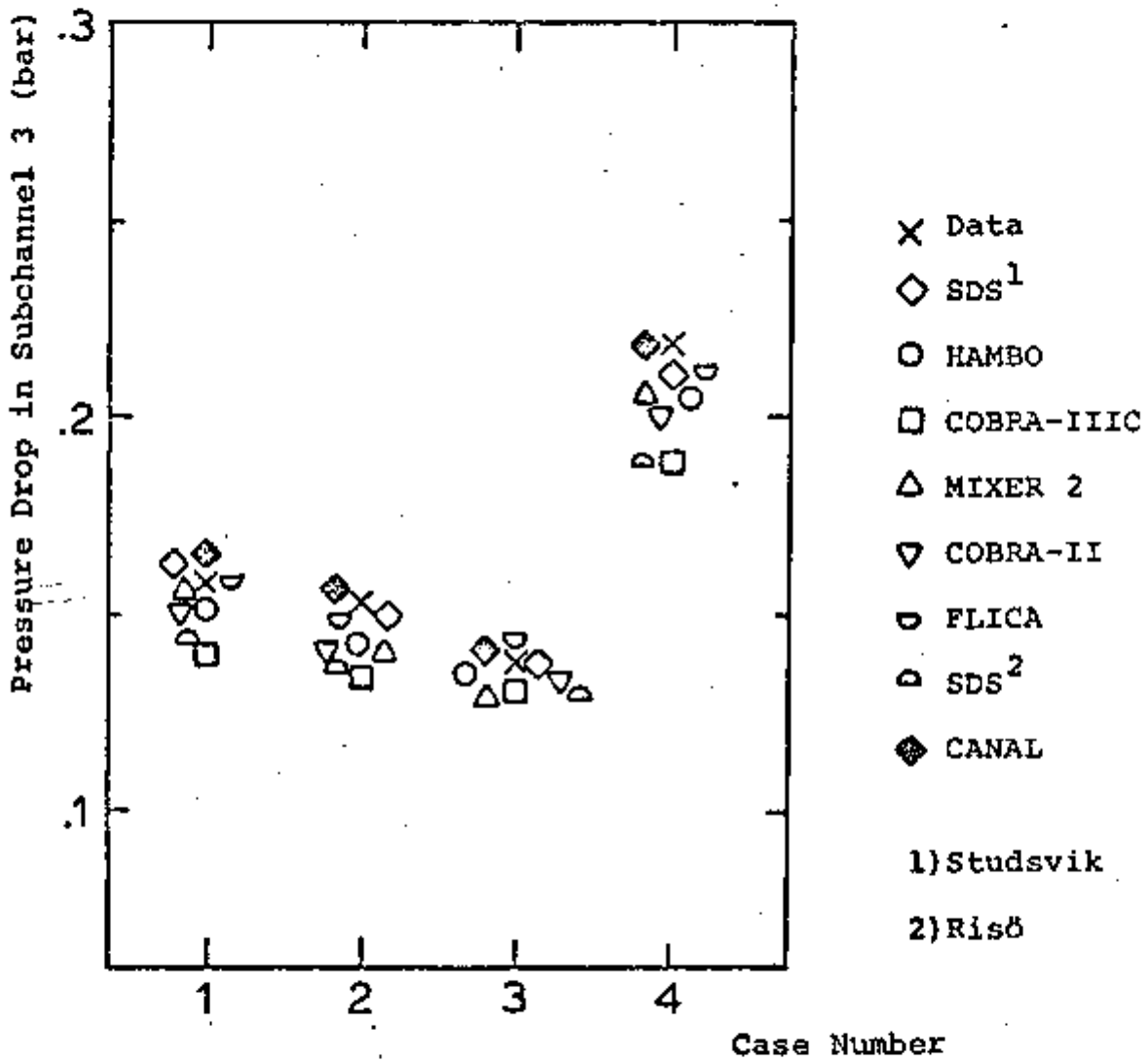

Fig. 3.24 - Comparison between Measured and Predicted Pressure Drop for Cases 1 to 4 of the Studsvik Test.

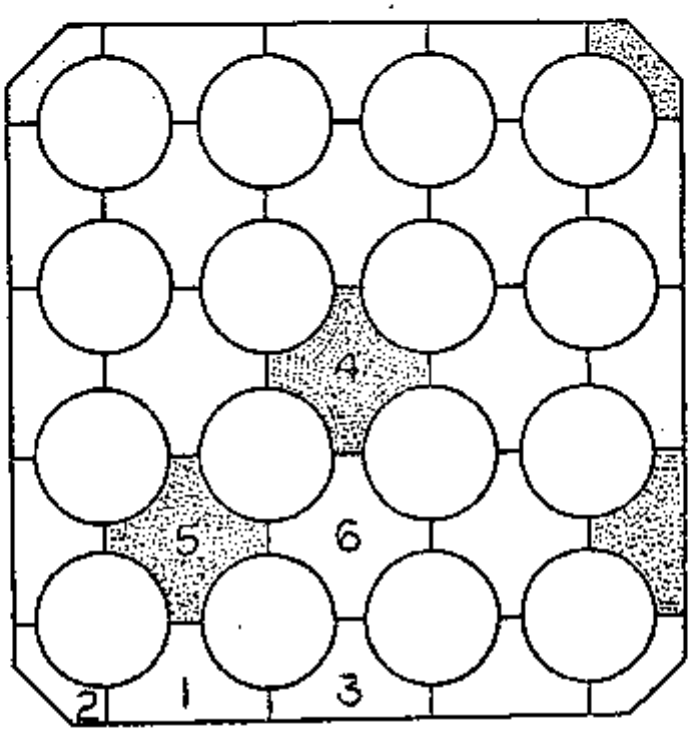

Fig 3.25 - Cross Section of the Ispra Sixteen-Rod Bundle

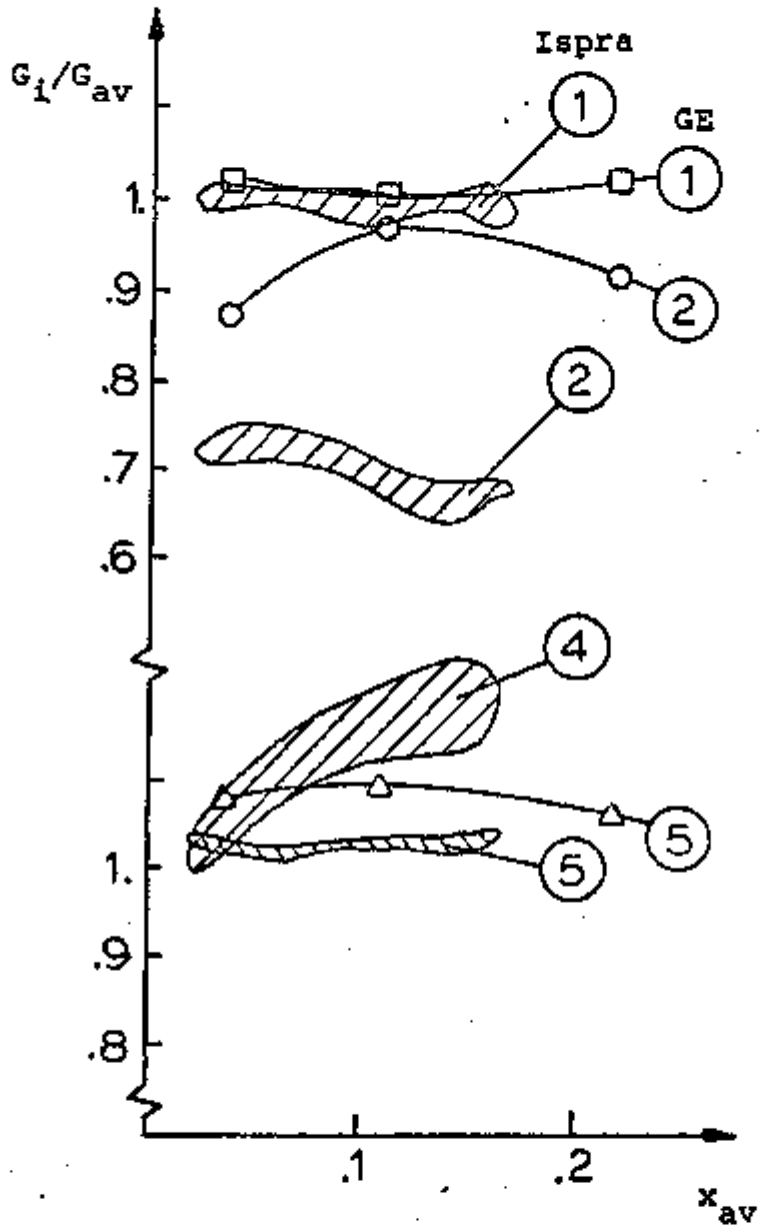

Fig. 3.26 - Comparison between Ispra and GE Exit Mass Velocity Distributions at $\bar{G}$ = 1500 Kg/m^{2}s .

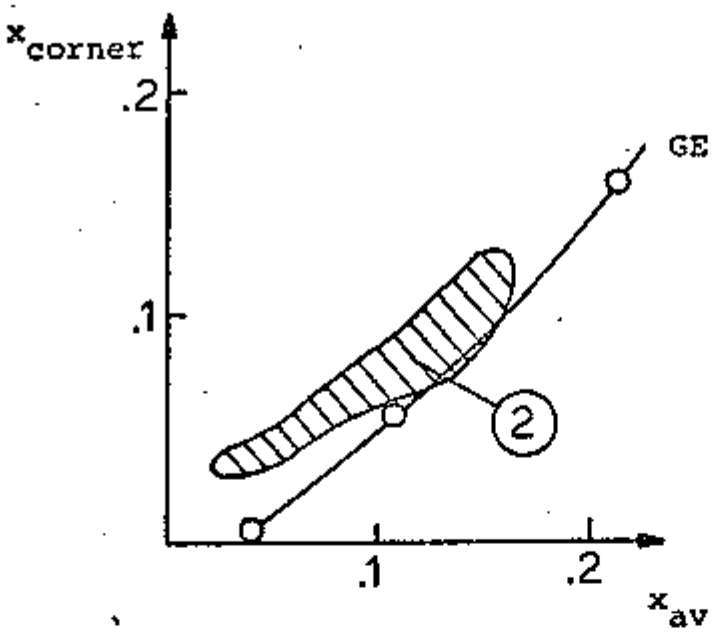

Fig. 3.27- Comparison between Ispra and GE Corner Subchannel Exit Quality at $\bar{G}$ = 1500 Kg/m^{2}s.

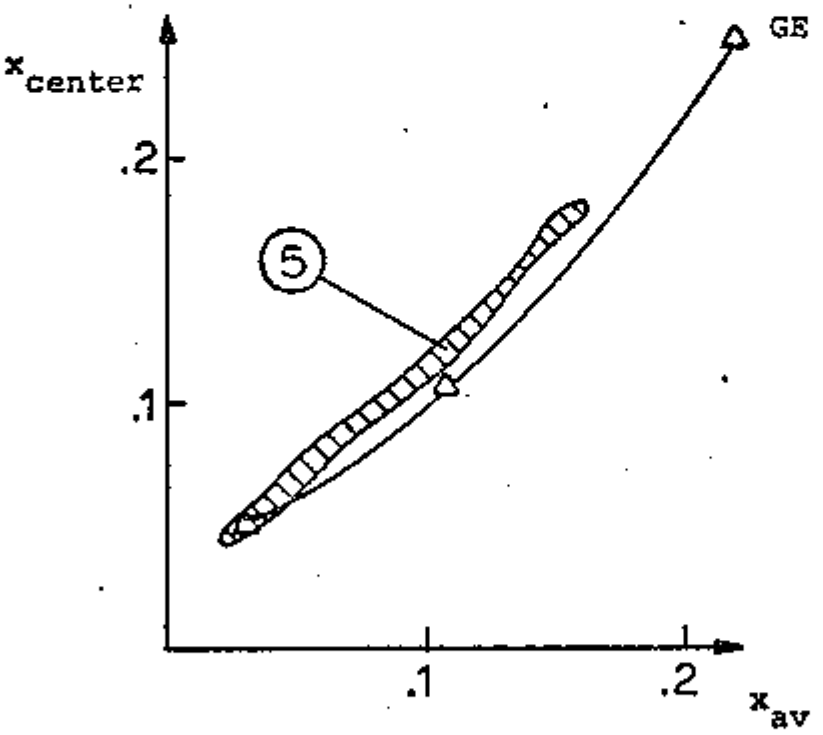

Fig. 3.28 - Comparison between Ispra and GE Center Subchannel Exit Quality at $\bar{G}$ = 1500 Kg/m^{2}s.

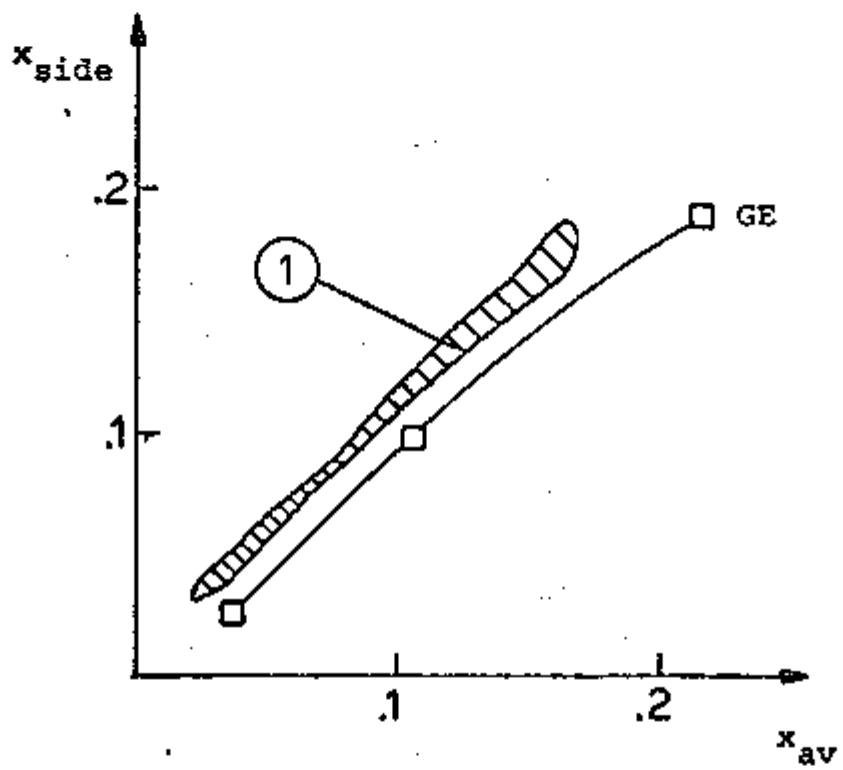

Fig. 3.29 - Comparison between Ispra and GE Side Subchannel Exit Quality at $\bar{G}$ = 1500 Kg/m^{2}s

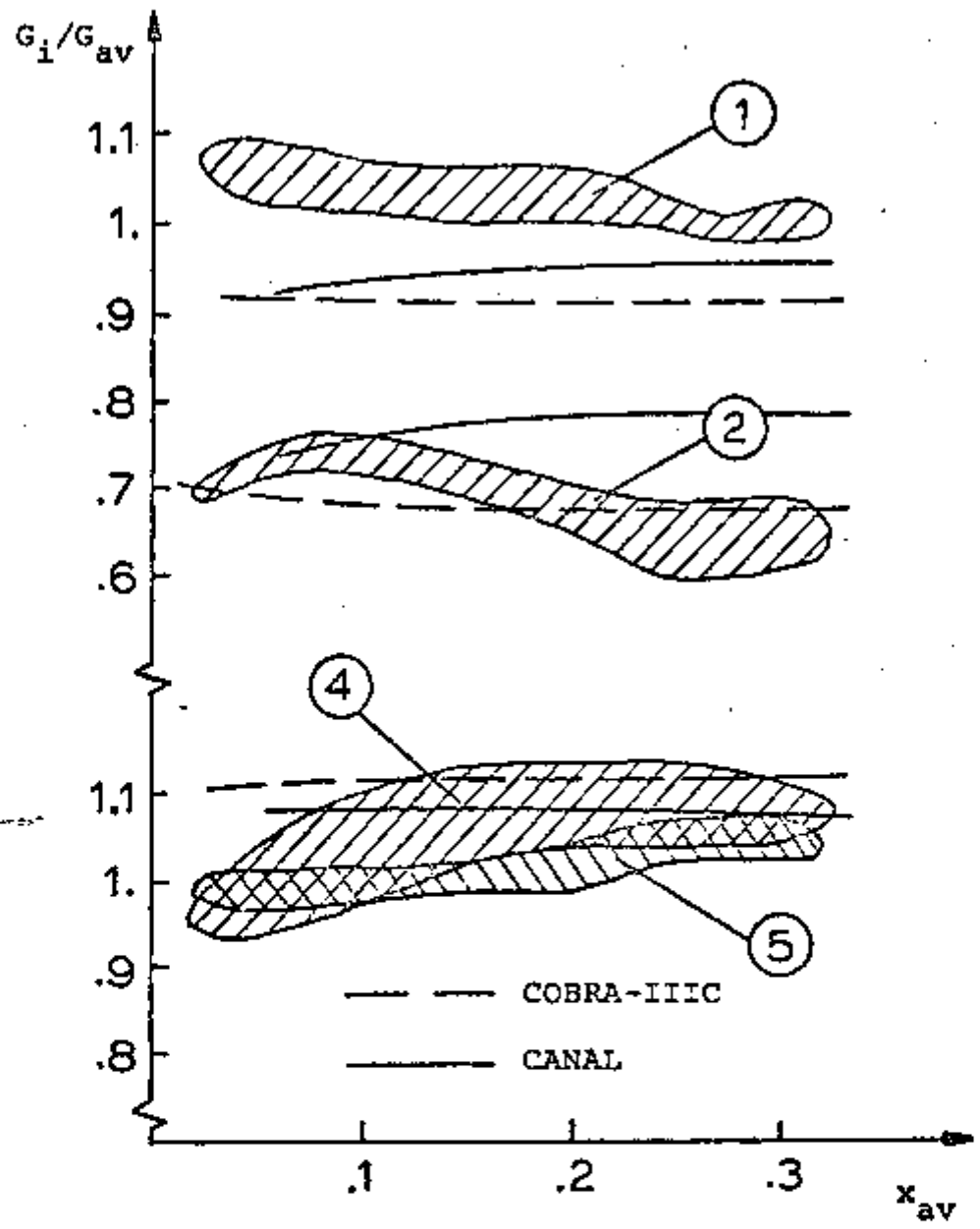

Fig. 3.30 - Comparison between Measured and Predicted Exit Mass Velocity Distribution for the Ispra Test at $\bar{G}$ = 1000 Kg/m^{2}s.

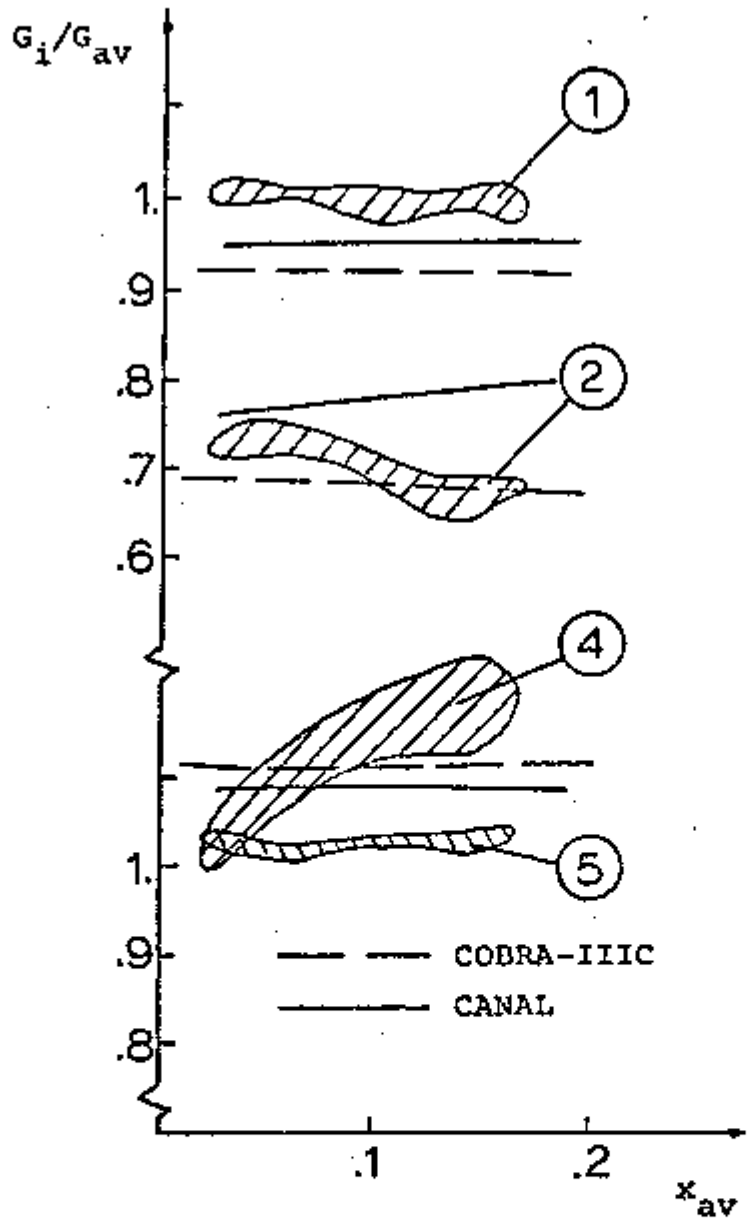

Fig. 3.31 - Comparison between Measured and Predicted Exit Mass Velocity Distribution for the Ispra Test at $\bar{G}$ = 1500 Kg/m^{2}s.

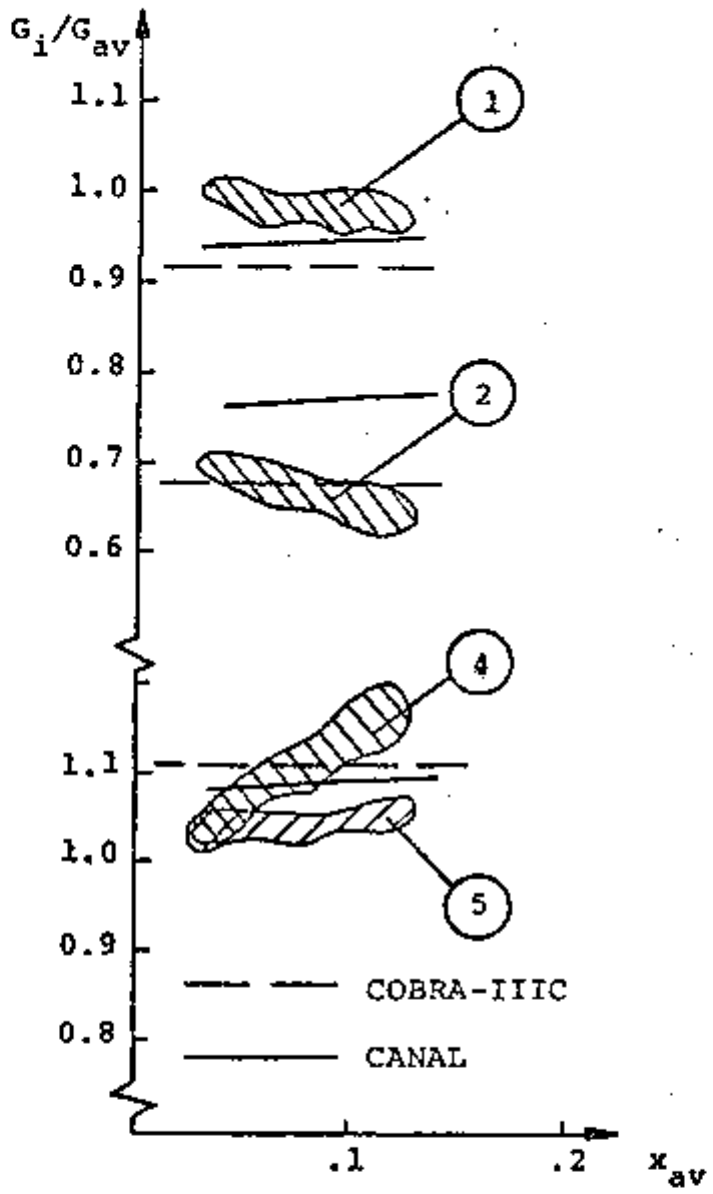

Fig. 3.32 - Comparison between Measured and Predicted Exit Mass Velocity Distribution for the Ispra Test at $\bar{G}$ = 2000 Kg/m^{2}s.

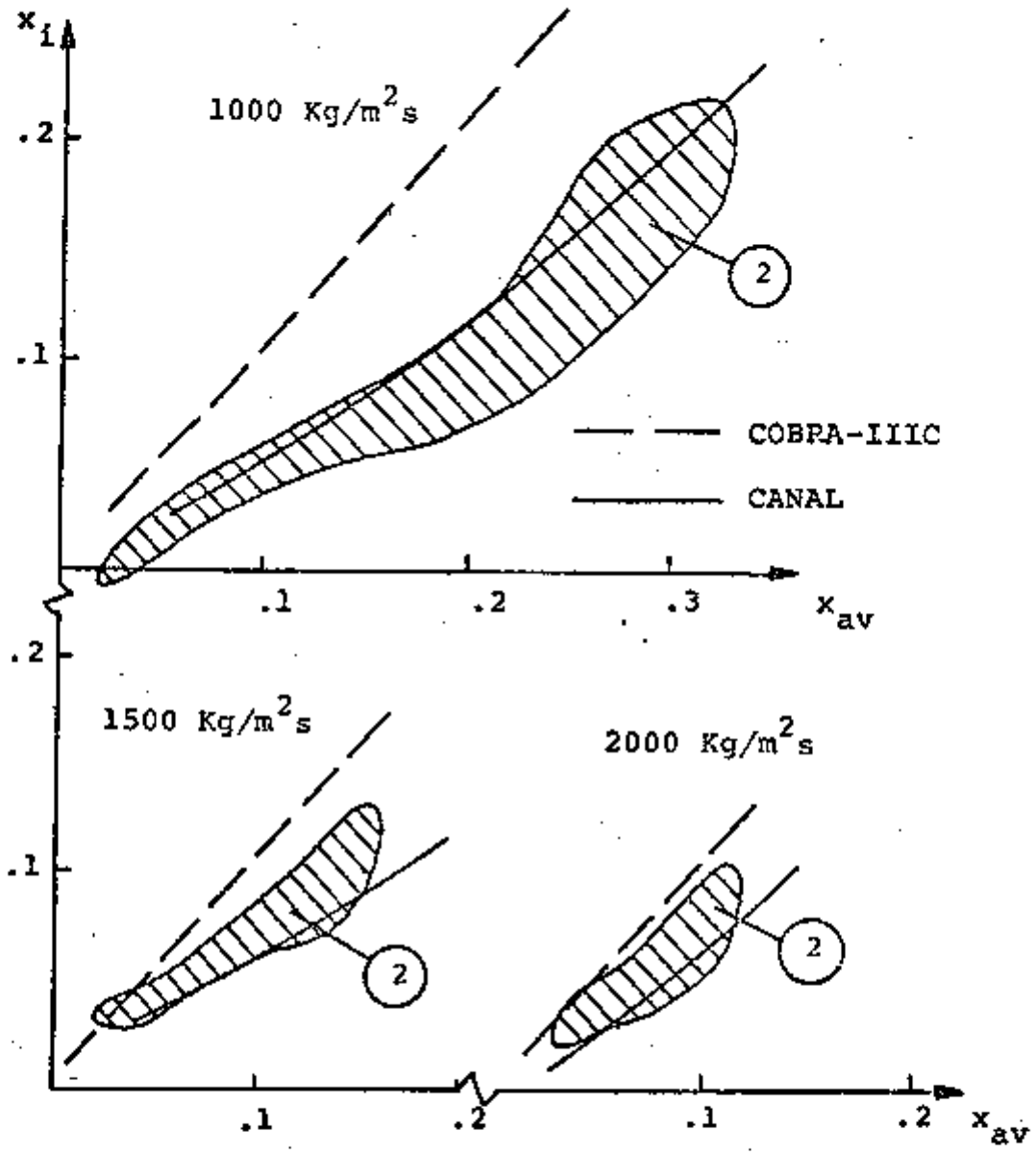

Fig. 3.33 - Comparison between Measured and Predicted Corner Subchannel Exit Quality for the Ispra Test.

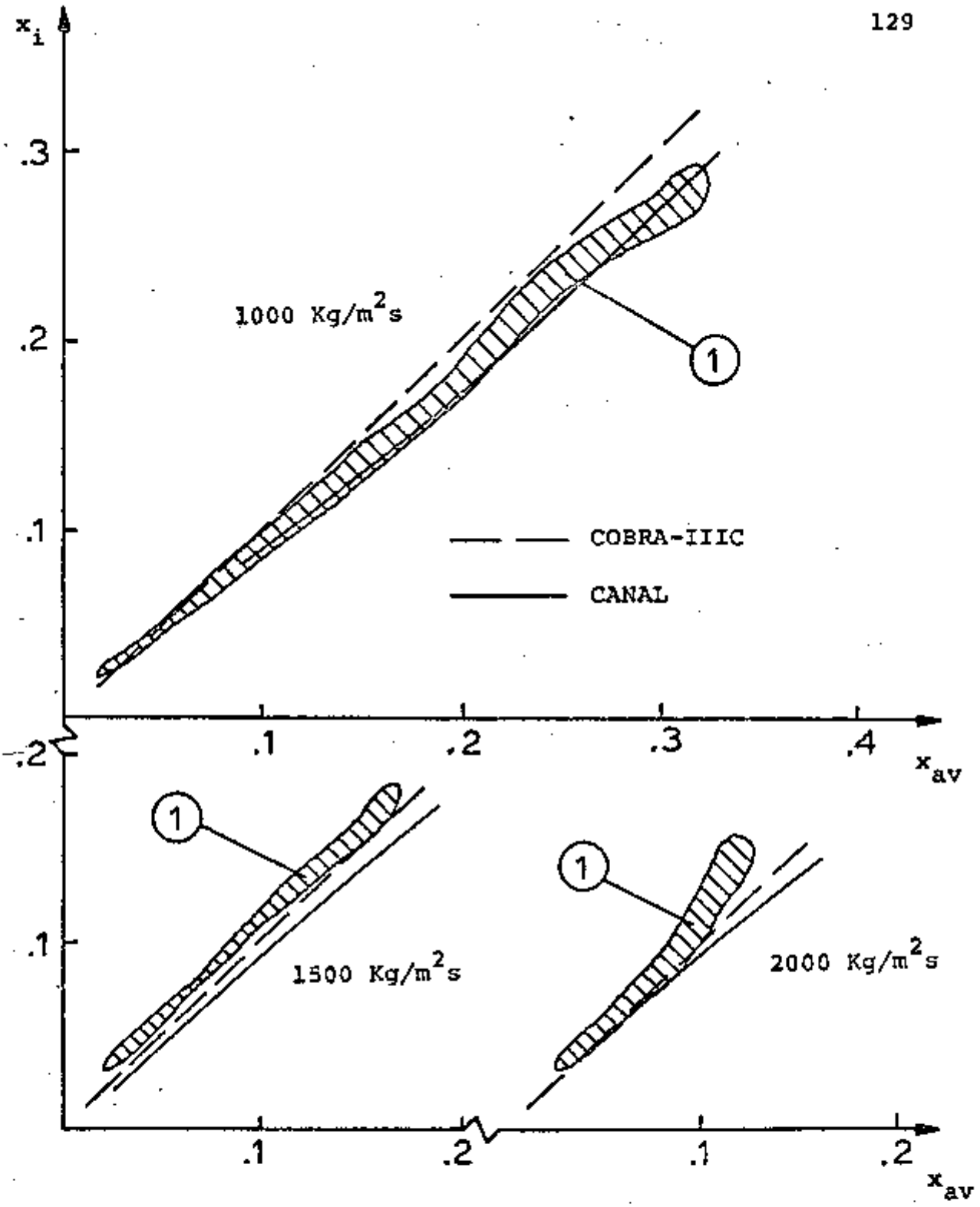

Fig. 3.34 - Comparison between Measured and Predicted Side Subchannel Exit Quality for the Ispra Test.

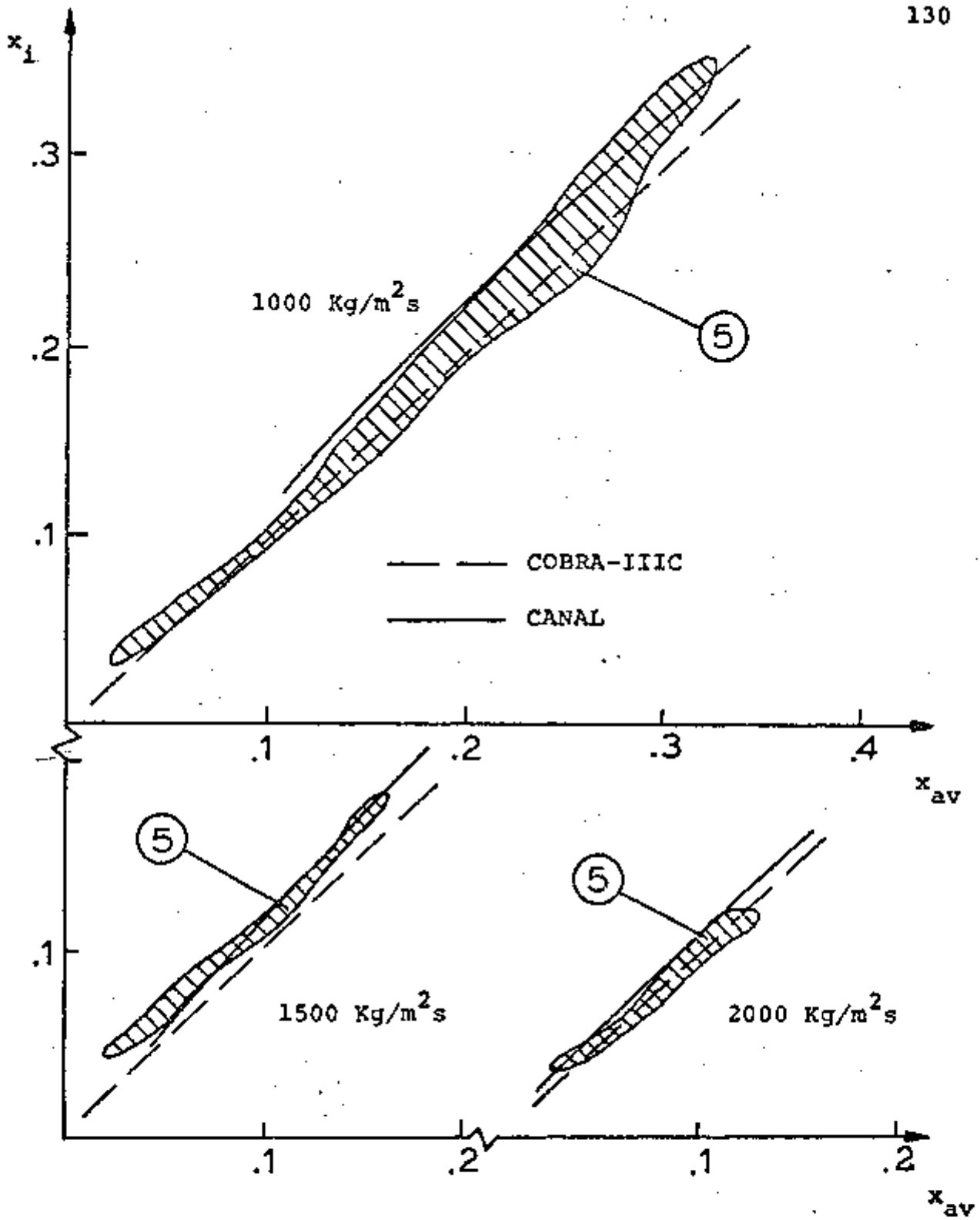

Fig. 3.35 - Comparison between Measured and Predicted Inner Subchannel Exit Quality for the Ispra Test.

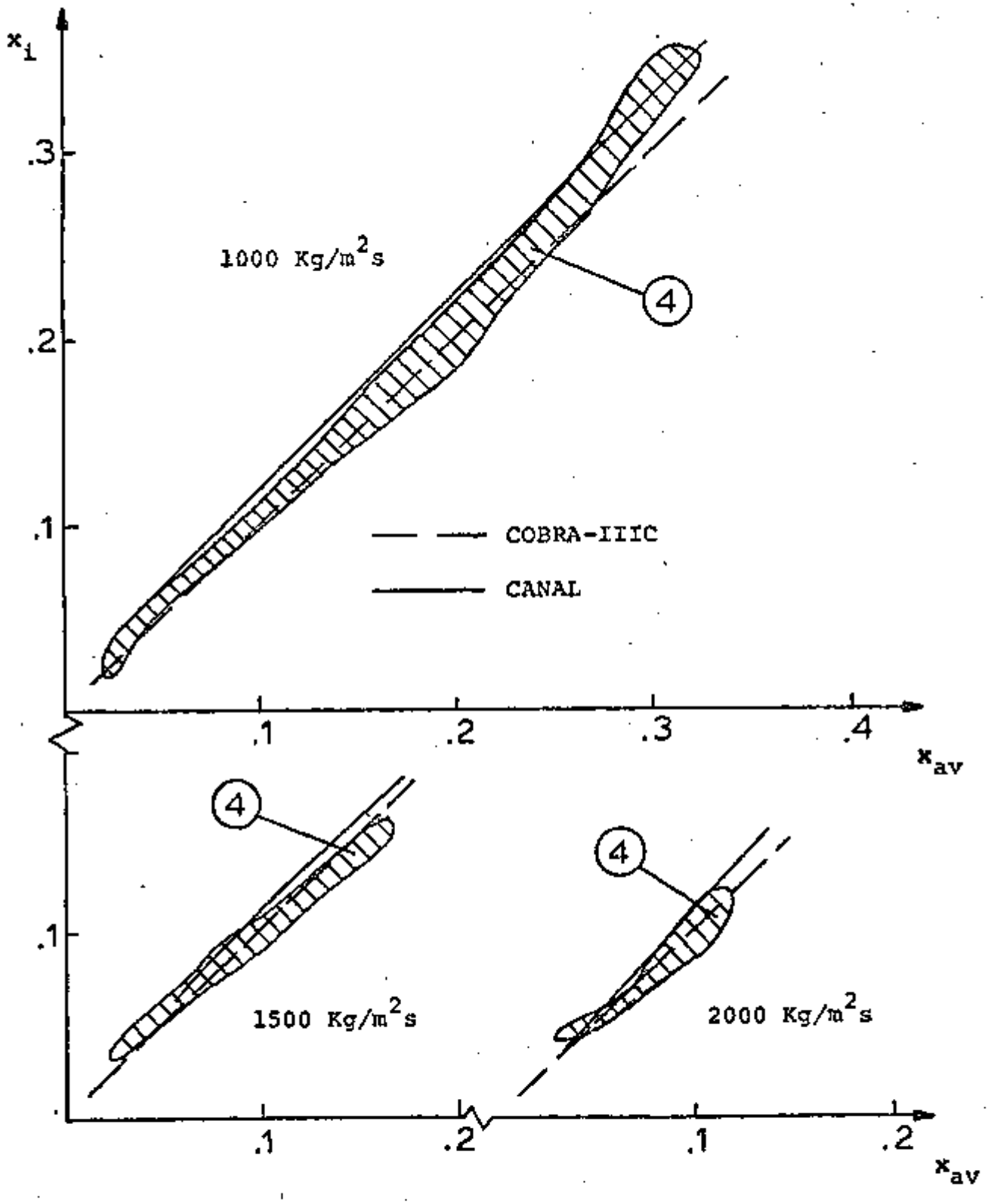

Fig. 3.36 - Comparison between Measured and Predicted Center Subchannel Exit Quality for the Ispra Test.

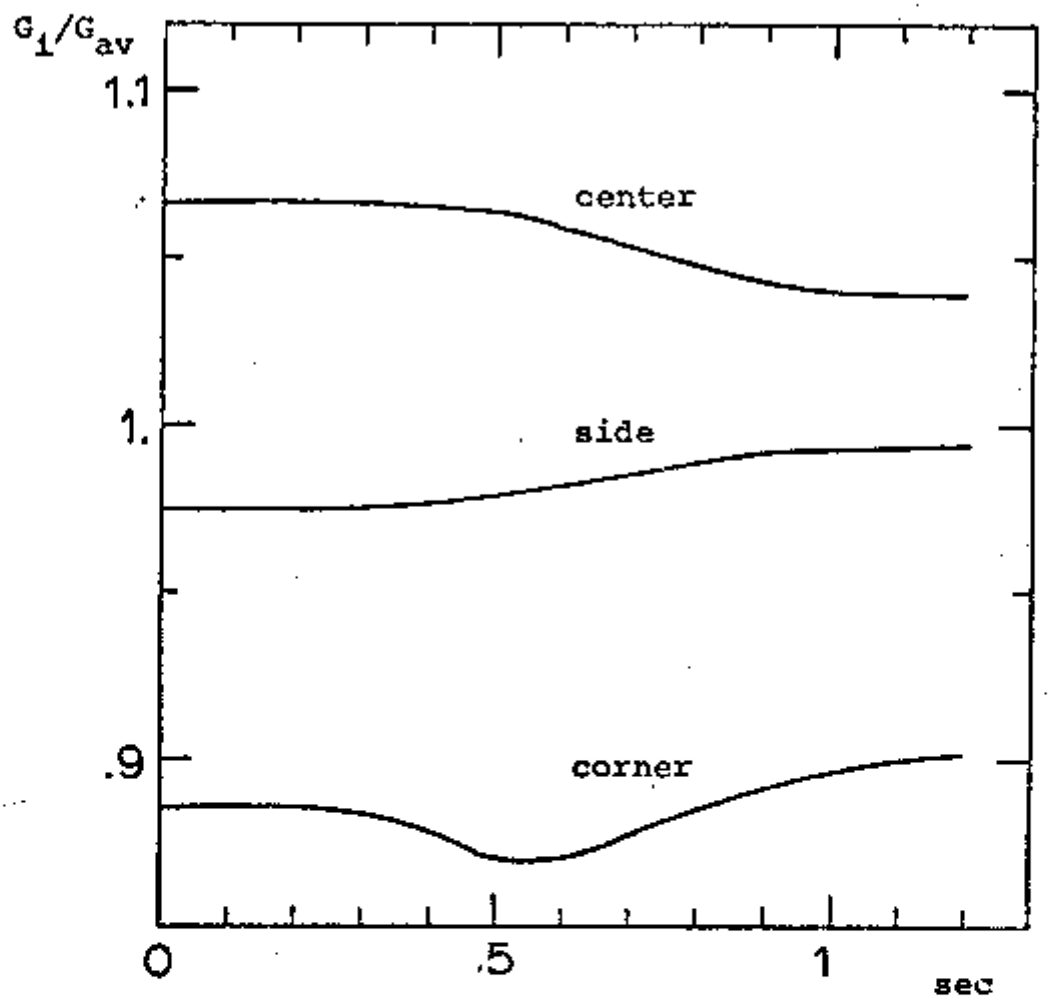

Fig. 3.37 - Exit Mass Velocity Distribution as Function of Time for the Mass Decay Transient.

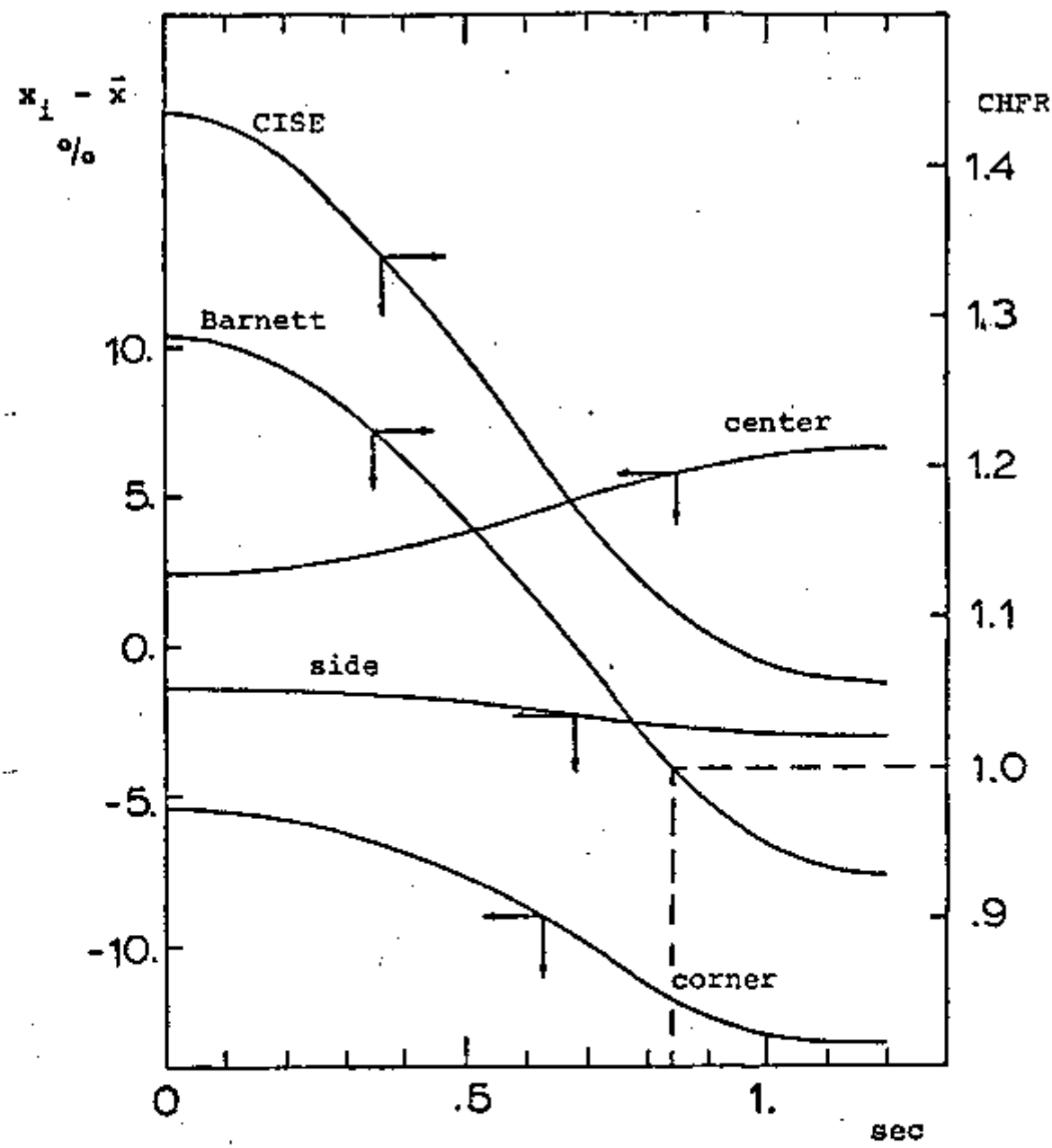

Fig. 3.38 - Deviation of Exit Quality from Bundle Average Exit Quality and CHFR as Function of Time for the Mass Decay Transient.

CHAPTER 4 - CONCLUSIONS

In this study the program CANAL has been developed and assessed against the following set of experimental data:

(A) GE nine-rod bundle under isothermal conditions;
(B) GE nine-rod bundle with uniform radial heating;
(C) GE nine-rod bundle with non-uniform radial heating;
(D) Studsvik nine-rod bundle with non-uniform radial heating;
(E) Ispra sixteen-rod bundle with uniform radial heating.

Besides benchmarking the code against actual test data, it was also the intention of this study to compare CANAL with the results of other commonly used subchannel codes. Fortunately, for all experiments considered a number of subchannel code results were available thus allowing a direct comparison of these codes against the experimental data and against CANAL. From the results displayed in Chapter 3 the following overall conclusions can be drawn:

(1) One of the most significant phenomena observed in experiments (B), (C) and (E) was the lateral drift of the vapor to the higher velocity regions of the bundle. That is, the center subchannel quality was measured as the highest whereas the corner subchannel exit quality was the lowest for all cases in spite of the corner subchannel displaying the highest power/flow area ratio. This phenomenon is incorporated in the mixing model of CANAL and, accordingly, CANAL predictions follow the observed trends mentioned above. The results of COBRA-IIIC, COBRA-IV, THINC-II and THINC-IV for these tests reveal that these programs fail to simulate the correct trends basically because the mixing models built into these codes are based on single-phase turbulent exchange considerations which are simply extended to two-phase conditions.

(2) CANAL is capable of simulating the phenomenon of turbulent mixing enhancement due to flow regime changes observed in experiment B (GE-2E1, -2E2 and -2E3). In CANAL the rate of mixing is assumed to be maximum at the slug-annular transition. However, this apparently leads to an underestimation of the mixing rate under bubble flow conditions (GE-2B2, -2C1, -2E1 and -2G1).

(3) CANAL results for experiment D are in satisfactory agreement with the measured data. The lateral vapor drift phenomenon in this case was overshadowed by the strong radial power tilt which is not typical of BWR design.

(4) In bundles typical of BWR design it seems appropriate to neglect transverse pressure gradients for single-phase conditions, for two-phase conditions with uniform radial heating and two-phase conditions with a moderate power tilt.

CHAPTER 5 - RECOMMENDATIONS

The following recommendations are made for future work:

1) As a final confirmation the code should be tested against experimental data for real size bundles, before using it for design purposes. Presently, however, this data is proprietary.

2) In order to analyze a larger set of problems an improvement of the present numerical scheme of CANAL is necessary. The use of a marching technique certainly provides a considerable payoff in terms of computational time but it lacks generality. It should be replaced by a numerical method that treats the real boundary value problem. J. Kelly* will investigate the use of the CANAL mixing model in the code THERMIT /R1/ which he is extending for subchannel analysis. THERMIT offers the choice of pressure or/and velocity boundary conditions.

3) The spectrum of currently available heat transfer correlations (Dittus-Boelter for single-phase and Chen for nucleate boiling) should be extended to include suitable post-CHF correlations. This would enable the user to test the calculations against clad temperature measurements under severe conditions.

4) It would be desirable to check the assumptions made in the formulation of the mixing model by means of an experiment. This experiment would be performed in a heated rod bundle operating at typical BWR conditions with an adiabatic length provided before the sampling location. The results would give information about the fully developed void fraction distuibution and its dependence on the mass velocity distribution. By varying the flow and power input it

---

* J. Kelly, Doctoral Thesis, MIT Nuclear Engineering Department (to appear)

would also be possible to investigate the rate of mixing between subchannels for a variety of flow regime conditions.

5) It would be desirable to examine the sensitivity of the calculated results to changes in the mixing parameters K_a and θ_M. Based on steady-state results presented in Chapter 3 the recommended values are K_a=1.4 and θ_M=5. However several experiments indicate that θ_M decreases as the mass velocity decreases. The GE, Studsvik and Ispra experiments would be valuable in assessing the dependence of θ_M on G for G in the range 0.5 - 1.5 Mlb/h-ft^2.

6) Future work should also consider the analytical models being developed by Drew et al./D3/ for determining radial void distribution in confined channels. Models have been derived for phase distribution mechanisms in two-phase pipe flow and the extension to subchannel geometry is certainly underway.

REFERENCES

B1) Bayoumi, M. et al., "Determination of Mass Flow Rate and Quality Distributions Between the Subchannels of a Heated Bundle", European Two-Phase Flow Meeting, Erlangen, Germany, (1976)

B2) Baroczy, C.J., "A Systematic Correlation for Two-Phase Pressure-Drop", Chem.Eng.Prog.Ser.64,

B3) Bennet, A.W. et al., "Flow Visualization Studies of Boiling Water at High Pressure", AERE-R 4874, (1965)

B4) Beus, S.G., "A Two-Phase Turbulent Mixing Model for Flow in Rod Bundles", WAPD-T-2438, (1971)

B5) Beus, S.G., J.H.Anderson and R.J.Decristofaro, "HOTROD-A Computer Program for Subchannel Analysis of Coolant Flow in Rod Bundles", WAPD-TM-1070, (1973)

B6) Bird, R.B., "Transport Phenomena", John Wiley & Sons, Inc., (1960)

B7) Boure, J.A., "On a Unified Presentation of the Non-Equilibrium Two-Phase Flow Models", ASME Symposium, Houston, (1975)

B8) Bowring, R.W., "Physical Model Based on Bubble Detachment and Calculations of Steam Voidage in the Subcooled Region of a Heated Channel", HPR-10, (1962)

B9) Bowring, R.W., "HAMBO - A Computer Program for the Subchannel Analysis of the Hydraulic and Burnout Characteristics of Rod Clusters. Part 2: the Equations", AEEW-R582, (1968)

B10) Barnett, P.G., "A Correlation of Burnout Data for Uniformly Heated Annuli and its Use for Predicting Burnout in Uniformly Heated Rod Bundles", AEEW-R-463, (1966)

B11) Bertoletti, S. et al., "Heat Transfer Crisis with Steam-Water Mixtures", Energia Nucleare 12, 121-172, (1965)

C1) Casterllana, F.S., and J.E. Casterline, "Subchannel Flow and Enthalpy Distribution at the Exit of a Typical nuclear Fuel Core Geometry", Nucl.Eng.Des.22, 3-18, (1972)

C2) Chawla, T.C. et al., "The Application of the Collocation Method Using Hermite Cubic Splines to Nonlinear Transient One-Dimensional Heat Conduction Problems", ASME Paper 76-HT-B, (1976)

C3) Chawla, T.C. and M. Ishii, "Equations of Motion for Two-Phase Flow in a Pin Bundle of a Nuclear Reactor", Int.J.Heat Mass Transfer 24, 1057-1068, (1978) also ANL/RAS 77-41

C4) Chelemer, H. et al., "An Improved Thermal Hydraulic Analysis Method for Rod Bundle Cores", Nuc.Eng.Des.41, 219-229, (1977)

C5) Chelemer, H. et al., "THINC-IV - An Improved Program for Thermal-Hydraulic Subchannel Analysis of Rod Bundle Cores", WCAP-7956, (1973)

C6) Chen, J.C., "A Correlation for Boiling Heat Transfer to Saturated Fluids in Convective Flow", ASME Paper 63-HT-34, (1963)

C7) Collier, J.G., "Convective Boiling and Condensation", McGraw-Hill, (1972)

D1) Douglas, J. and T. Dupont, "A Finite Element Collocation Method for Quasilinear Parabolic Equations:, Math.of Comp. 27, 17-28, (1973)

D2) Dukler, A.E. and Y.Taitel, "Flow Regime Transitions for Vertical Upward Gas Liquid Flow - A Preliminary Approach through Physical Modeling", NUREG-0162, (1977)

D3) Drew, D. et al., "Radial Phase Distribution Mechanisms in Two-Phase Flow", Second CSNI Specialist Meeting on Transient Two-Phase Flow, Paris, 12-14th June (1978)

F1) Finlayson, B.A., "The Method of Weighted Residuals and Variational Principles with Applications in Fluid Mechanics, Heat and Mass Transfer", Academic Press, N.Y., (1972)

F2) Forster, H.K. and N. Zuber, "Dynamics of Vapor Bubbles and Boiling Heat Transfer", A.I.Ch.E.J. 1, 474-488, (1954)

F3) Forti, G. and J.M. Gonzalez Santalo, "A Model for Subchannel Analysis of BWR Rod Bubbles in Steady State and Transient", Int.Conf. Reactor Heat Transfer, Kaulsruhe, Germany, (1973)

G1) Gaspari, G.P. et al., "Critical Heat Flux Prediction in Complex Geometries (annuli and clusters) from a Correlation Developed for Circular Conduits", CISE-R-276, (1968)

G2) Gaspari, G.P. et al., " Some Considerations of Critical Heat Flux in Rod Clusters in Annular Dispersed Vertical Upward Two-Phase Flow", 4th Int.Conf. Heat Transfer, Paris, (1970)

G3) Ginoux, J.J., "Two-Phase Flows and Heat Transfer", Hemisphere Publishing Corporation, (1978)

G4) Gonzalez-Santalo, J.M., "Two-Phase Flow Mixing in Rod Bundle Subchannels", Ph.D. Thesis, Dept. Mechanical Eng., M.I.T., (1972)

G5) Govier, G.W. and K. Aziz, "The Flow of Complex Mixtures in Pipes", Van Nostrand Reinhold Co., New York, (1972)

G6) Gustafsson, B. and J. Gransell, "Boundary Conditions for the Exercise at the European Two-Phase Flow Meeting 1976", AP-RL-7431, (1976)

H1) Harlow, F.H. and A-A. Amsden, "Flow of Interpenetrating Material Phases", Journal of Com.Phys.18, 440-464, (1975)

H2) Herkenrath, H. and Hufschmidt, W., "The Pressurized and Boiling Water Loops BOWAL and PRIL for Boiling Mixing Studies of the Heat Transfer Division JRC ISPRA/ Italy", EUR-6045, (1978)

H3) Herkenrath, H. et al., "Experimental Subchannel Investigation in a 15-Rod Test Section by Means of the Isokinetic Sampling Technique", 2nd Multi-Phase Flow and Heat Transfer Symposium Workshop, Miami, April 16-18, (1979)

H4) Hewitt, G.F. and N.S. Hall-Taylor, "Annular Two-Phase Flow", Pergamon Press, Oxford, (1970)

H5) Hsu, Y.Y. and R.W. Graham, "Transport Processed in Boiling and Two-Phase Systems", Hemisphere Publishing Corporation, (1976)

H6) Hughes, E.D., R.W. Lyczkowski and J.H. McFadden, "An Evaluation of State-of-the-Art Two-Velocity Two-Phase Flow Models and Their Applicability to Nuclear Reactor Transients", Vol.2 - Theoretical Bases, NP-143, (1976)

I1) Ishii, M., "One-Dimensional Drift Flux Model and Constitutive Equations for Relative Motion Between Phases in Various Two-Phase Flow Regimes", ANL-77-47, (1977)

I2) Ishii, M., T.C. Chawla and N. Zuber, "Constitutive Equation for Vapor Drift Velocity in Two-Phase Annular Flow", AIChe Journal 22, 283-289, (1976)

I3) Ishii, M., "Thermo-Fluid Dynamic Theory of Two-Phase Flow", Eyrolles, (1975)

J1) Jones, A.B., "Hydrodynamic Stability of a Boiling Channel", KAPL-2170, Knolls Atomic Power Laboratory, (1961)

L1) Lahey, R.T. and H.A. Schraub, "Mixing Flow Regimes and Void Fraction for Two-Phase Flow in Rod Bundles", Two Phase Flow and Heat Transfer in Rod Bundles, ASME Booklet, (1969)

L2) Lahey, R.T. et al., "Out-of-Pile Subchannel Meas urements in a Nine-Rod Bundle for Water at 1000 Psia", Int. Symposium on Two-Phase Systems", Haifa, Israel Aug.29-sep.2, (1971)

L3) Lahey, R.T. et al., "Mass Flux and Enthalpy Distribution in a Rod Bundle for Single and Two-Phase Flow Conditions", J. Heat Transfer 93, 197, (1971)

L4) Lahey, R.T., JR., "Two-Phase Flow in BWR", NEDO-13388, (1974)

L5) Lahey. R.T. and F.J. Moody, "The Thermal Hydraulics of a BWR", ANS Monograph (1975)

L6) Liles, D.R. and Wm.H. Reed, "A Semi-Implicit Method for Two-Phase Fluid Dynamics", J. of Computational Physics, vol 26, 390-407, (1978)

L7) Levy, S., "Forced Convection Subcooled Boiling - Prediction of Vapor Volumetric Fraction", GEAP-5157, (1966)

M1) Marinelli, V. and I. Pastori, "Pressure Drop Calculations in BWR Rod Bundles", European Two-Phase Flow Group Meeting, Casaccia, Rome, Italy, (1972) also CONF-720686-6, CONF-720607-38

M2) Martinelli, R.C. and D.B. Nelson, "Prediction of Pressure Drop During Forced Circulation Boiling of Water", Trans ASME 70, 695-702, (1948)

M3) McClellan, "Flow Stability in BWR Coolant Channels During Transients", M.S. Thesis, Dept.Mech.Eng., M.I.T., (1974)

M4) Meyer J.E., "Conservation Laws in One-Dimensional Hydrodynamics", WAPD-BT-20, (1960)

R1) Reed, W.H. and H.B. Stewart, "THERMIT - A Computer Program for Three-Dimensional Thermal-Hydraulic Analysis of Light Water Reactors", Internal M.I.T. Report, Dep. Nucl.Eng., (1978)

R2) Rogers, J.T. and N.E. Todreas, "Coolant Interchange Mixing in Reator Fuel Rod Bundles Single-Phase Coolant", Heat Transfer in Rod Bundles, ASME Booklet (1968)

R3) Rogers, J.T. and R.G. Rosehart, "Mixing by Turbulent Interchange in Fuel Bundles. Correlation and Inferences", ASME 72-HT-53, (1972)

R4) Rouhani, S.Z., "Calculation of Steam Volume Fraction in Subcooled Boiling", AE-286, (1967)

R5) Rouhani, S.Z. and E. Axelsson, "Calculation of Void Volume Fraction in the Subcooled and Quality Boiling Regions", AE-336, (1968)

R6) Rouhani, S.Z., "Axial and Transverse Momentum Balance in Subchannel Analysis", AE-480, (1973)

R7) Rowe, D.S., "Crossflow Mixing Between Parallel Flow Channels During Boiling -Part I - COBRA-Computer Program for Coolant Boiling in Rod Arrays", BNWL-371, Part 1, (1967)

R8) Rowe, D.S. and C.W. Angle, "Crossflow Mixing Between Parallel Flow Channels During Boiling -Part II- Measurement of Flow and Enthalpy in Two Parallel Channels", BNWL-371, Part 2, (1967)

R9) Rowe, D.S. and C.W. Angle, "Crossflow Mixing Between Parallel Flow Channels During Boiling -Part III- Effect of Spacers on Mixing Between Two Channels", BNWL-371, Part 3, (1969)

R10) Rowe, D.S. "A Mathematical Model for Transient Subchannel Analysis of Rod-Bundle Nuclear Fuel Elements", Journal of Heat Transfer, 211-217, (1973)

R11) Rowe, D.S., "COBRA-IIIC: A Digital Computer Program for Steady-State and Transient Thermal Hydraulic Analysis of Rod Bundle Nuclear Fuel Elements", BNWL-1695, (1973)

S1) Saha, P. and N. Zuber, "Point of Net Vapor Generation and Vapor Void Fraction in Subcooled Boiling", 5th Int. Heat Transfer Conf., Japan, (1974)

S2) Schraub, F.A. et al., "Two-Phase Flow and Heat Transfer in Multirod Geometries; Air-Water Flow Structure Data for a Round Tube, Concentric and Eccentric Annulus, four and Nine-Rod Bundle", GEAP-5739, (1969)

S3) Sha, W.T., "Boundary-Value Thermal Hydraulic Analysis of a Reactor Fuel Rod Bundle", Nucl.Sci Eng.59, (1976)

S4) Shiralkar, B.S. et al., "Transient Critical Heat Flux: Experimental Results", GEAP-13295, (1972)

S5) Stewart, C.W. et al., "Core Thermal Model: COBRA-IV Development and Applications", BNWL-2212, (1977)

T1) Thom, J.R.S., "Prediction of Pressure Drop During Forced Circulation Boiling of Water", Int.J. Heat Mass Transfer 7, (1964)

T2) Tong, L.S., "Boiling Heat Transfer and Two-Phase Flow",

U1) Ulrych, G. and H. Kemner, "Exercise of the European Two-Phase Flow Group Meeting 1976 - Survey on the Experimental and Computed Results", Erlangen, Germany, (1977)

W1) Wallis, G.B., "One-Dimensional Two-Phase Flow", McGraw-Hill, (1969)

W2) Weisman, J. and R.W. Bowring, "Methods for Detaited Thermal Hydraulic Analysis of Water Cooled Reactors", Nucl.Sci.Eng.57, 225-276, (1975)

W3) Whalley P.B., "The Calculation of Dryout in a Rod Bundle", Int. Journal of Multiphase Flow 2, 501-515, (1977)

W4) Wheeler, C.L. et al., "COBRA-IV-I: An Interim Version of COBRA for Thermal-Hydraulic Analysis of Rod Bundle Nuclear Fuel Elements and Cores", BNWL-1962, (1976)

W5) Wolf, 1. et al., "WOSUB - A Subchannel Code for Steady-State and Transient Thermal Hydraulics Analysis of BWR Fuel Pin Bundles Vol I - Model Description", Energy Lab., MIT-EL-78-023, (1978)

Y1) Yadigaroglu, G. and A. Maganas, "Quality and Mass Flux Distribution in an Adiabatic Three-Subchannel Test Section", UC-B/NE-3342, (1978)

Y2) Yeung, M.K., "The Application of the Collocation Method Using Hermite Cubic Polynomials to LWR Fuel-Pin Transient Conduction Problems", Special Problem in Nuclear Engeneering, M.I.T. Dept.of Nucl.Eng., (1975)

Z1) Zuber, N. and J.A. Findlay, "Average Volumetric Concentration in Two-Phase Flow Systems", Journal of Heat Transfer,

Z2) Zuber, N. et al., "Steady-State and Transient Void Fraction in Two-Phase Flow Systems", GEAP-5417, (1966)

Z3) Zuber, N. et al., "Vapor Void Fractions in Subcooled Boiling and Saturated Boiling Systems", 3rd Int. Heat Transfer Conf., Chicago, (1966)

APPENDIX A - FUEL PIN HEAT CONDUCTION

A collocation method (see Finlayson /F1/) is employed for the solution of the parabolic partial differential equation that governs the heat conduction in the fuel. Collocation methods have the desirable characteristic of generating point values as contrasted to nodal values yielded by finite difference methods. The high order accuracy of collocation schemes is another important advantage since it permits a reduction in the number of algebraic equations to be solved. The use of Hermite piecewise cubic polynomials as subspace functions together with Gaussian quadrature points as collocations points results in an accuracy of order $O(\Delta r^4)$ whereas $O(\Delta r^2)$ is obtained from finite difference schemes /D1/ (Δr represents the spatial mesh size). The method that follows was initially developed by Chawla et al./C2/ and, following Yeung /Y2/ closely, it is adapted here for temperature-independent physical properties in the fuel and cladding regions.

The cross section of a typical BWR fuel pin with UO_2 pellets and Zircaloy cladding is shown in Fig.A.1. In order to establish the appropriate heat conduction equation and boundary conditions pertinent to that geometry the following assumptions are made:

(1) Radially uniform power density in the fuel region whereas no heat generation is considered in the gap and cladding regions.
(2) Only radial conduction is considered.
(3) Physical properties of the fuel rod are isotropic and temperature independent.
(4) Effective heat transfer coefficient simulates the energy transport in the gap region.
(5) Outer surface of the cladding is convectively cooled by

single or two-phase flow fluid for which the heat transfer coefficient is determined from Chen's correlation.

By virtue of assumptions (1) through (3) the one-dimensional heat conduction equation in cylindrical coordinates can be written as

$$\frac{1}{r}\frac{\partial}{\partial r}\left(r\frac{\partial T}{\partial r}\right) + \frac{q'''}{k} = \frac{1}{\alpha}\frac{\partial T}{\partial t} \qquad \text{(A.1)}$$

where q''' is the power density ($q'''=0$ in the cladding), k is the thermal conductivity and α the thermal diffusivity. The following boundary conditions must be satisfied:

Fuel Center Line

$$\left.\frac{\partial T}{\partial r}\right|_{r=0} = 0 \qquad \text{(A.2)}$$

Fuel Surface

$$-k_f \left.\frac{\partial T}{\partial r}\right|_{r=R_{FS}} = h_{gap}\left[T(R_{FS}) - T(R_{CI})\right] \qquad \text{(A.3)}$$

Cladding Inner Surface

$$-k_c \left.\frac{\partial T}{\partial r}\right|_{r=R_{CI}} = h_{gap}\left[T(R_{FS}) - T(R_{CI})\right] \qquad \text{(A.4)}$$

Cladding Outer Surface

$$-k_c \left.\frac{\partial T}{\partial r}\right|_{r=R_{CS}} = h_{fc}(T(R_{CS})-T_B) + h_{nb}(T(R_{CS})-T_S) \qquad (A.5)$$

T_B is the fluid bulk boiling temperature and T_S the saturation temperature; h_{fc} and h_{nb} are heat transfer coefficients for forced convection and nucleate boiling respectively; h_{gap} is the effective heat transfer coefficient in the gap region.

An approximate solution is sought for Equation (A.1). For this purpose fuel and cladding are subdivided by N radial points as shown below

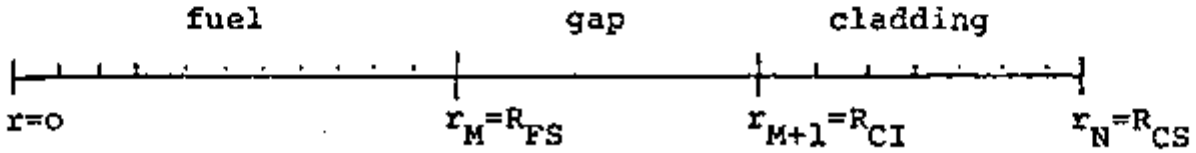

In each interval the r-dependence of the temperature is approximated by combining a set of functions $\{f(r)\}$ which must have the following properties

(a) $\{f(r)\}$ and $\{f'(r)\}$ are continuous in each interval

(b) $\{f(r)\}$ satisfies the boundary conditions mentioned earlier

The Hermite cubic polynomials form a convenient basis for generating $\{f(x)\}$. For the i^{th} interval these polynomials are

$$V_i(x) = \begin{cases} 1 - 3x^2 + 2x^3 & 0 \leq x \leq 1 \\ 1 - 3x^2 - 2x^3 & -1 \leq x < 0 \\ 0 & |x| > 1 \end{cases} \qquad (A.6)$$

$$S_i(x) = \begin{cases} x(1-x^2) & 0 \leq x \leq 1 \\ x(1+x^2) & -1 \leq x < 0 \\ 0 & |x| > 1 \end{cases} \qquad (A.7)$$

where x is the normalized distance from the i^{th} node,

$$x = \frac{r-r_i}{\Delta r}$$

It is also assumed that $V_1(x)$ and $S_1(x)$ vanish to the left of r_1 while $V_N(x)$ and $S_N(x)$ vanish to the right of r_N. It is easy to verify that properties (a) and (b) are satisfied by both $V_i(x)$ and $S_i(x)$.

The temperature field is then approximated by

$$T(x,t) = \sum_{i=1}^{N} \{C_{V_i}(t)(t)V_i(x) + C_{S_i}(t)S_i(x)\} \qquad (A.8)$$

where C_{V_i} and C_{S_i} are the unknown coefficients to be determined. The number of radial nodes, N, is given by $N = N_F+N_C+2$ where N_F and N_C are number of space intervals in the fuel and in the cladding respectively. Therefore the number of unknown coefficients is $2N = 2(N_F+N_C+2)$. The coefficients are found by requiring equation (A.8) to satisfy equation (A.1) at $2N_F$ points in the fuel and $2N_C$ points in the cladding along with the four relations provided by the boundary conditions.

Following Douglas and Dupont /D1/ the $2N_F$ points in the fuel and $2N_C$ points in the cladding are taken as the Gauss-Legendre quadrature points of order two. At each interval they are given by

$$\gamma_{ik} = \frac{1}{2}(r_i + r_{i+1}) + (-1)^k \frac{\Delta r}{2\sqrt{3}} \qquad (A.9)$$

$$i=1,\ldots,(N_F+N_C) \qquad k=1,2$$

The transient heat conduction equation (A.1) can be put into the simplest finite-difference form as

$$\frac{1}{r}\frac{\partial}{\partial r}\left(r\frac{\partial T^+}{\partial r}\right) + \frac{(q''')^+}{k} = \frac{1}{\alpha}\left[\frac{T^+(r)-T^-(r)}{\Delta t}\right] \qquad (A.10)$$

where the superscripts + and - refer to the new and the old time step values respectively. The initial temperature distribution is obtained by simply performing a analytical steady state solution of equation (A.10) together with the four boundary conditions and the initial condition $q'''(0)$.

The solution to the transient heat conduction equation is assumed to be

$$T(r,t) = \sum_{i=1}^{N} \{C_{V_i} V_i(x) + C_{S_i}(t) S_i(x)\} \qquad (A.11)$$

Substituting (A.11) into (A.10) and rearranging results

$$\sum_{i=1}^{N} \left\{ C^+_{V_i}\left[V_i(x) - \frac{\alpha\Delta t}{\Delta r}\left(\frac{V_i'(x)}{r} + \frac{1}{\Delta r}V_i''(x)\right)\right]\right.$$

$$\left. + C^+_{S_i}\left[S_i(x) - \frac{\alpha\Delta t}{\Delta r}\left(\frac{S_i'(x)}{r} + \frac{1}{\Delta r}S_i''(x)\right)\right]\right\} =$$

$$= (q''')^{+} \frac{\alpha \Delta t}{k} + \sum_{i=1}^{N} \left[C_{V_i}^{-} V_i(x) + C_{S_i}^{-} S_i(x) \right] \qquad \text{(A.12)}$$

Equation (A.12) is applied to the $2N_F$ collocation points in the fuel and to the $2N_C$ points in the cladding. Thus a total of $2(N_F+N_C)$ equations are obtained. The remaining four equation needed to make the system determined are provided by the boundary conditions as follows.

Boundary Condition at Fuel Centerline

Equation (A.2) denotes that the radial temperature distribution is symmetrical with respect to the fuel centerline. Substituting (A.11) into (A.2) it follows that

$$\sum_{i=1}^{N} \frac{1}{\Delta r} \left[C_{V_i}^{+} V_i'(x) + C_{S_i}^{+} S_i'(x) \right] \Big|_{r=0} = 0 \qquad \text{(A.13)}$$

Using the definitions of $V_i(x)$ and $S_i(x)$ results

$$C_{S_1}^{+} = 0 \qquad \text{(A.14)}$$

Boundary Condition at the Fuel Surface

Equation (A.3) relates the temperature gradient at the fuel surface to the temperature difference across the gap through an effective gap heat transfer coefficient. Substituting (A.11) into (A.3) and rearranging results

$$\sum_{i=1}^{N}\left\{C_{V_i}^{+}\left[\frac{k_f}{h_{gap}\Delta r}\,V_i'(x)+V_i(x)\right]_{r=r_M} + C_{S_i}^{+}\left[\frac{k_f}{h_{gap}\Delta r}\,S_i'(x)+S_i(x)\right]_{r=r_M}\right\}$$

$$= \sum_{i=1}^{N}\left[C_{V_i}^{+}V_i(x)+C_{S_i}^{+}S_i(x)\right]_{r=r_{M+1}}$$

or

$$C_{VM}^{+} + \frac{k_f}{h_{gap}\Delta r}\,C_{SM}^{+} = C_{VM+1}^{+} \qquad \text{(A.15)}$$

Boundary Condition at the Clad Inner Surface

Equation (A.4) relates the temperature gradient at the cladding inner surface to the temperature difference across the gap. Again, by substituting (a.11) into (A.4), rearranging and using the definitions of $V_i(x)$ and $S_i(x)$ it follows

$$C_{VM+1}^{+} - \frac{k_c}{h_{gap}\Delta r}\,C_{SM+1}^{+} = -C_{VM}^{+} \qquad \text{(A.16)}$$

Boundary Condition at the Cladding Outer Surface

Finally, equation (A.5) expresses the relationship between the cladding outer surface temperature and its gradient to the bulk coolant temperature, T_B, which is obtained from sub-channel analysis. Substituting (A.11) into (A.5) results

$$C_{VN}^{+} + \frac{k_c}{(h_{nb}+h_{fc})\Delta r}\,C_{SN}^{+} = \frac{h_{nb}T_S+h_{fc}T_B}{h_{nb}+h_{fc}} \qquad \text{(A.17)}$$

Equations (A.12), (A.14), (A.15), (A.16) and (A.17) form a set of $2(N_F+N_C+2)$ equations to be solved for the $2(N_F+N_C+2)$ unknows.

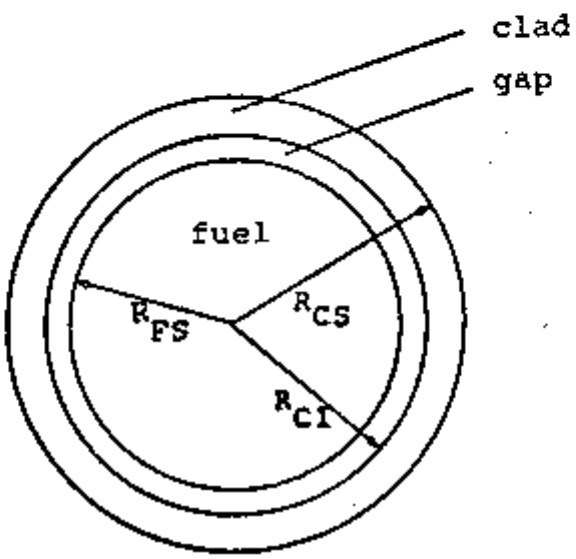

Fig A.1 - Cross Section of the Fuel Pin.

APPENDIX B - HEAT TRANSFER COEFFICIENTS

B.1 Single-Phase Flow Heat Transfer

The Dittus-Boelter correlation is applied for the single-phase flow heat transfer,

$$h_{1\phi} = 0.0023\, Re^{0.8}\, Pr^{0.4} \left(\frac{k}{D_e} \right) \tag{B.1}$$

B.2 Two-Phase Flow Heat Transfer

The Chen correlation /C6/ is used for subcooled and saturated boiling conditions. The heat flux is divided into two components: 1) nucleate boiling and 2) forced convection,

$$q''_{chen} = h_{nb}(T_w - T_{sat}) + h_{fc}(T_w - T_\ell) \tag{B.2}$$

The forced convection heat transfer coefficient, h_{fc}, is evaluated by

$$h_{fc} = 0.0023\, Re_{tp}^{0.8}\, Pr^{0.4} \left(\frac{k_\ell}{D_e} \right) \tag{B.3}$$

where

$$Re_{tp} = Re_\ell F^{1.25} \tag{B.4}$$

with

$$Re_\ell = \frac{G(1-x)D_e}{\mu_\ell} \tag{B.5}$$

Finally h_{fc} becomes

$$h_{fc} = 0.023\left[\frac{G(1-x)D_e}{\mu_\ell}\right]^{0.8}\left[\frac{\mu c_p}{k}\right]_\ell^{0.4}\left(\frac{k_\ell}{D_e}\right) F \qquad (B.6)$$

The Reynolds number factor, F, is plotted as a function of the Martinelli parameter, X_{tt}, in Fig.B.1. For subcooled conditions the value of F is set equal to one /C7/.

For the nucleate boiling heat transfer coefficient Chen used the Forster-Zuber correlation /F3/ times a nucleation supression factor, S,

$$h_{nb} = 0.00122\left[\frac{k_\ell^{0.79}\, c_p^{0.45}\, \rho_\ell^{0.49}}{\sigma^{0.5}\, \mu_\ell^{0.29}\, h_{fg}^{0.24}\, \rho_g^{0.24}}\right]\Delta T_{sat}^{0.24}\, \Delta p_{sat}^{0.75}\, S \qquad (B.7)$$

where

$$S = \left(\frac{\Delta T_{av}}{\Delta T_{sat}}\right)^{0.99} \qquad (B.8)$$

ΔT_{av} is the average superheat in the liquid film and $\Delta T_{sat}=T_w-T_{sat}$. S is shown in Fig.B.2. as a function of Re_{tp}. ΔT_{sat} and Δp_{sat} can be related using Clapeyron's equation,

$$\Delta T_{sat} = \frac{T_{sat}}{h_{fg}}\, v_{fg}\, \Delta p_{sat} \qquad (B.9)$$

Using this result in (B.6) it comes

$$h_{nb} = 0.00122\left[\frac{k_\ell^{0.79}\, c_p^{0.45}\, \rho_\ell^{0.49}}{\sigma^{0.5}\, \mu_\ell^{0.29}\, h_{fg}^{0.24}\, \rho_g^{0.24}}\right]\left(\frac{h_{fg}}{v_{fg}T_{sat}}\right)^{0.75}(\Delta T_{sat})^{0.99}\, S \qquad (B.10)$$

B.3 Curve Fits for the Parameter F and S

For computational purposes the parameters F and S can be fitted by curves developed by McClellan /M3/.

a) Reynolds Number Factor, F

$$F = 0.5\left(\frac{1}{X_{tt}}\right)^2 + 0.95\left(\frac{1}{X_{tt}}\right) + 1. \qquad \text{if} \quad \frac{1}{X_{tt}} < 0.5$$

$$= 1.6\left(\frac{2}{X_{tt}}\right)^{0.738} \qquad \text{if} \quad \frac{1}{X_{tt}} \geq 0.5$$

where

$$X_{tt} = \left(\frac{1-x}{x}\right)^{0.9}\left(\frac{\rho_g}{\rho_\ell}\right)^{0.5}\left(\frac{\mu_\ell}{\mu_g}\right)^{0.1}$$

(Martinelli parameter)

b) Supression Factor, S

$$S = 0.17 - 0.232\ \ln\left(\frac{Re_{tp}}{3.x10^5}\right) \qquad \text{if} \quad 2.x10^4 \leq Re_{tp} \leq 3.x10^5$$

$$= 0.17 - 0.0617\ \ln\left(\frac{Re_{tp}}{3.x10^5}\right) \qquad \text{if} \quad 3.x10^5 < Re_{tp} \leq 1.x10^6$$

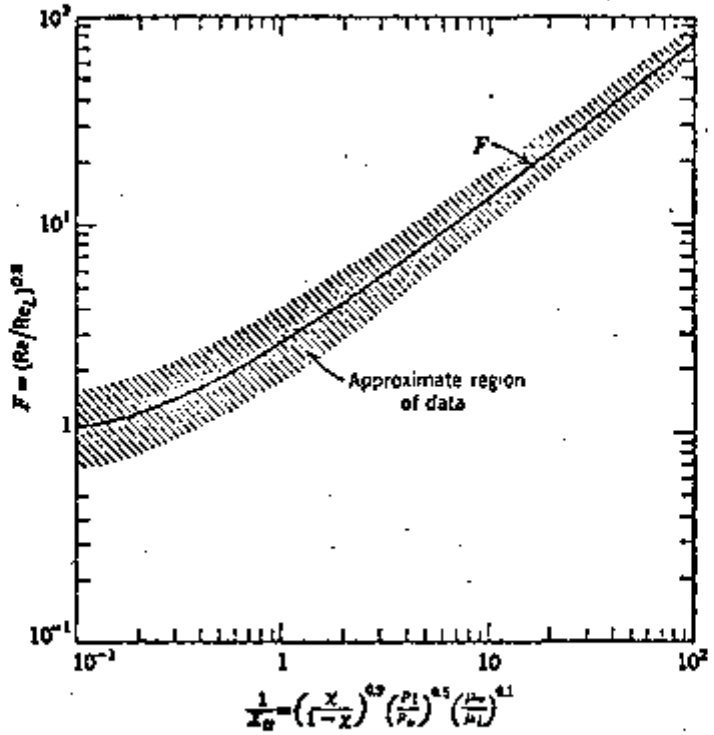

Fig. B.1 - Reynolds Number Factor

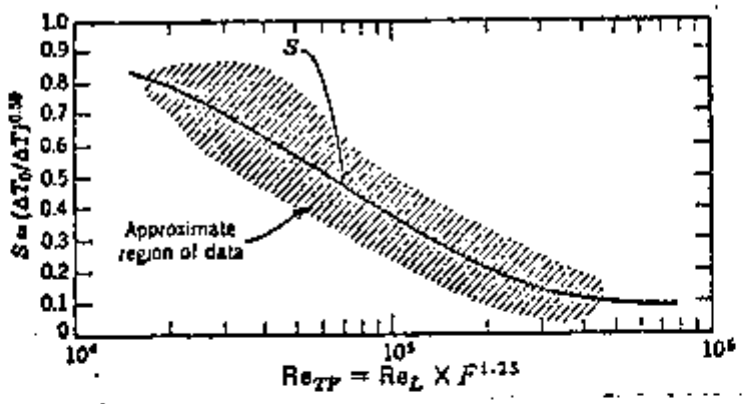

Fig. B.2 - Supression Factor

APPENDIX C - PROGRAM ABSTRACT

1. Program Identification: CANAL
2. Computer and Language: Multics on Honeywell 6180, FORTRAN IV
3. Description of Function: CANAL uses the drift-flux model to predict flow and enthalpy distribution in BWR fuel rod bundles under steady-state and operational transient conditions.
4. Method of Solution: The method of solution is based on the assumption that there is no transverse pressure gradients. At a given axial step CANAL iterates on the crossflow rates until a condition is reached where all subchannels achieve the same planar pressure. Then the solution marches to the nest axial step.
5. Restrictions: Presently the program will solve up to 45 subchannels and 35 fuels rods which is enough for half of a 8x8 BWR bundle. However these limits can be arbitrarily extended due to the virtual memory capability of the Multics systems.
6. Running time: For steady-state cases 20-30 msec per subchannel per axial node is a typical running time on the Honeywell 6180.
7. Availability: See report MIT-EL-79-028.

APPENDIX D - DRIFT FLUX PARAMETERS

D.1 Drift Velocity, V_{vj}

Vapor drift velocity correlations for various flow regimes have been studied by Ishii /I2/. For vapor-dispersed flow regimes Ishii recommends that the churn-turbulent drift velocity correlation alone can be used with satisfactory results. It is as follows

$$\bar{V}_{vj} = 2\left[g\,\frac{\sigma(\rho_f-\rho_g)}{\rho_f^2}\right]^{0.25} \qquad (D.1)$$

It should be noticed that this expression was derived from the vapor momentum equation in a confined channel under the assumptions of steady-state, no phase change and negligible mass effects and phasic interfacial drag forces. In short, it was assumed that gravity effects are dominant.

Ishii also derived an expression for the drift velocity the vapor in the annular flow regime starting from the one-dimensional, adiabatic, steady-state phasic momentum equations in a confined channel. The final expression can be approximated as

$$\bar{V}_{vj} \simeq \frac{1-\langle\alpha\rangle}{\langle\alpha\rangle + 4\sqrt{\rho_g/\rho_f}}\left[\langle j\rangle + \sqrt{\frac{(\rho_f-\rho_g)D(1-\langle\alpha\rangle)}{0.015\rho_f}}\right] \qquad (D.2)$$

Presently CANAL is only using equation (D.1) for all flow regimes. Attempts to incorporate equation (D.2) in CANAL have failed because it is not clear how to provide a smooth transition from (D.1) to (D.2). Discontinuities in $\bar{V}_{vj}$ have caused numerical instabilities in the solution scheme since they also imply discontinuities in the void fraction $\langle\alpha\rangle$ which is related to $\bar{V}_{vj}$ through equation (2.32). It must be

mentioned that in a real BWR core flow regime changes are really abrupt causing sharp changes in the relative velocity between vapor and liquid.

D.2 Concentration Parameter, C_o

Correlations for C_o are also available for several flow regimes but again sharp changes in C_o imply sharp changes in the void fraction $\langle\alpha\rangle$ leading to numerical instabilities. Therefore it was decided to approximate C_o as a constant (C_o=1.3 to 1.5 is recommended). This is satisfactory for BWR steady-state conditions where bulk boiling conditions predominante along most of the bundle length and for these conditions void and velocity profiles do not change considerable in the axial direction.

APPENDIX E - CRITICAL HEAT FLUX CORRELATIONS

In BWR technology the term critical heat flux (CHF) characterizes the rapid local deterioration of the heat transfer coefficient. As described by Hewitt and Hall-Taylor /H4/ as well as Collier /C7/ and Tong /T2/ this phenomenon is always associated with two-phase annular conditons. It is primarily governed by the dryout of the liquid film on the heated surface. The interested reader is referred to Lahey and Moody /L5/ for a review on simple mechanistic descriptions of the film dryout process as well as a summary on the main techniques employed to estimate CHF in BWR design.

The user of CANAL is provided with the following set of CHF correlations:

1) Hench-Levy lines
2) Barnet correlation
3) CISE correlation

E.1 Hench-Levy lines /L5/

These are limit lines constructed in the heat flux vs. exit quality plane. They were developed by GE based on single-, four- and nine-rod bundle experiments with uniform axial heat flux. The Hench Levy lines are given by the following expressions at 1000 psia:

$$(q''_c/10^6) = \begin{cases} 1. & \text{for } x<x_1 \\ 1.9 - 3.3x - 0.7\tanh^2(3G/10^6) & \text{for } x_1 \leq x \leq x_2 \\ 0.6 - 0.7x - 0.09\tanh^2(2G/10^6) & \text{for } x>x_2 \end{cases} \quad (E.1)$$

where $x_1 = 0.197 - 0.108(G/10^6)$

$x_2 = 0.254 - 0.026(G/10^6)$ (E.2)

This correlation is in the British System of Units and covers the range of system parameters:

P	600 - 1450 psia
D_h	0.324 - 0.485 in
G	0.2 - 1.6 Mlb/hr-ft^2
S_{ik}	greater than 0.06 in

For pressures other than 1000 psia the following correction has been recommended:

$$q_c''(P) = q_c''(1000)\left[1.1 - 0.1\left(\frac{P-600}{400}\right)^{1.25}\right] \quad (E.3)$$

E.2 Barnett Correlation /B10/

Barnett correlated the CHF data for annuli by a Macbeth type correlation. This correlation is given by the following mathematical expression at 1000 psia:

$$(q_c''/10^6) = \frac{A + B(\Delta h_{sub})}{C + Z} \quad (E.4)$$

where

$$A = 67.45\, D_h^{0.68}(G/10^6)^{0.192}\left[1 - \left[0.744\exp(-6.512 D_e G/10^6)\right]\right]$$

$$B = 0.2587\, D_h^{1.261}(G/10^6)^{0.817} \quad (E.5)$$

$$C = 185.\, D_e^{1.415}(G/10^6)^{0.212}$$

If D_i and D_o are respectively the internal and external diameters of the annulus the hydraulic equivalent diameter is

given by $D_e=D_o-D_i$ and the equivalent heated diameter D_h by $(D_o^2-D_i^2)/D_i$. Barnett reported that his correlation gives accurate prediction for CHF in rod bundles with uniform axial heat flux with D_i and D_o given by

$$\begin{aligned} D_i &= D_R \text{ (rod diameter, in)} \\ D_o &= \left[D_R(D_R + D_h^*)\right] 0.5 \end{aligned} \tag{E.6}$$

where

$$D_h^* = \frac{4 \times \text{(Flow Area)}}{S \times \text{(Heated Rod Perimeter)}} \tag{E.7}$$

with

$$S = \sum_{\substack{\text{all} \\ \text{rods}}} \frac{\text{local rod power}}{\text{maximum rod power}} \tag{E.8}$$

The correlation is in the British System of Units and covers the following range of system parameters

P	600 - 1400 psia
Z	24 - 108 in
$G/10^6$	0.14 - 6.2 lb/hr-ft^2
Δh_{sub}	0 - 412 BTU/lb
D_o	0.551 - 4.0 in
D_i	0.375 - 3.798 in

For pressures other than 1000 psia Barnet suggests multiplying the coefficient A in equation (E.6) by $h_{fg}(P)/649$.

A correction for nonuniform axial heat flux is suggested as follows. Radially nonuniform patterns are handled through the S factor, equation (E.8) which appears in the formula for

the equivalent heated diameter.

For nonuniform axial heat flux cases S will be changed to

$$S = \frac{1}{\xi_{ax}} \sum_{m=1}^{n} \frac{\bar{q}''_m}{\bar{q}''_{max}} \tag{E.9}$$

where n is the total number of rods in the bundle,

$$\bar{q}''_m = \frac{1}{H} \int_0^H q''_m(z)\,dz \tag{E.10}$$

$\bar{q}''_{max} = \max\{\bar{q}''_m\}$ and ξ_{ax} is the axial peaking factor (assuming all rods have the same axial power shape). Equation (E.9) can be simplified by defining $(q''_{av})_{radial}$

$$(q''_{av})_{radial} = \frac{1}{n} \sum_{m=1}^{n} \bar{q}''_m \tag{E.11}$$

Finally equation (E.9) becomes

$$S = \frac{n}{\xi_{ax}\,\xi_{rad}} \tag{E.12}$$

where ξ_{rad} is the radial peaking factor defined by

$$\xi_{rad} = \frac{\bar{q}''_{max}}{(q''_{av})_{radial}} \tag{E.13}$$

E.3 CISE Correlation /G1/

The CISE correlation developed at CISE, Italy accounts for upstream history effects on CHF by using the "global condition hypothesis" according to which if cross section, pressure and mass velocity are known the critical heat flux condition can be described by the relation

$$f(Q_{si}, L_{si}) = 0 \tag{E.14}$$

where Q_{si} is the critical power relevant to the surface i affected by and L_{si} is the boiling length on that surface. In this approach the upstream history enters implicitly on L_{si}. The CISE correlation built into CANAL has the following specific form in the British System of Units:

$$\frac{Q_{si}}{G_i A_i h_{fg}} = \frac{\dot{q}_{avg}}{\dot{q}_{local}} n \frac{a}{1 + b/L_{si}} \frac{A_i}{A_{tot}} \tag{E.15}$$

where

$$a = \frac{1 - P/P_c}{(1.35\ G_i/10^6)^{1/3}}$$

$$b = 168.(P_c/P - 1.)^{0.4} (G_i/10^6) (D_{hi})^{1.4} \tag{E.16}$$

n is the total number of rods in the bundle, A_{tot} is the bundle flow area and P_c=3204. psia.

It should be kept in mind that this correlation was set up for rod-centered subchannel codes since it is based on an annulus correlation. In order to apply it to CANAL which uses the coolant-centered subchannel scheme it was thought that it should be only used for interior subchannels. In the coolant centered subchannel scheme corner and side sub-

channels include large portions of the unheated bundle wall and, for this reason, the hydraulic diameter of these subchannels are too small compared to their annular counterparts. The presence of the cold bundle wall also affects the subchannel boiling length. On the other hand the coolant-centered and rod-centered subchannel schemes are the same so that the correlation can be safely applied.

In addition to this the term for the correction of radially nonuniform heat fluxes needs to be modified. This factor appears as $\dot{q}_{avg}/\dot{q}_{loc}$ in the correlation but it can simply be interpreted as the inverse of the radial peaking factor in a rod-centered subchannel. However for a coolant center subchannel which faces four possibly differently heated rods, this factor must be modified. One option which has been proposed by A. Levin /W5/ is

$$\frac{\dot{q}_{avg}}{\dot{q}_{loc}} = \frac{1}{n} \sum_{rods} \frac{\dot{q}_{avg}}{\dot{q}_{loc}} \qquad \text{(E.17)}$$

where n=4.